The Formation and Run-off of Condensate on a Vertical Glass Surface: An Experimental Study

by

Vivek Kansal

A thesis
presented to the University of Waterloo
in fulfilment of the
thesis requirement for the degree of
Master of Applied Science
in
Mechanical Engineering

Waterloo, Ontario, Canada, 2006

I hereby declare that I am the sole author of this thesis. This is a true copy of the thesis, including any required final revisions, as accepted by my examiners.

I understand that my thesis may be made electronically available to the public.

ABSTRACT

An experimental study of condensate was performed by exposing a sheet of glass, cooled at its bottom edge, to an enclosure with a controlled environment. The air in the enclosure was maintained at a constant relative humidity (RH) and a constant dry bulb temperature (T_{db}). Experiments were conducted at T_{db} = 22.1°C and RH of 30%, 35%, 40%, 45%, and 50%.

It was found that the time until initial condensation run-off was sensitive to low RH (RH = 30%, 35%, 40%) and insensitive to high RH (RH = 45%, 50%). Time until run-off decreased with increasing RH. It was found that, at first, condensation run-off occurred near the bottom of the glass and left one to believe that the remaining condensate was in steady state with the enclosure. Over a 16 hour period however, it was found that the condensation run-off front, in every case, progressed upward to include the entire condensate area. Similar to time of initial run-off, speed of condensation front movement increased with RH and was also insensitive at high RH.

A summary plot showing run-off front position is presented. This chart can be used to predict initial run-off and front progression at the bottom edge of any window if the surface temperature profile is known.

ACKNOWLEDGMENTS

I would like to thank the Canadian Window & Door Manufacturers Association for the scholarship that allowed me to conduct my research.

I would like to thank my supervisor, Prof. J.L. Wright for his support and guidance throughout my project.

The hours of support provided by the Engineering Machine Shop and the Engineering Student Machine Shop were greatly appreciated and were of great importance in construction and trouble-shooting of the apparatus.

Thanks to Chris, Nathan, and Sohel for providing support, whether it be for CFD, theory, or general questions; the help was appreciated.

Thanks to the rest of the solar lab for providing me with daily distractions and making my time in the lab a great experience.

Finally, thanks to my family and Bhagawan for always supporting me during my project.

TABLE OF CONTENTS

LIST OF FIGURES

Nomenclature

a_w	water activity, dimensionless
B_Y	Spalding transfer number, dimensionless
CRF	condensation resistance factor, dimensionless
d	divider, m
D	droplet diameter, m
D_{AB}	component diffusion coefficient, m^2/s
D_O	initial droplet diameter, m
FT	frame temperature, °C
FT_I	weighted frame temperature on warm side, °C
FT_{II}	weighted frame temperature on cold side, °C
FT_p	average temperature of 14 predetermined thermocouples on frame, °C
FT_r	average temperature of 4 roving thermocouples, °C
g	gravity, m/s^2
GT	average temperature of 6 predetermined thermocouples on glazing, °C
h	convective heat transfer coefficient, W/m^2K
h_x	local convective heat transfer coefficient, W/m^2K
H_{glass}	height of glass section, m
H_{post}	height of section below glass, m
H_{pre}	height of section above glass, m
I	temperature index , dimensionless
k_c	mass transfer coefficient, cm^3/s
K	droplet evaporation constant, dimensionless
L	length of enclosure, m
N_u	Nusselt number, dimensionless
Nu_l	Nusselt number based on length, dimensionless
Nu_s	Nusselt number based on fin spacing, dimensionless
Nu_x	local Nusselt number, dimensionless
P	pressure, kPa
Pr	Prandtl number, dimensionless
q	heat flux, W/m^2
q_x	local heat flux, W/m^2
R_{RH}	Condensation run-off front progression rate based on RH, mm/min
Ra	Rayleigh number, dimensionless
Ra_s	Rayleigh number based on fins spacing, dimensionless
Ra_L	Rayleigh number based on length, dimensionless
RH	relative humidity, %
RH_{dp}	relative humidity based on for T_{dp} = 0°C and given T_{db}, %
S	fin spacing, m
S_{opt}	fin spacing for maximum heat transfer from each individual fin, m
S_{max}	fin spacing for maximum heat transfer for the entire array, m
Sc	Schmidt number, dimensionless
Sh	Sherwood number, dimensionless
t	time, min

t_{cst}	condensate layer thickness, m
t_{drop}	condensate droplet layer thickness, m
$t_{between}$	condensate layer between droplets thickness, m
t_{ir}	time at initial run-off, min
T	temperature, K
T_{cold}	glass surface temperature, K
T_{db}	dry bulb temperature, °C
T_{dp}	dew point temperature, °C
T_{hot}	heated surface temperature, K
T_{mean}	enclosure air temperature, K
w	humidity ratio, $g_{H2O}/kg_{dry\ air}$
W	weighting factor, dimensionless
x_v	mole fraction of water vapour in a mixture, $mole_{H2O}/moles_{mixture}$
x_s	mole fraction of water vapour in a saturated mixture, $mole_{H2O}/moles_{mixture}$
y_g	distance up the glass surface ($y_g = 0$ is the bottom), m
$y_{g,ir}$	distance up the glass surface where initial run-off occurs, mm
α	thermal diffusivity, m^2/s
μ	dynamic viscosity, kg/m.s
ν	kinematic viscosity, m^2/s
ρ	density, kg/m^3

Chapter 1

1 Background

1.1 Mould

Mould (fungi) growth within a building envelope can be extremely hazardous to its occupants. Through touch or inhalation, the effects of mould can vary from mild allergic reactions to fatality. Mould growth in the building envelope occurs when moisture is present on common building materials, such as; house dust, wallpaper, textiles, wood, paint, gypsum board, fiber board, and glue [Dalton, 2004; IOM, 2004]. Symptoms of mould include headaches, sneezing, eye and skin irritation, runny nose, difficulty breathing, and asthma [EPA 2002]. In 1994, Dr. David Sherris of the Mayo Clinic, determined mould to be the cause of chronic sinus infections in 93% of his 210 test patients [Underwood 2000]. Studies at the Lawrence Berkeley National Laboratory concluded with statistical significance that mould and building dampness are associated with a 30% to 80% increase in respiratory and asthma related problems [Fisk et al., 2006]. More serious health effects caused by repeated contact with mould include hypersensitivity pneumonitis, pulmonary haemorrhaging, cancer of the liver, brain haemorrhaging, and narcosis; all potentially fatal [EPA 2001, Dearborn et. al. 1999, Barrett 2000, Wang et al. 2001]. These symptoms are caused when mycotoxins are found in the mould.

The severity of mycotoxins was brought to the public eye when a group of infants in Cleveland, Ohio showed bleeding in the lungs [Jarvis & Miller 2005]. Studies into the incidents found an association with mould growth in homes of the infants, in particular, a toxic mould known as Stachybotrys chartarum (S. chartarum). S. chartarum is typically found in carpet or gypsum board (drywall) [McNeel & Kreutzer 1996]. In total, 37 infants were diagnosed, 19 of whom passed away [Dearborn et al. 1999]. It should be noted that although S. chartarum does contain mycotoxins, its correlation with the Ohio infants is questioned because other fungi were also found in the infants homes [Robbins et al. 2003]. The incidents in Ohio led to numerous studies on S. chartarum in an effort to better understand its presence in households and effects on the human body. It was found that the occurrence of S. chartarum in building envelopes was minimal; of 1717 buildings examined across the U.S., 6% contained S. chartarum with an average concentration of 12 colony-forming units per meter cubed of air (CFU/m^3) [Shelton et al. 2002], of 68 allergy patient's homes in southern California, 2.9% were populated with an average concentration of 0.3 CFU/m^3 [Kozak et al. 1979]; 1 out of 50 Canadian homes contained S. chartarum with no mention of concentration levels [Miller at al., 1988]. In perspective, the levels found in the homes of the children from Ohio were 43 CFU/m^3 [Eztel et al. 1998]. Unfortunately, not enough data exists showing what concentration levels are detrimental to human health [Brasel et al. 2005]. The state of New York and the U.S. federal government have both acknowledged mould to be a serious health issue, but agree that so little information is available that they can not release any regulations for evaluating potential health effects based on fungal contamination levels [D'Andrea 2004].

More common moulds found indoors are Penicillium, Aspergillus, and Cladosporium [Altman et al. 2000]. Often, when a building is contaminated, it is done so by many mould types, not just one. This makes it extremely difficult to associate human health effects to one particular type of mould. Research papers discussed in this thesis used what the researchers believed to be the cause of the health symptoms discovered. The goal is to inform the reader of the health concerns presented for each type of mould in everyday situations. It is beyond the scope of this thesis to question the validity of the researcher's claims.

Penicillium, found on wallpaper, carpet, paint, cotton, wood, and polyvinyl chloride (PVC) [Carlson 2006, McNeel & Kreutzer 1996, Upsher 1984] is also known to produce mycotoxins [Mortensen et al. 2006]. It has been found to cause health problems in schools surveyed in the U.S. and in British Columbia. The most common health effects shown in the U.S. study were nasal congestion (19.8% of teachers surveyed) and itchy/watery eyes (14.3%). Concentration levels of Penicillium in the U.S. schools averaged 180 CFU/m^3 in all of the schools studied and close to 250 CFU/m^3 in 20 schools where Penicillium was the dominant contaminant. Cladosporium was the dominant fungi in schools where Penicillium was not but were not considered a threat because the levels were significantly lower than outdoor levels at the same locations. Penicillium and Aspergillus were the only fungi found to be at higher levels indoors relative to outdoors [Cooley et al. 2006, Bartlett et al. 2003]. A study of 1002 "high risk for asthma" infants from Connecticut and western Massachusetts concluded that those

exposed to high levels of Penicillium were at a significant risk for wheeze and persistent cough relative to those who were not. High risk infants are those with at least one older sibling diagnosed with asthma [Gent at al. 2002]. Again, researchers say it is difficult to have upper limits on what concentration levels pose a threat because every human is different and react differently at various levels [Davis 2001].

Aspergillus, found on wood, carpet, house dust, and wall paper glue [dehs.umn.edu 2006, McNeel & Kreutzer 1996], can also produce mycotoxins [Godish 1995, dehs.umn.edu 2006]. It has been known to cause liver and kidney disease through inhalation [Al-Doory et al. 1984]. A Korean study of various bars, cafes, schools, and homes found an extremely high occurrence of Aspergillus, 70%-100%, depending on season, sampling method, and business category. The average concentration levels varied from 24 CFU/m^3 to 34 CFU/m^3, all at levels greater than found outdoors. The total fungal concentration levels varied from 209 CFU/m^3 to 1002 CFU/m^3. No mention was made of what health effects were experienced at the various locations [Jo & Seo 2005].

Cladosporium, usually found on cotton, wood, paint, PVC, rubber, and glass [Carlson 2006, McNeel & Kreutzer 1996, Upsher 1984] is typically known as an allergen and can cause mycosis or extrinsic asthma [Crissy et al. 1995]. Cladosporium is most often found in larger quantities outdoors relative to indoors and therefore is not generally considered a significant pollutant in a building environment [Carlson 2006, Jo & Seo 2005, Cooley et al. 2006].

1.1.1 Legal Risks

The presence of mould not only poses a health threat to building occupants, but also a financial threat to insurance companies, building owners, architects, and the various engineers associated with construction. Numerous lawsuits have been filed in the U.S. over the past few years over mould found in buildings. In New York, 300 tenants of an apartment building filed a $10 billion law suit for mould related damages [Herdon & Yang 2000]. Ed McMahon sued his insurance company for $20 million after his family started to get sick from mould in his house [O'Neill 2002]. A paper published by Sarah E. Carson stated that there were over 400 cases pending in the New York judicial system in regards to mould related damage [Carson 2003]. Mould claims in Texas cost insurance companies over $850 million in 2001 [Porter 2003]. A 47 year old woman was advised after testing to leave her home due to mould growth. She subsequently filed a $75 million law suit against the builder – Fischer Homes [Clark 2002]. Two women were awarded $1.07 million when a landlord's failure to respond to mould problems resulted in asthma attacks and other health problems. The case made it all the way to the Delaware Supreme Court in appeals where the original ruling was upheld [Ridder 2002]. The county of Martin in Florida was awarded $8.8 million from a construction company when a courthouse and office building were evacuated after inspection due to mould problems [Carson 2003]. The legal proceedings mentioned above are merely a few of many. Lawsuits in reference to mould damage increase annually and more money is lost by insurance companies, builders, and engineers. There is significant financial benefit to eliminating mould in the building envelope.

1.1.2 Structural Damage

Mould can also pose a financial risk when it infiltrates and damages the substance it grows on. Mould and bacteria have the ability to penetrate various materials and compromise their structural integrity. Wood has been an area of significant study as it is usually a significant load bearing material in construction. Bacterial decay of wood can be classified under three categories as mentioned by Greaves (1971). Change permeability but not strength, attack structure, and work in association with other bacteria to break down wood. Two types of bacteria that affect a wood structure are tunnelling bacteria and cavitation bacteria. Tunnelling bacteria, as the name suggests, tunnel through the wood and can only be seen as a single cell at the surface. Tunnelling bacteria have been known to attack pine, a common building material found in residential homes, more specifically in window frames [Nilsson & Daniel 1983].

Cavitation bacteria hollow out sections of wood from within and are not visible on the surface. Cavitation bacteria, like tunnelling bacteria, have been known to attack pine [Nilsson 1984]. Decay of pine under extreme circumstances, complete submergence in water for long periods of time, has been well documented. Studies conducted in Sweden and the U.S. show the potential for 72.8% substance loss in pine wood after two months of decay [Nilsson & Rowell 1983]. A study out of the University of Portsmouth in the United Kingdom showed 30% weight loss of untreated pine after six months. The samples from Portsmouth were tested in a cooling tower and were directly under the sprinklers. The cooling tower was functional 24h a day except for periods of maintenance [Eaton 1994].

1.1.3 Growth

Mould growth potential is defined as the minimal moisture required for microbial growth in terms of water activity, a_w. Water activity is defined as the ratio of the moisture content of the material in question to the moisture content of the same material when it is saturated. A material is considered to have an a_w value of 1 when the material is fully saturated and surrounded by air at an RH of 100% [IOM 2004]. Penicillium and Aspergillus can start growing at a_w = 0.76, while Cladosporium and S. chartarum can start growing at a_w =0.83 and 0.91, respectively [Grant et al. 1989]. Aside from water, mould needs nutrients to grow. These nutrients can be carbohydrates, proteins, lipids or even nonbiologic compounds [IOM 2004]. These nutrients are usually found in house dust, wallpapers, textiles, wood, paints, gypsum board, fiber board, and glue [Dalton 2004, IOM 2004]. Once present, the rate at which mould grows varies depending on mould type and environmental conditions. Some types of micro organisms can multiply from one cell to one billion in 18 hours [White and Kuehl 2002]. A study of Penicillium on wallpaper showed growth in as little as 5 hours [Pasanen et al. 1992]. The final necessity for mould growth indoors is temperature. Mould thrives at temperatures of 40-100 F (4-38 ºC) [Post 1999] which is common.

The typical household will be well with in the temperature range for mould growth and hence temperature is not a limiting factor in growth sites. To find potential mould growth locations it is best to look for sitting water on building materials. Main sources of water in the household are moisture from a shower in a bathroom, cooking, a leaky pipe, or water from sinks and tubs. Another obvious source is a window. Condensation that

forms on a window, under the right circumstances, may run-off the window and begin to pool in the window sill or on the window frame. If the condensation persists, water can flow down the frame on to the wall below the window or seep behind the surface into the insulation. Mould growth on or around windows frames has been well documented. A study of 200 houses with water incursions in Texas cited window frames as one of the locations for surface fungal growth [Kuhn et al. 2005]. Morrell (2002) highlighted the types of mould typically found on window frames in a study of wood-based construction. McNeel and Kreutzer (1996) also identified household moulds found on window sills. Grant et al., (1989) stated gloss paint on window joinery supports mould growth. Surveys conducted by Statistics Canada for Natural Resources Canada found that 42% of houses surveyed reported window condensation and cited it as a problem that could lead to mould growth [NRC 2006]. The U.S. Environmental Protection Agency lists prevention of condensation on windows as way to reduce the risk of mould in the building envelope [EPA 2002]. Condensation on windows has been cited, in numerous references, as the cause of mould growth on window glass and frames [Baily & Hall 2006, Godish 2006]. The University of New Brunswick lists mould and condensation on windows as a check box on an inspection form, created by the student union, to be completed by students before commencing residence in off-campus housing [Fredericton Student Housing 2006]. It is hoped the author has shown the link between condensation on the indoor surface of windows and mould growth is common and detrimental.

1.2 Windows

Windows have always been a significant part of building design. They provide many functions and play a significant role in daily building operations. Of benefit, they allow natural light into a building and in some cases fresh outdoor air. Of hindrance, they provide very poor thermal resistance compared to wall sections and are sources of sometimes unwanted solar heat gain. Windows vary in construction, style, and performance. Initially, windows consisted of a single plane of glass. Through the need to improve thermal resistance, windows began to change and additional panes of glass were added creating a sealed, insulated pocket of air between the panes. The most common window found in today's residential buildings are double paned and hence, will be the only windows discussed in the remainder of this thesis. These insulating windows, also known as Insulated Glazing Units (IGU) developed further through the addition of low emissivity coatings, alternate fill gasses, new spacer construction, and various other innovations.

A double-pane IGU consists of five components as can be seen in Figure 1.1; two panes of glass (with potential coatings), a fill gas, a spacer assembly, and a sealant. The spacer assembly consists of a desiccant tube and a primary sealant. The IGU is surrounded by a sash and a frame which hold the unit in place. The panes of glass are the main portion of the window which allow light transmission and the fill gas acts as an insulating pocket. The spacer assembly and sealant support and separate the two panes also acting as a barrier, preventing moisture and gas from entering or leaving the cavity.

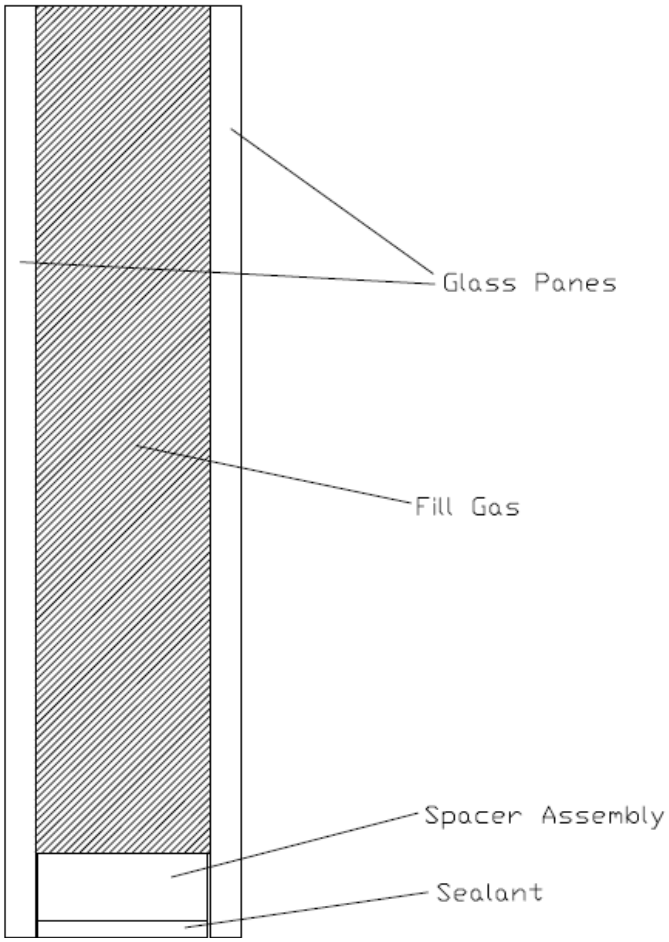

Figure 1.1: Components of a double glazed Insulated Glazing Unit (IGU)

1.2.1 Condensation

The amount of moisture present in an air mixture can be described with the relative humidity (RH) and the humidity ratio (w). The relative humidity is the ratio of the mole fraction of water vapour of a mixture (x_v) and the mole fraction of water vapour in a saturated mixture (x_s) at the same temperature (T) and pressure (P). The humidity ratio,w, is the mass of water in the mixture to the mass of dry air. Both are shown in Equations 1.1 and 1.2.

$$RH = \left[\frac{x_v}{x_s} \right]_{t,P} \tag{1.1}$$

$$w = \frac{m_{water}}{m_{dryair}} \tag{1.2}$$

For regular building operations and human comfort, it is recommended by the American Society of Heating, Refrigeration and Air-Conditioning Engineers (ASHRAE) that RH range between 30-60% at normal room temperatures for human comfort [ASHRAE 2004].

Another important property of a conditioned space is the dew point temperature (T_{dp}). The dew point temperature is the temperature at which the water in the air will change phase from vapour to liquid. It varies with RH, where T_{dp} increases as RH increases at a constant T_{db}.

For condensation to occur on the indoor surface of a window, the glass surface must be at or below T_{dp} of the surrounding air. This scenario typically occurs in cold climates where the outdoor air temperature is much lower than the temperature of the indoor conditioned space. This temperature differential causes heat transfer from the conditioned space to the outdoor environment through the window. This heat loss is apparent when one touches a window and notices it to be cold. When the temperature differential is sufficient, certain portions of the glass drop below T_{dp} resulting in condensation. This will be discussed in further detail in the next section with an energy analysis of a double paned IGU.

1.2.2 Heat Transfer Analysis

Heat transfer through an IGU is complex in nature. It is simplest to model by splitting the IGU into three parts as described by ASHRAE [ASHRAE 2005]; a 2-D edge-glass region, a 1-D center-glass region, and a 2-D frame region. All are shown in Figure 1.2. The edge-glass consists of an area 65mm from the sightline. The center glass is the remaining area within the sightline and the frame is the area surrounding the sightline. Under winter time conditions, the outdoor environment is colder than indoors. Hence, energy is transferred from the indoor space to the outdoor space. This energy transfer occurs via convection, conduction, and radiation. Of importance in describing radiation through a glazing unit is short-wave (solar) radiation and long-wave radiation. Short wave radiation is transferred from the sun while long-wave radiation is transferred from surrounding objects (e.g., trees, grass, furniture, and walls). Typically, for a sheet of glass, 8% of the incident solar radiation is reflected, 5-50% is absorbed, depending on glass thickness and the remainder is transmitted [McQuiston et al. 2000].

Heat transfer through a glazing can be quantified using a two-step analysis. First, the solar radiation is tracked while accounting for multiple reflections (figure 1.3), determining how much energy is transmitted, reflected, and absorbed at each glazing layer [Edwards 1977, Wright & Kotey 2006]. This is followed by an overall energy balance using the values from the first step and accounting for long-wave radiation, conductive and convective energy transfer.

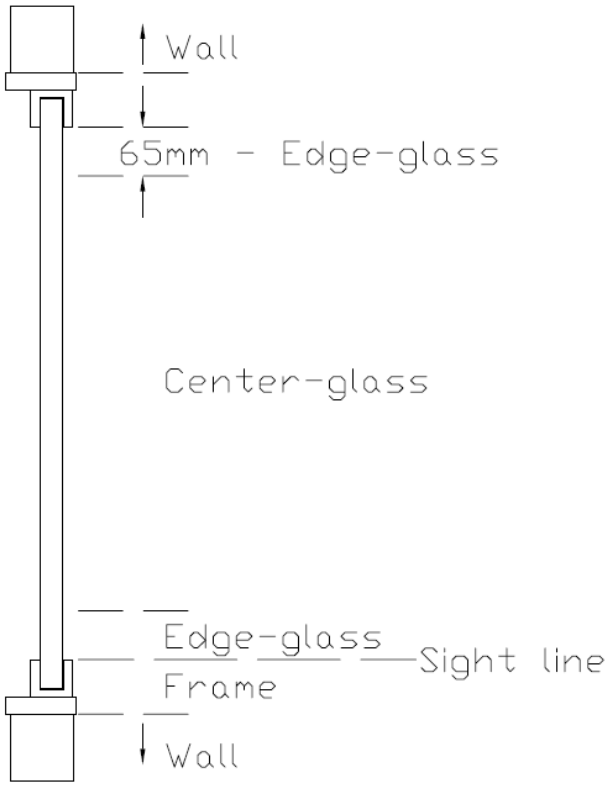

Figure 1.2: Sections of a window used for computer models

Heat transfer through the center glass region can be explained with the aid of a resistance network. The majority of heat transfer through a glazing occurs through the center-glass region [Wright 1998a]. Energy is exchanged between the outer most pane of glass and the outdoor environment via convection and radiation. Energy is then exchanged between panes of glass via convection and radiation. The convective portion is due to the pocket of fill-gas between panes. The flow is strictly buoyancy driven and travels up the warm pane of glass and then down the cold pane. Energy is exchanged between the inner pane of glass and the indoor environment via convection and radiation. A detailed heat transfer analysis through a glazing using a resistance network and formula can be found in the literature [e.g., Hammond 2001].

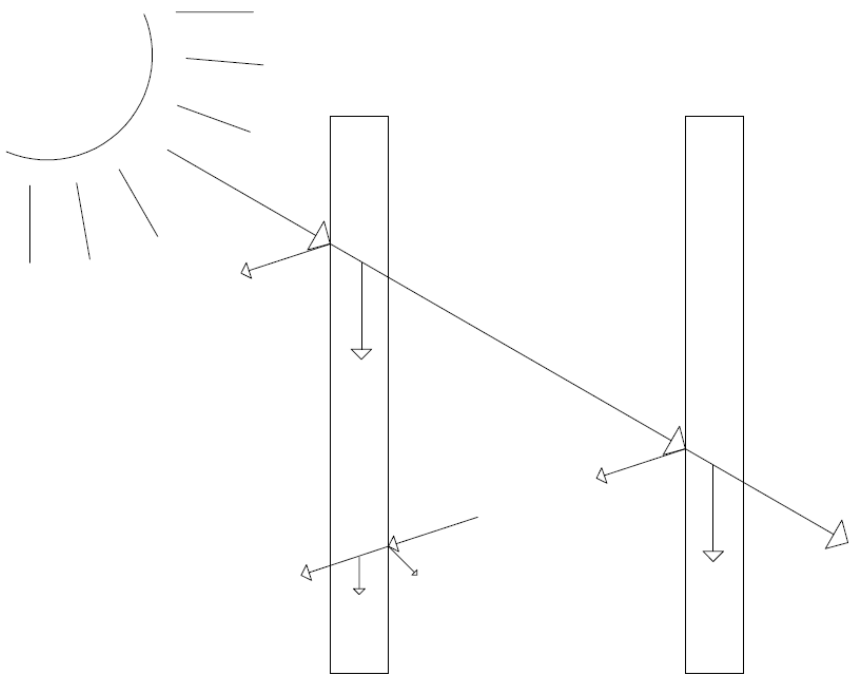

Figure 1.3: Solar irradiation energy transfer for a double paned glazing unit

1.2.3 Edge-glass Region

The edge glass region is defined as, *"...the area of the glass where the glass temperature changes until it reaches the constant value of the center of the glass..."* [Elmahdy & Frank 1993]. It is different from the center glass for two main reasons; there is conduction between the frame components and the edge glass and fill gas circulates from one pane to the next, as can be seen in Figure 1.4. The fill gas motion is described in more detail below. A major contributor to heat transfer through this region is the spacer used. The spacer acts as a thermal short allowing heat to transfer via conduction from one pane of glass to the next. This conduction causes the indoor edge glass region to be colder (under winter conditions) than the center region. Elmahdy & Frank (1993) tested four different types of spacers and evaluated the effects on the indoor glass temperature

in the edge-glass region. It was found that a silicone foam spacer yielded best results, followed by a corrugated metal strip, a thermally broken metal, and an aluminum strip. This is as expected as a solid piece of aluminum would provide the least thermal resistance, while a silicone foam spacer would provide the most. A Japanese study looked at the use of a resin spacer. The resin, however, was porous to water and over time, water vapour infiltrated the glazing cavity [Matsuyama et al. 2005]. A 2-D computer simulation model called FRAME was developed specifically for simulating heat transfer through the glazing spacer and frame components. A study using this software determined that using a wooden frame over an aluminum frame could reduce the rate of heat loss (U-value) through a window by as much as 50% for a small window with a well insulated IGU. It also concluded that an insulated spacer could reduce the total window U-value by as much as 6% over an aluminum spacer [Carpenter & McGowan 1989].

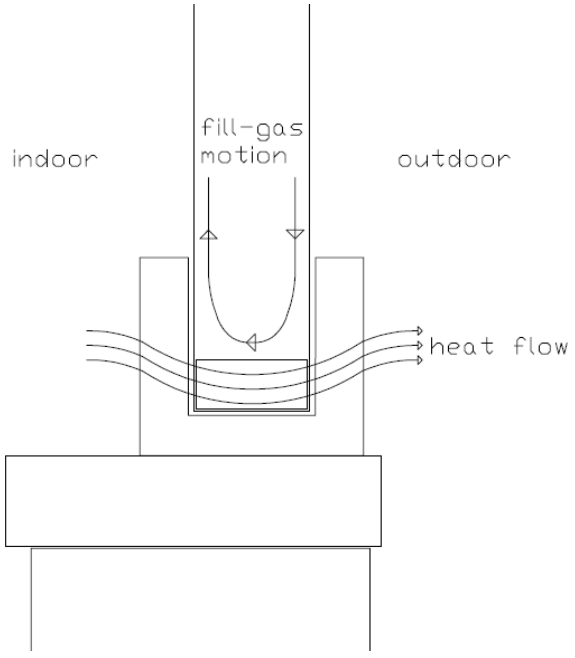

Figure 1.4: Conduction through frame and fill-gas motion

1.2.4 Fill Gas Motion

The fill gas motion and associated heat transfer creates a location varying temperature profile along the glass panes. To better clarify how this occurs one must follow a pocket of air as it travels through the glazing cavity. This will be done starting at the bottom of the warm pane of glass. The pocket of air will be warmed by the pane of glass, reduce in density, and rise. As it rises it continues to gain heat from the glass until it reaches the top of the cavity. The pocket then crosses to the cold pane and is cooled as it descends. The process is then repeated. This motion causes the temperature of the indoor glass to be coldest at the bottom. To fully understand the convective portion of energy transfer inside the cavity one must be familiar with the Rayleigh number (Ra) Eq 1.3,1.4 Nusselt number (Nu), and heat transfer coefficient (h) Eq 1.5.

$$Ra = \frac{g\beta(T_1 - T_2)L^3}{\alpha\nu} \tag{1.3}$$

$$\beta = \frac{2}{(T_1 + T_2)} \qquad \text{(ideal gas)} \tag{1.4}$$

$$h = \frac{Nu \cdot k}{L} \tag{1.5}$$

Where:

g = gravity
$T_{1,2}$ = temperature of glazing surface (1,2)
L = distance between panes of glass
α = thermal diffusivity of fill gas
ν = kinematic viscosity

The Nusselt number is a non-dimensional representation of the convective heat transfer rate. Nu is a function of cavity geometry, Ra, and Pr, where Ra describes the nature

(buoyancy versus viscous forces) of the flow in the cavity and where Pr describes the ratio of momentum diffusivity and thermal diffusivity for the gas in the cavity. Many studies have looked at determining correlations for Nu as a function of Ra and Pr for natural convection through vertical cavities of different dimensions. Initial correlations derived by ElSherbiny et al. (1982) were widely accepted and later modified to be more accurate at lower Ra by Wright (1996). The motion in the cavity varies depending on Ra, more specifically the temperature differential between the indoor and outdoor environment. With greater Ra, cells form within the core of the cavity while the primary flow remained [Wright & Sullivan 1989]. Typically Ra does not exceed 12,000 under even severe winter conditions [Wright & Sullivan 1995]. As mentioned previously, changing the fill gas to a substance of high viscosity can inhibit this convective flow. One study looked at the effects of using infrared absorbing gasses in the cavity rather then ones with high kinematic viscosity. It was concluded that the benefits of an infrared absorbing gas do not outweigh one with a high kinematic viscosity for a vertical glazing unit. The study did however conclude that infrared absorbing gasses would be beneficial in horizontal glazing units where convection does not play a significant role [Reilly et al. 1990]. A model using convection in the fill gas to determine an optimal gap thickness between panes in a double glazed window for four different cities in Turkey found an optimal thickness between 12mm – 21mm. It should be noted, however, that these thicknesses were determined based on assuming a constant outdoor and indoor glass temperature [Aydin 2006]. Wright (Wright 1996, Hollands et al. 2001) shows that the optimum pane spacing corresponds to Ra = 8104. A detailed review of the flow inside

the glazing cavity can be found in the literature [Wright & Sullivan 1989, Wright et al. 2006].

In summary, it should be seen that the bottom portion of the glass will be the coldest section because of the effects of fill gas motion and conduction via the edge seal. This is important because it is more likely this area of the glass will be below the conditioned spaces dew-point temperature and hence will be where condensation forms. It should also be apparent that by increasing the thermal resistance of a glazing unit the resistance to condensation is improved by increasing the temperature of the indoor facing pane of glass.

1.2.5 Computer Simulation

Two main computer models were developed to determine heat transfer through glazing units. VISION developed by Wright [UW 1995] and WINDOW developed by the Lawrence Berkeley National Laboratory [LBL 1993]. These programs, alone, model only the center-glass region and are 1-D [Wright 1995]. VISION used correlations developed by ElSherbiney et al. (1982) while WINDOW used correlations developed by Rubin (1982). Wright later developed more accurate models for energy transfer through the center glass region [Wright 1998a]. As the programs developed they each picked up a "partner" program to model the 2-D edge glass and frame areas. VISION4, the most recent version, can be coupled with FRAME 4.0 [EEL 1995], where WINDOW 5 can be coupled with THERM5 [Mitchell et al. 2003].

1.3 Current Rating Systems

There are three main governing bodies that deal with condensation resistance in the fenestration industry in North America; National Fenestration Rating Council Incorporated (NFRC), Canadian Standards Association (CSA), and American Architectural Manufacturers Association (AAMA). All three have their own standards and rating systems. For the sake of simplicity it is useful for all three to agree to the same standard. Two rating parameters that are energy related, widely used, and well established are the Solar Heat Gain Coefficient (SHGC) and the U-Factor. Both are discussed by all three governing bodies. SHGC is a dimensionless constant that shows how much radiant energy is transferred from the sun to the conditioned space through the fenestration. The U-factor is a value that measures a fenestration ability to resist heat transfer.

Condensation resistance is a fairly new topic of interest in the fenestration industry. Currently all three North American groups have their own rating systems. NFRC developed standard NFRC 500, CSA amended standard A440.2, and AAMA developed standard AAMA 1503.

The AAMA 1503 rating uses a condensation resistance factor (CRF) that ranges from 0-100. Typically a CRF of 10 is associated with a glazing of poor performance and a CRF of 60 is a well performing glazing. AAMA 1503 started in 1972 as AMMA 1502.3; a voluntary standard to rate the thermal performance of fenestration. It developed to include condensation resistance in 1988 and took on the title AAMA 1503.1. The CRF

value is determined experimentally and the same test procedure can be used to determine the U-factor of the window. The CRF is the lower of either the weighted frame temperature (FT) or the average glazing temperature (GT), equations shown below. The procedure calls for the use of a guarded hot box test procedure [ASTM C1363-71] and 20 thermocouple readings on the indoor surface. The thermocouple locations vary depending on the type of fenestration. The formula use a weighting factor (W) shown below which is a function of the average of 14 predetermined thermocouple temperatures (FT_p) and the average of the coldest sash or frame temperature obtained from four of ten roving cold point seeking thermocouples (FT_r). Cold point seeking locations are said to be chosen based on the operator's experience. The CRF is a whole number and will be rounded up or down accordingly.

$$W = \frac{FT_p - FT_r}{FT_p - (T_{II} + 10)} \times 0.40 \tag{1.6}$$

$$FT = FT_p(1 - W) + W \times FT_r \tag{1.7}$$

Where:

T_{II} = cold side air temperature

The CRF values for the glass (CRF_G) and frame (CRF_F) are then calculated using Equations 1.8 and 1.9, the lower being the final CRF value as mentioned above.

$$CRF_G = \frac{GT - T_{II}}{T_I - T_{II}} \tag{1.8}$$

$$CRF_F = \frac{FT - T_{II}}{T_I - T_{II}} \tag{1.9}$$

Where:

GT = average of 6 pre-determined thermocouple glazing temperatures
T_I = warm side air temperature

It should be noted that the CRF value is optional [AAMA, 2004].

The CSA 440.2 standard uses a temperature index (*I*) factor that ranges between 0 and 100. The first completed publication of CSA 440.2 came in 1991 with subsequent revisions in 1993 and 1998. The standard also covers simulation and test procedures for the U-value, solar heat gain coefficient (SHGC) and various other properties related to fenestration. The test procedures are described in the standard along with calculations for *I*. The test procedure does not state the use of a guarded hot box; instead it lists the minimum requirements of whatever apparatus is chosen. Similar to AAMA 1503, thermocouples are placed in pre-determined locations (positions vary depending on the fenestration being evaluated). In total, 16 thermocouples are placed on the test unit; three are to be placed at the bottom of each glazing unit 50mm from the frame, three are the placed at the bottom edge of the glazing unit 12.5mm from the frame and four roving thermocouples are to be placed on the frame at the four coldest point locations (as with AAMA 1503). Data from the four roving thermocouples are not used in the standard and are just extra points of interest as stated by the CSA. The remaining thermocouple locations vary with fenestration type. The procedure states a steady state must be achieved for 5 hours and all data must be averaged into 10 minute blocks. Data used for the *I* rating must be averaged from five consecutive 10 minute blocks. The calculations

specifically require the use of the coldest frame temperature (T_f) and coldest glazing temperature (T_g). The temperature index is calculated as shown in Eq. 1.10 [CSA 2004].

$$I = \left(\frac{T - T_c}{T_h - T_c} \right) \times 100 \tag{1.10}$$

Where:

T = the lower of T_f and T_g
T_c = the cold air chamber temperature
T_h = the warm air chamber temperature

The CSA standard is considered a stricter test of a fenestrations ability to resist condensation because it only uses the coldest temperature where in the AAMA standard a spatially averaged cold-side temperature is used. As with CRF, evaluation of *I* is not a building code requirement.

The NFRC condensation resistance rating is perhaps the least used in North America. AAMA 1503 dominates in the United States and CSA in Canada [Baker 2006]. NFRC 500 uses a condensation resistance (CR) factor that ranges from 1 to 100 and was first released in 2001. This standard is the only one of the three systems to discuss the use of computer simulation as well as test procedures. The standard specifies the 2-D software used must be an NFRC approved tool and must include a detailed grey-body diffuse radiation model and detailed convection modelling inside the glazing cavity. The standard uses two different procedures to calculate the CR depending on whether data were obtained from simulation or experimentation. Both computer simulation and experimentation calculations require three different relative humidity levels; 30%, 50%,

and 70%. The final CR value will be the lowest of three CR values; frame (CR_f), edge-of-glazing (CR_e), and center-of-glazing (CR_c). The calculations for simulation results use an average over a segment of cells (subdivided element) in the simulation at pre-determined locations for each data point. Each segment is averaged by dividing by the length of the segment in terms of cells; calculations shown below.

$$CR_f = \left[1 - \left(\frac{\sum_k \left(SS_{f_k} A_{f_k}\right)}{A_f}\right)^{\frac{1}{3}}\right] \times 100 \tag{1.11}$$

$$SS_{fk} = \frac{\sum_j \left(S_f\right)_{j=RH@30\%,50\%,70\%}}{3} \tag{1.12}$$

$$S_f = \frac{\sum_i \left(T_{dp} - T_{f_i}\right)^+ \cdot \Delta L_{f_i}}{\left(T_{dp} - T_o\right) L_f} \tag{1.13}$$

Where:

$$CR_c = \left[1 - \left(\frac{\sum_k SS_{d_k} A_{d_k} + \sum_k SS_{deog_k} A_{deog_k} + \sum_k SS_{cog_k} A_{cog_k}}{\sum_k A_{d_k} + \sum_k A_{deog_k} + \sum_k A_{cog_k}}\right)^{\frac{1}{3}}\right] \times 100 \tag{1.14}$$

$$SS_{x_k} = \frac{\sum_j \left(S_x\right)_{j=RH@30\%,50\%,70\%}}{3};\ for, x = d, deog, cog \tag{1.15}$$

$$S_x = \frac{\sum_i \left(T_{dp} - T_{x_i}\right)^+ \cdot \Delta L_{x_i}}{\left(T_{dp} - T_o\right)};\ for, x = d, deog, cog \tag{1.16}$$

Where:

T_{dp} = condensation reference point temperature (dew point temperature + 0.3°C)
T_o = outside temperature
k = frame section
i = subdivided element

ΔL = length of segment
$^{+}$ = positive values only
d = divider
deog = edge-of-divider
cog = center-of-glazing

Special amendments must be made to deog and d formulae if the glazing unit is not composed of true divided lites.

$$CR_e = \left[1 - \left(\frac{\sum_k SS_{eog_k} A_{eog_k}}{\sum_k A_{eog_k}} \right)^{\frac{1}{3}} \right] \times 100 \tag{1.17}$$

$$SS_{eog_k} = \frac{\sum_j \left(S_{eog} \right)_{j=RH@30\%,50\%,70\%}}{3} \tag{1.18}$$

$$S_{eog} = \frac{\sum_i \left(T_{dp} - T_{eog_i} \right)^{+} \cdot \Delta L_{eog_i}}{\left(T_{dp} - T_o \right) L_{eog}} \tag{1.19}$$

Where:

k = edge-of-glazing sections
eog = edge-of-glazing

The calculations for experimental CR values use thermocouples to obtain temperatures. The locations are pre-determined and are defined in NFRC standard 102; measuring the steady state thermal transmittance of fenestrations [NFRCa 2004]. Once data is obtained the following Equations are to be used to determine CR [NFRCb 2004];

$$CR_f = \left[1 - \frac{1}{3} \left(\sum_{j=1}^{3} \left(\frac{\sum_i \left(T_{dp_j} - T_{f_i} \right)^+ \cdot A_{f_i}}{\left(T_{dp_j} - T_o \right) A_f} \right)_{j=RH\,@\,30\%,50\%,70\%} \right)^{\frac{1}{3}} \right] \times 100 \qquad (1.20)$$

$$CR_c = \left[1 - \frac{1}{3} \left(\sum_{j=1}^{3} \left(\frac{\sum_i \left(T_{dp_j} - T_{x_i} \right)^+ \cdot A_{x_i}}{\left(T_{dp_j} - T_o \right) A_x} \right)_{j=RH\,@\,30\%,50\%,70\%} \right)^{\frac{1}{3}} \right] \times 100;\ for, x = d, deog, cog \qquad (1.21)$$

$$CR_e = \left[1 - \frac{1}{3} \left(\sum_{j=1}^{3} \left(\frac{\sum_i \left(T_{dp_j} - T_{eog_i} \right)^+ \cdot A_{eog_i}}{\left(T_{dp_j} - T_o \right) A_{eog}} \right)_{j=RH\,@\,30\%,50\%,70\%} \right)^{\frac{1}{3}} \right] \times 100 \qquad (1.22)$$

The NFRC rating is differs from AAMA and CSA because it factors in area, where the others found the coldest point(s). Hence, NFRC 500 looks more at the severity of condensation by factoring in how much of the glazing area is below the dew-point temperature.

1.4 Motivation and Methodology

While current rating systems for windows do aid the consumer in making an educated purchase, there is still room for improvement. A global condensation resistance rating system must be implemented to prevent confusion. Even more importantly, perhaps even as a replacement for the condensation resistance rating, is the need for a condensation run-off resistance rating. As mentioned above it is of more value to the consumer to know if water will run-off and pool or simply form and remain on the glass.

Condensation that forms on glass during the night at colder temperatures and then re-evaporates into the air once the sun rises is irrelevant to the consumer. The research described here is an initial attempt to examine the conditions under which window condensate will run and pool.

This was done by observation of condensate on a vertical sheet of glass. An experimental apparatus was built for this purpose. A sheet of glass on one wall of an enclosure was cooled and exposed to air at controlled levels of RH. Observations were made to determine if condensate that forms on the glass runs off and if so how long after start-up. Multiple experiments were conducted each at a T_{db} of approximately 22.6 and at different RH values (30%, 35%, 40%, 45%, and 50%). Tests spanned 950 minutes, a typical length for the longest night in a southern Canadian winter. The longest night in Waterloo, Ontario (43.30N x 80.32W) occurs on December 21 and spans 915 minutes [Duffie & Beckman 2001].

Chapter 2

2 Literature Review

2.1 Condensation on Windows

Much of the literature related to condensation on glazing units is in reference to determining the indoor glass temperature profile and the indoor heat transfer coefficient profile, thereby determining where on the glass condensation will form.

A major collaborative research project conducted by four different laboratories across North America looked at determining the indoor temperature profile of seven different flush mounted IGUs. Flush mounting meaning the glazing unit was installed, without a frame, flush with the wall in which it was mounted. Different computer simulation and experimental studies, each blind to the others, were undertaken with a net research objective of determining the answer the three questions:

- *"Knowing that different laboratories were given almost identical units, how well do different laboratories compare in terms of measured absolute temperature profiles?*
- *Similarly, how well do different simulation programs compare in terms of predicted temperature profiles?*

- *Do simulations agree well with experimental measurements?"* [Sullivan et al. 1996]

All experiments were conducted using ASHRAE winter design conditions; indoor room temperature of 21.1°C±0.1, indoor heat transfer coefficient of 8.0±0.4 W/m^2K, outdoor air temperature of -17.78°C±0.05, and an outdoor heat transfer coefficient of 30±2 W/m^2K. Computer simulations were also run using winter design conditions and a constant indoor heat transfer coefficient of 8.3 W/m^2K [Sullivan et al. 1996].

The first laboratory used infrared thermography [Arasteh et al. 1992] on the glazing units surrounded by two climate chambers. This lab found IGU # 6 to have the highest average indoor temperature while IGU # 3 had the lowest. The study concluded thermography to be effective although requiring a great deal of data post processing [Griffith et al. 1996].

The second laboratory used a guarded hot box [Elmahdy 1992] to maintain the required environmental conditions. Results showed for the most part the edge-glass region was warmer at the top in comparison to the bottom, as expected, due largely to edge-seal conduction and fill gas motion. Elmahdy's results showed that varying spacer material to be the only factor that caused a variance in temperature differential between the edge-glass and center-glass regions. Results also showed that as pane spacing increased the minimum temperature at the bottom of the glass increased and the temperature differential between the top and of the glass and the bottom of the glass increased. A

low-emissivity coating also acted to increase the temperature of the indoor glass surface. The final observation was that a triple glazed unit resulted in higher temperatures on the glass in comparison to a double glazed unit.

The third and fourth laboratories conducted computer simulations on the glazing units. The first of these labs performed two different simulations of the units using software called BRAVO (developed for 2-D analysis of windows) [De Abreu 1997] and a more simplified code; a combination of VISION4/FRAME 4.0 [EEL 1995]. VISION4 and FRAME 4.0 were used in conjunction as VISION4 accounted for the center-glass region and FRAME 4.0 the edge-glass region. Three models were run with the VISION4/FRAME 4.0 combination; in all three VISION4 used a correlation for the convective heat transfer coefficient and a 1-D analysis to model the heat transfer in the center-glass region. FRAME 4.0 was varied for the models. The first model treated the space between panes in the edge-glass region as a solid and used an effective conductivity with data taken from VISION4 to model the heat transfer [Wright 1998a]. The second took velocity data from VISION4 and performed CFD calculations to model the heat transfer between panes in the edge-glass region. The third used the CFD calculations and imposed a convective heat transfer coefficient on the indoor side of the window. It was found that the third model was closest to data obtained through thermography.

The center glass was modelled as a solid with an effective conductivity equivalent to the convective heat transfer associated with the fill-gas motion [Wright 1998a]. Results from

the two models were very similar and the researchers concluded VISION4/FRAME 4.0 to be an effective simple method for conducting heat transfer analysis through glazing units

The final laboratory conducted computer simulations using three different simulation models. The first simulation was conducted in CFD software known as FIDAP using convection, radiation, and conduction while the second program was a combination of THERM and WINDOW 4.1 and used only conduction. The third program used a "variable-h" condensation model to account for fill-gas. It was concluded that the THERM/WINDOW combination was a good simulation for over all U-Factor in a fenestration but was inaccurate at the edge seals where it was unable to account for the fill gas convection. The variable-h model, however, proved to be an accurate model for the temperature profile at the edge-glass region and hence a good simulation for condensation potential [Zhao et al. 1996]. The results from all four laboratories were summarized and found to be within good agreement [Sullivan et al. 1996].

Further tests used a more detailed analysis of the guarded hot box method in conjunction with thermography for determining a temperature profile on glass in a glazing unit. Two window units and a calibrated standard unit were tested and simulated. Thermography was also tested against thermocouples taped to the glass surface. Results were similar showing discrepancies of less than 0.5 °C for the most part (between thermocouples and thermography). The study concluded thermography to be an effective tool in determining temperature profiles of glass [Elmahdy & Devine 2005].

A further study took thermography data from IGU#1 and IGU#2 and in conjunction with a 2-D computer simulation attempted to determine local heat transfer coefficients along the surface of the glass. Currently computer simulations assume a constant heat transfer coefficient, a method considered acceptable as most of the heat transfer in a glazing unit occurs through the center-glass portion where the heat transfer coefficient is essentially constant. The simulations used two different methods of calculations; T-proportional to h method and a downhill simplex method. Both methods use temperatures from measurements and temperatures from simulation. The results for heat transfer profiles for one of the units varied between the data from each of the laboratories. The authors concluded the T-proportional-to-h method to be a fast, rough estimate of local heat transfer coefficients [Schrey et al. 1998].

Griffith et al. (2002) repeated thermography experiments with windows recessed in frames, something more common for residential applications. The windows were scanned in four separate sections; sill region, bottom half, top half, and header region. A point infrared thermometer with a transversing system was also tested. Values were compared to direct contact thermocouples. Test results showed good agreement in general trend of the temperature profile, but were in poor agreement for exact values. Experimental error, poor calibration, and deficiencies with the data acquisition system were cited as possible reasons. It was concluded that the procedure and equipment used by the lab were not an effective method for consistent measurement [Griffith et al. 2002].

The experiments conducted by Griffith et al. (2002), were then simulated using VISION4 and FRAME 4.0, as with the original 1996 study, by Wright & McGowan (2003). Three different computer simulations were conducted, all using the VISION/FRAME software package and the same software changes as Wright & McGowan (2003). It was found that all simulations took the same general temperature profile shape, and that both fill-gas models were within the error band of the thermography data. It was also observed that the frame temperatures were noticeably higher in simulations compared to thermography data. The authors concluded computer simulation to be favourable over thermography in determining edge-glass temperature profiles, mainly due to ease and simplicity [Wright & McGowan 2003].

The simplified CFD model mentioned above was derived and presented by Wright (1998b) in conjunction with VISION/FRAME. Simulations were compared to those produced by De Abreu et al. (1996), thermocouple measurements [McGowan 1995], and thermography [Griffith et al. 1996, Elmahdy 1996]. Results were in good agreement and were calculations were simple enough to limit computational requirements [Wright 1998b].

A study using thermocouple measurement and a guarded hot-box was conducted and compared to a finite element analysis (FEA) and FRAME results. Results showed an agreement of within 2°C for IGUs with non-metal frames and within 5°C for units with metal frames. It was also shown that tape material for mounting thermocouples to the glass surface could be attributed to about a 1°C difference [McGowan 1995].

A study by Carpenter & Hanam (2001) looked at the effects of air leakage on the indoor temperature profile (more specifically TI) and the effect of varying the outdoor environment temperature from the ASHRAE winter design standard. This was done through experimentation and computer simulation. Experimentation was conducted in a climate chamber with thermocouples taped to the glass and frame surface. Simulations were run under different seal conditions to model air infiltration. Changing the outdoor temperature showed no significant affect on the TI for the glazings. It was seen that temperatures changed by a small amount as air leakage rate increased, so long as the air infiltration rate met CSA standards. [Carpenter & Hanam 2001].

A further study determining the effects of air leakage on Temperature Index, *I*, was conducted by Elmahdy (2003). Experiments were conducted on three different glazing units each at five different air leakage rates. Thermocouples were used to determine the indoor side temperatures. Results were similar to the Carpenter & Hanam (2001) study where *I* increased (for some of the windows) with air leakage rate, again showing air was moving from the warm side to the cold side. The author concluded experimentation would have to be modified to cause the air flow in the other direction something more common in an actual glazing unit [Elmahdy 2003].

Muneer & Abodahab (1998) developed a model to estimate the number of occurrences of condensation formation on glazing units in dwellings over a span of 10 years. Using meteorological data from Edinburgh, Manchester, and London they predicted the frequency of condensation formation for six given glazing units. The study then looked

at the effect of placing a fence in the fill-gas cavity of a seventh unit using the same data and simulations. The purpose of the fence was to disrupt the flow of fill gas to the bottom edge of the window thereby increasing the temperature. It was found that the frequency of condensation formation on the seventh unit was significantly lower than the other six units.

Bong et. al., (1998) used a 3-D CFD model to predict condensation on a window in a large viewing gallery. Different simulations used varying supply air temperatures and ambient temperatures. It was found that condensation would occur at the top portion of the glass rather than at the bottom. This was the case because the cold air supply was cooling the top portion of the glass causing it to drop below the dew point temperature of the indoor air. The study concluded that by increasing the supply air from 17°C to 18°C the number of hours during which condensation could occur (between 10am – 10pm) reduced from 52 to 10 over one year.

Chapter 3

3 Motivation and Objectives for this Research

3.1 Introduction

The objective of this study is to determine how condensate will form and if condensate will run-off a cooled vertical sheet of glass exposed to air at controlled properties (T_{db}, RH).

Figure 3.1 is an image of condensation on a glazing unit. From the image it can be seen that condensation on the glazing unit can be separated into two bands; one where condensation runs (band 1) and one where it does not (band 2).

Unfortunately, it is impossible to tell from the image if the condensation in the second band is at a steady state or if over a longer period of time will run as in the first band. A development of water droplets can be seen in the second band where at the bottom, closest to the first band, the droplets are largest. Progressing up the band the droplets decrease in size and eventually become small enough to appear as a uniform, thin, layer at the top of the band. To fully understand this idea it is best to briefly review the principles of heat and mass transfer.

Figure 3.1: Multiple bands of condensation with run-off

When looking at condensation on a window surface one must also look at mass transfer as well as heat transfer. Fortunately, the two are very similar, in fact, analogous. Equations 3.1, 3.2, 3.3 are x-momentum, energy, and water vapour diffusion balances for flow over a horizontal, flat, isothermal, plate [Duffie & Beckman 1991].

$$u\frac{\partial u}{\partial x}+v\frac{\partial u}{\partial y}=\nu\frac{\partial^2 u}{\partial y^2} \tag{3.1}$$

$$u\frac{\partial T}{\partial x}+v\frac{\partial T}{\partial y}=\alpha\frac{\partial^2 T}{\partial y^2} \tag{3.2}$$

$$u\frac{\partial C}{\partial x}+v\frac{\partial C}{\partial y}=D\frac{\partial^2 C}{\partial y^2} \tag{3.3}$$

It can be seen that the equations are similar differing only at the coefficient associated with the diffusion term (right hand side). Non-dimensionalizing the equations yield;

$$u'\frac{\partial u'}{\partial x'}+v'\frac{\partial u'}{\partial y'}=\frac{1}{\mathrm{Re}}\frac{\partial^2 u'}{\partial y'^2} \tag{3.4}$$

$$u'\frac{\partial T'}{\partial x'}+v'\frac{\partial T'}{\partial y'}=\frac{1}{\mathrm{Re}\cdot\mathrm{Pr}}\frac{\partial^2 T'}{\partial y'^2} \tag{3.5}$$

$$u'\frac{\partial C'}{\partial x'}+v'\frac{\partial C'}{\partial y'}=\frac{1}{\mathrm{Re}\cdot Sc}\frac{\partial^2 C'}{\partial y'^2} \tag{3.6}$$

For water vapour in air the equations can be further simplifying assuming Pr = Sc; a reasonable approximation given Pr ≈ 0.71 and Sc ≈ 0.61 for air at T = 300K.

As well, there are similarities in the heat transfer coefficient and mass transfer coefficient. Knowing Nu = G (Re, Pr, L/D), one can calculate the Sherwood number (Sh), assuming, Sh = G (Re, Sc, L/D), shown in Equation 3.7, where G represents the same function.

$$Sh=\frac{K_c L}{D_{AB}} \tag{3.7}$$

K_c and D_{AB} are defined as the overall mass transfer coefficient and the component diffusion coefficient respectively. The point of importance here is that the local mass

transfer coefficient will change with respect to location similarly to how the local heat transfer coefficient changes with location.

3.2 Condensation at Steady State without run-off

As mentioned above, at any given time, it is unknown if the condensation on the window is at a steady state or in an intermediate step en route to a steady state, or if it will ever reach a steady state. It is unknown if a window will progress to steady state with run-off or if a fine layer will form and create enough of a thermal resistance to stop mass transfer and hence remain in a steady state.

A fictitious scenario is discussed to better illustrate the idea of a layer with no mass transfer. If it is assumed that the small droplets of condensation that form on the glass can be treated as a thin liquid layer then two phenomena must occur for a steady state without run-off to be reached. Condensate on the glass surface acts as a thermal resistance resulting in a temperature increase across the condensate layer (t_{cst}) and a higher temperature at the exposed surface in the conditioned space as shown in Figure 3.2. For a steady state to be achieved the temperature at the exposed surface (T_2) must be at the dew point temperature (T_{dp}) of the conditioned space. The condensate layer thickness cannot, however, be too large as, eventually, the more mass accumulated on the glass surface the more likely run-off will occur. Hence, a sufficiently large t_{cst} is required to allow for the exposed surface to reach T_{dp}, yet t_{cst} cannot be large enough to cause run-off. Once this steady state is achieved mass transfer will cease even though heat transfer still occurs.

If droplet formation progresses water on the glass surface will coalesce. These droplets result in different water thickness resistance layers on the glass surface, as shown in Figure 3.3. It is clearly shown that T_3 will be greater than T_4 due to the difference in t_{drop} and $t_{between}$. These sections between will condense more moisture and cause adjacent droplets to further coalesce thereby creating larger droplets.

In summary, the following questions are to be discussed with this research;

1. Can a water layer exist indefinitely on a glass surface without running (i.e., at steady state with no further condensation)?
2. If so, under what conditions does this occur?
3. If not, how long does it take before run-off occurs and how does the condensate progress with respect to time?

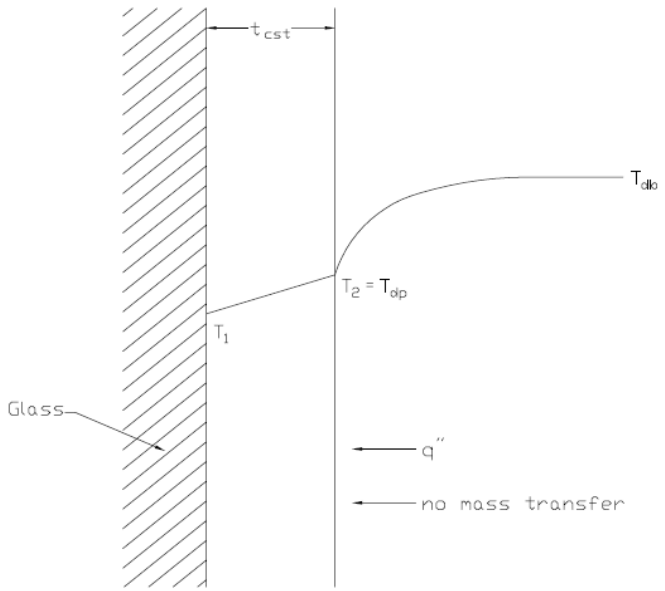

Figure 3.2: Temperature profile through condensate at steady state with no additional condensation

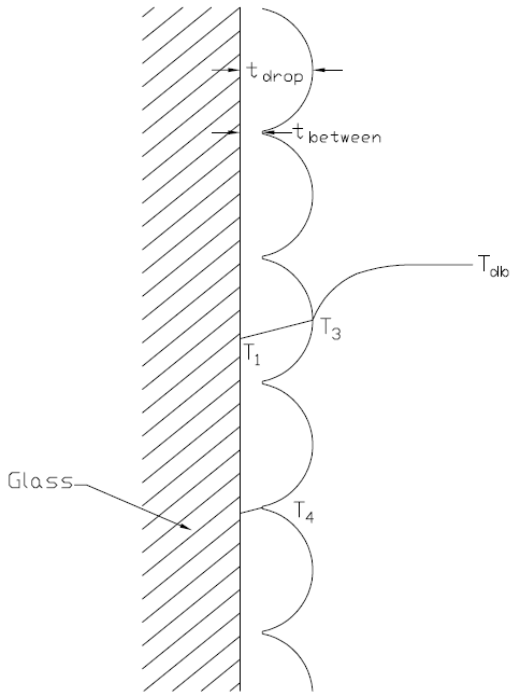

Figure 3.3: Temperature profile through droplet condensate

Chapter 4

4 Test Apparatus

4.1 Introduction

The experimental apparatus will be discussed in detail in this chapter. First an overview will be given of its functions and construction. This will be followed by the design process for major components.

The enclosure is required to create an environment consisting of a vertical cooled sheet of glass exposed to air that is held at a controlled RH and T_{db}. Ideally, the convective heat transfer coefficient along the glass surface would be constant. This would simplify heat transfer calculations and will be discussed later in this chapter. At the very minimum a constant heat transfer coefficient should be present over the portion of the glass to be observed. The temperature profile of the glass surface can vary, similar to that of a glazing unit.

The magnitude of the local heat transfer coefficient would, ideally, be similar to what would occur at a window in a typical household. The ASHRAE winter design condition includes an indoor heat transfer coefficient of 8.3 W/m^2K [ASHRAE 2005]. Knowing that glass has an emissivity of 0.84 [ASHRAE 2005], the radiation portion of the total

heat transfer coefficient is approximately 5 W/m^2K. Thus, the convective portion is approximately 3 W/m^2K. Hence, the convective heat transfer coefficient for the experiment at the glass surface should be close to 3 W/m^2K which corresponds to natural convection.

The enclosure consists of cooled vertical sheet of glass exposed to a conditioned space. The conditioned space is held at a constant relative humidity and dry bulb temperature. Copper fins and a constant temperature bath were used to control the dry bulb temperature while a pipette and heating element were used to add water and control the relative humidity.

Figures 4.1, 4.2, and 4.3 are detailed assembly drawings of the apparatus. The conditioned space assembly (item 1) and the vertical glass assembly (item 2) from Figure 4.1 are shown in more detail in Figures 4.2 and 4.3. The conditioned space assembly forms most of the enclosure for the space. Copper fins (item 10) are used to heat the air in the conditioned space. The fins consist of ¼" outer diameter (OD) copper tubing soldered to a flat copper sheet. The copper fins are discussed in more detail in the following sections. The tubes protrude through the back plate (item 3) of the enclosure. The tubes are held in place with rubber grommets (item 11) in the back plate. The rubber grommets provide an air tight seal between the controlled space and the environment. The tubes were soldered to copper manifolds (item 12). The top manifold acted as the supply line of a water/glycol mixture from a HAAKE A81 water bath while the bottom was a return line. The manifolds were pipes with a 1½" OD and a ¾" inner diameter

(ID). A thick wall was required to allow for sufficient material contact between manifold and fin tubes for a strong solder joint. One end of each manifold was plugged with a copper disk (item 13). The other end was tapped for a ½" NPT fitting. In the back plate, not shown in the Figures, is a 2" diameter hole covered by a 5mm thick sheet of glass. This was used to observe the condensate formation on the cooled sheet of glass.

The back plate and fin arrangement was attached to a stainless steel sleeve (item 5). This sleeve completed the conditioned space. The sleeve was attached to the back plate with 48 M4 x 10 screws, washers, and nuts. Neoprene gaskets (item 4) were used to create an air tight seal. On top of the sleeve are three holes (items 6, 7, and 8). They secure the humidity sensor, pipette, and pressure hose respectively. All three are sealed for air tightness with rubber grommets. The humidity sensor, discussed in more detail later in this chapter, uses a probe to detect RH. The pipette controlled water input to the conditioned space, and a hose was connected from the enclosure to the water feed system to ensure the feed system was at the same pressure as the conditioned space. Any change in pressure could alter the flow rate.

The vertical glass assembly was used for cooling the sheet of glass and completing the enclosure. The sheet of glass (item 26) was bounded to an aluminum plate (item 17). This was achieved with a Loctite two-part adhesive (speedbonder and activator) and a low pressure roller. The speedbonder (Loctite 324) was applied to the glass surface and spread evenly with minimal thickness using a hand roller while the activator (Loctite

7075) was sprayed on the aluminum sheet. The glass was then placed on the aluminum and compressed with a printing press roller.

Nine type-T thermocouples were installed in the aluminum plate. Thermocouple junctions were all located on the vertical centre-line of the plate and the leads run 150mm along horizontal channels machined into the plate in order to reduce lead losses. The channels are 0.5mm deep and the thermocouple beads are 0.5mm in diameter thus ensuring the beads are in close contact with the glass surface. The wires exit through holes drilled through the plate. An OMEGA HH501T hand held thermocouple reader was used.

An aluminum manifold (item 25) was attached to the plate. The manifold contains four parallel channels that run along its length. Each end is tapped to a 1/8" NPT. Chilled water/glycol from a HAAKE DC10 water bath was run through the manifold. The first and third paths through the manifold were connected via fittings and tubes as were the second and fourth (the first path is closest to the aluminum plate). The chilled water was run through the manifold passages in alternating directions to minimize temperature change along the length of the manifold. On the front side of the aluminum plate (in the conditioned space) is a condensate collection system. An acrylic collector (item 24) is clamped to the aluminum plate with an aluminum bar (item 22). A neoprene gasket (item 23) was placed between the two acting as an extra layer of thermal resistance. The clamp, acrylic, and aluminum plate were all drilled, and threaded fasteners held them in place against the tapped manifold. The acrylic collector is comprised of 11 collection

zones which drain condensate into a channel running the length of the collector. This system ensures the condensate does not pool along the floor of the enclosure thus minimizing the possibility of condensate re-evaporating.

The cooling system and glass was attached to the enclosed space section via a stainless steel collar (item 19). Between the collar and the aluminum plate, also between the collar and the rest of the enclosure, are 9mm thick pieces of foam weather stripping (item 18). The weather stripping creates an air-tight seal. The collar was clamped in place with butterfly clips. The rubber foam was soft enough to create an effective seal between all parts under this clamping pressure. This method of clamping was chosen because of it allowed for easy access to the chamber.

The collar was used instead of attaching the sleeve directly to the plate because it provides the option for interferometry at a later date. The stainless steel collar can be easily replaced with a glass collar allowing for the laser transmission required for interferometry to measure the convective heat transfer coefficient.

In the stainless steel collar is a 1" diameter hole sealed by 1½" x 1½" piece of acrylic (item 20). This was used to illuminate the glass surface for viewing.

The following sections describe the design process involved in sizing the condensate surface, sizing the enclosure, reading the relative humidity and dry bulb temperature, and maintaining the desired levels of relative humidity and dry bulb temperature.

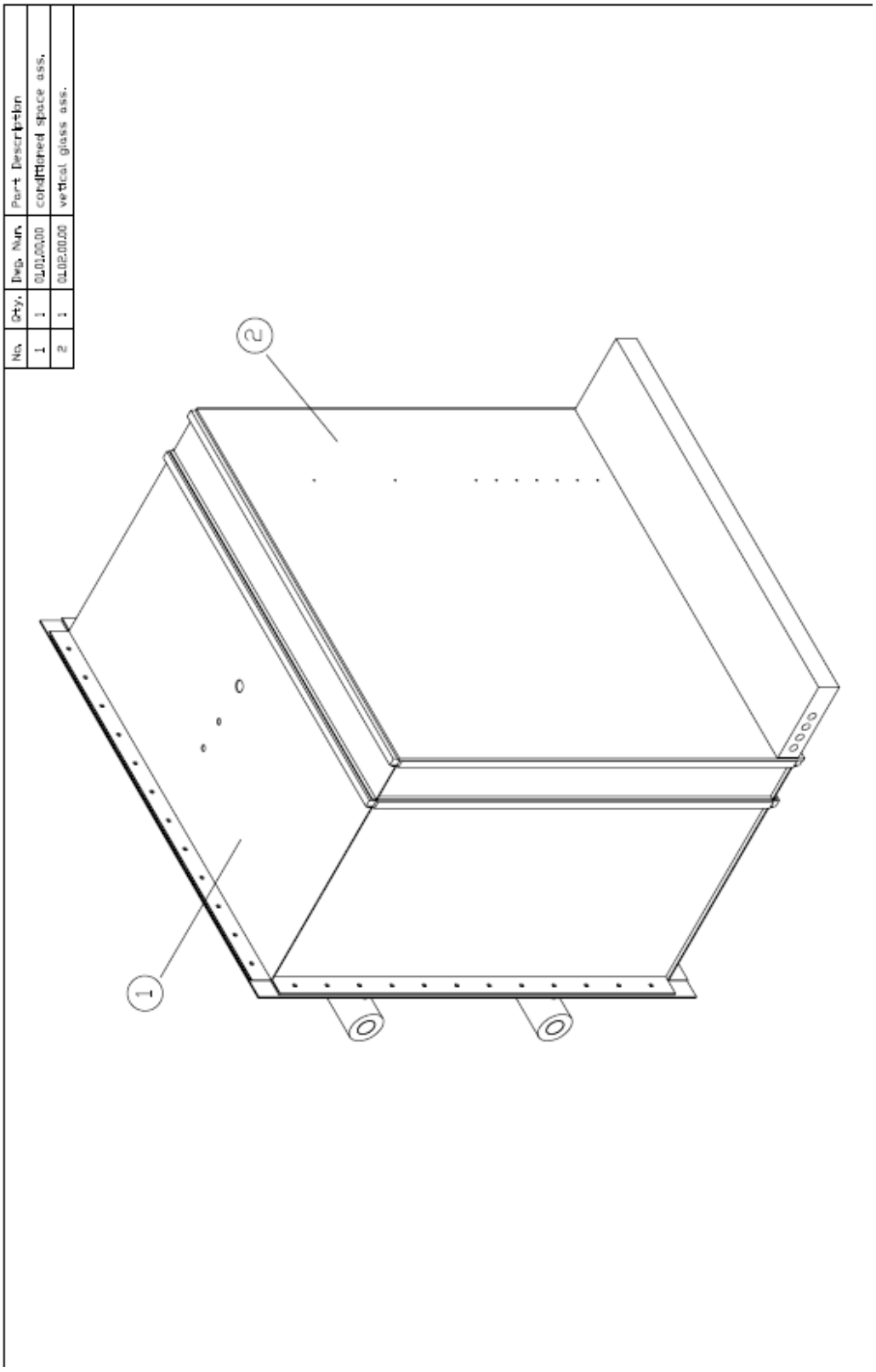

Figure 4.1: Apparatus assembly drawing

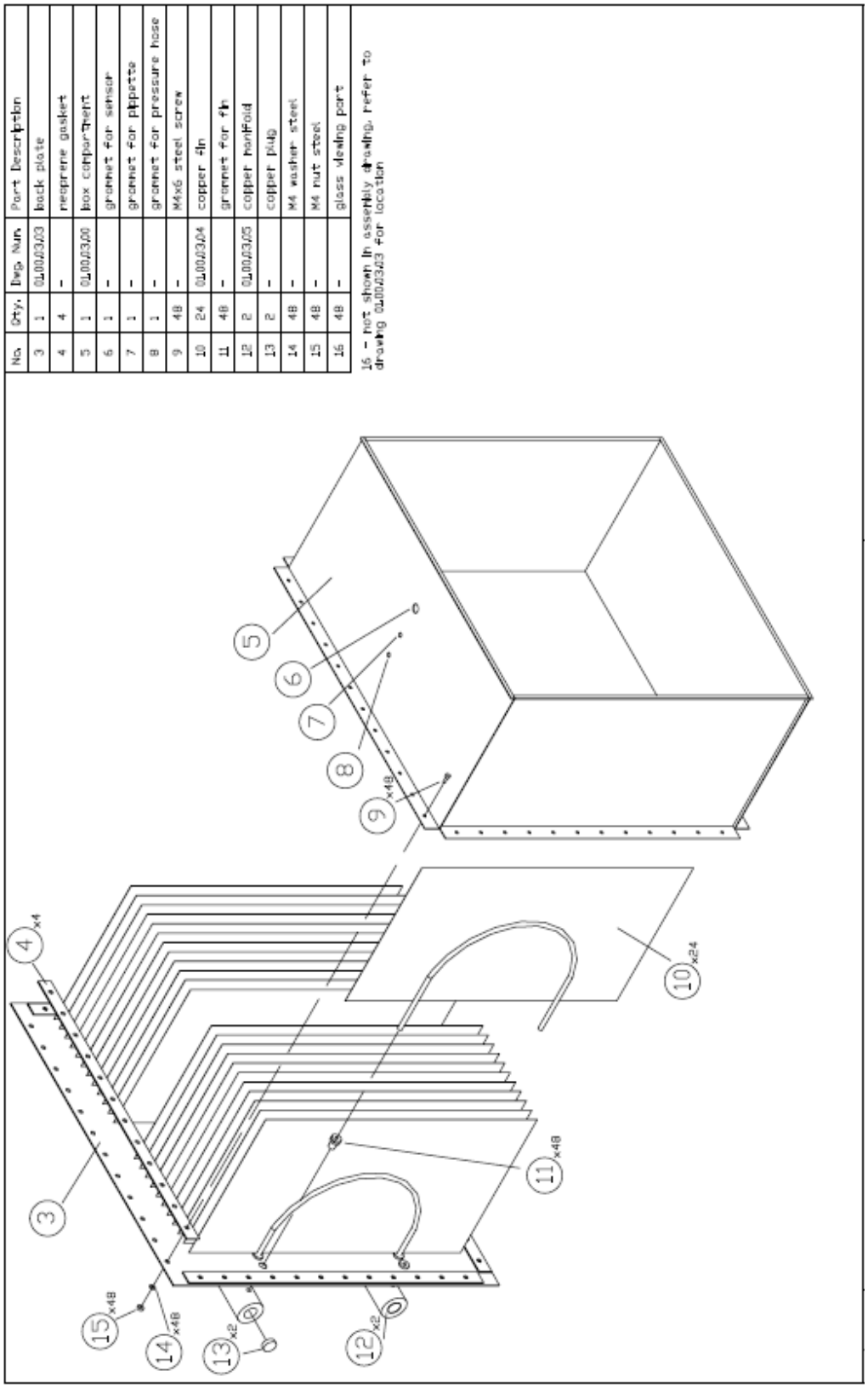

Figure 4.2: Conditioned space assembly drawing

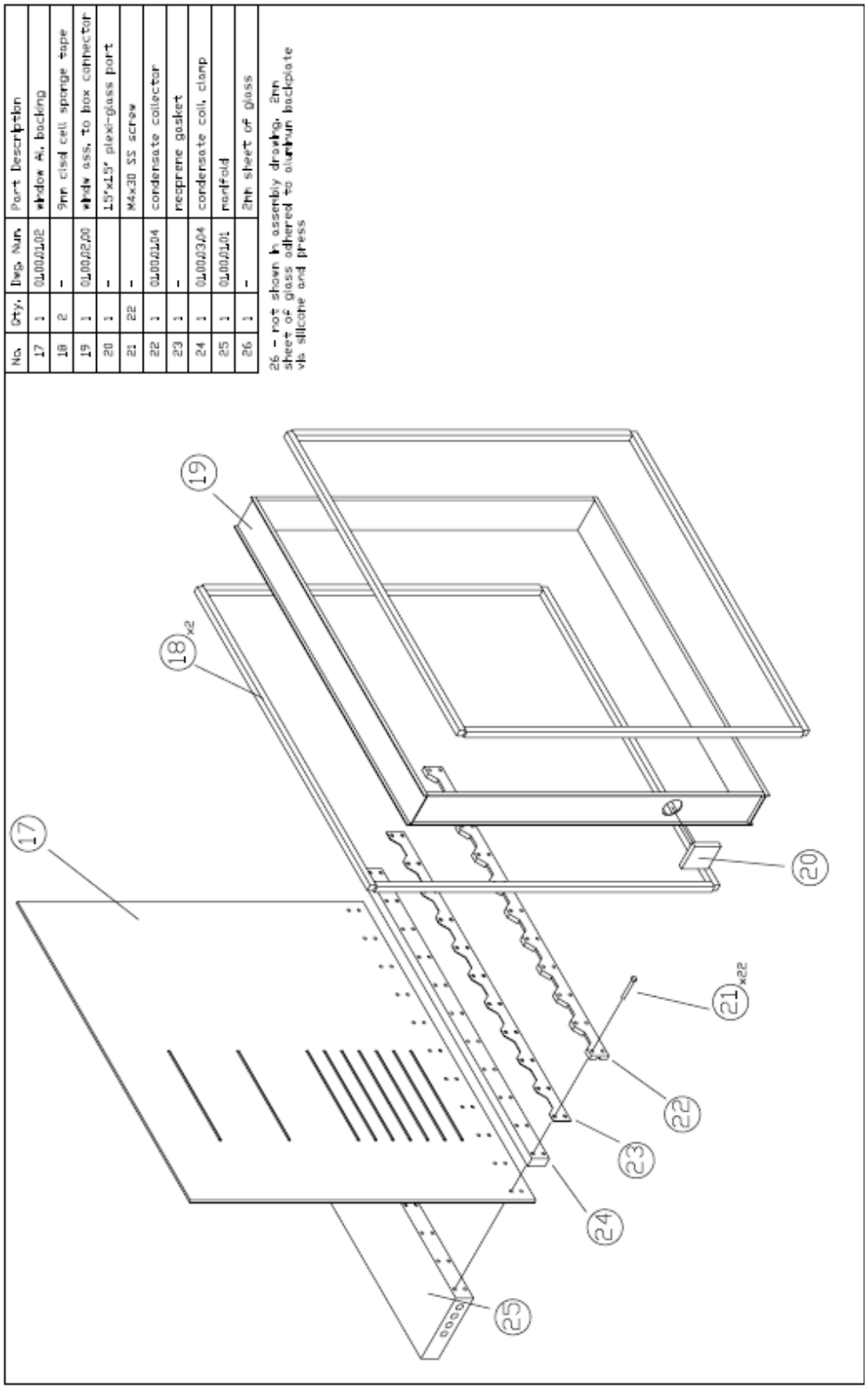

Figure 4.3: Vertical glass assembly drawing

4.2 Sizing the Enclosure

To understand the convective heat transfer coefficient and its spatial variations A Computational Fluid Dynamics (CFD) software was used. The software, StarCD V3.105A [CD Adapco 2004], was used as a design tool to seek conditions that would produce a constant heat transfer coefficient along a cooled vertical surface.

It is important to determine if the flow in the enclosure is laminar or turbulent before any CFD modelling can begin. This can be done by calculating Ra_L. Natural convective flow along a vertical flat surface becomes turbulent as Ra_L approaches $Ra_{L,c} = 10^9$. Nominal temperatures to be used in the enclosure are 0°C for the cooled, vertical, glass and 20°C for T_{db}. Under these conditions the length of the vertical sheet of glass can be as large as 0.75m before the flow trips to turbulence. A glass height of 0.5m, yielding a Ra_L of 3.2 x 10^8, was chosen as it was of practical size for a table-top experiment and Ra_L remains below $Ra_{L,c}$ by an order of magnitude.

4.3 CFD Validation

The local heat transfer coefficient for laminar free convection at a flat, vertical, cooled surface was used for validation. Specifically, the known solution to this problem was compared to a CFD model in order to confirm the correct set-up of the model. The flat plate was chosen because it is similar to the vertical cooled glass surface to be used in the enclosure. A semi-empirical solution for the Nusselt number (Nu_x), shown below in Equations 4.1 and 4.2 [Incropera & DeWitt 2002] was used to compare with CFD results.

$$Nu_x = \left(\frac{Gr_x}{4}\right)^{1/4} g(\mathrm{Pr}) \tag{4.1}$$

$$g(\mathrm{Pr}) = \frac{0.75\,\mathrm{Pr}^{1/2}}{\left(0.609 + 1.221\,\mathrm{Pr}^{1/2} + 1.238\,\mathrm{Pr}\right)^{1/4}} \tag{4.2}$$

Figure 4.4 is a detailed schematic of the CFD model used. The cold section was made small relative to the enclosure in order to approximate a free standing plate in quiescent air. The enclosure spanned 1.5m x 3m. The cold wall was 0.5m in length and was located on a side wall as shown in figure 4.4.

The mesh size chosen had to be small enough to get a significant number of data points in the boundary layer along the cold wall and large enough to yield reasonable computation time. Manipulation of memory also presented difficulty as the software began to misbehave when mesh size became too fine. It was discovered that a mesh size of 2mm x 5mm satisfied all criteria.

The parameters and equations discussed here were applied to the validation model as well as the enclosure model. It was assumed that the enclosure would be sufficiently wide and 2-D modelling would apply to the flow near the center-plane of the enclosure. Simulations were conducted assuming the air density varied as a function of temperature, using a PISO solution algorithm, and a MARS differencing scheme for density, pressure, and temperature. These variables were chosen as suggested by the STARcd tutorial guide for free convection on a heated vertical surface [CD adapco 2004].

STARcd simulations produced the local heat flux (q_x) along the wall which was used to determine the local heat transfer coefficient using;

$$h_x = \frac{q_x}{T_{hot} - T_{cold}} \tag{4.3}$$

Figure 4.5 shows the local heat transfer coefficient obtained from both STARcd and the semi-empirical formula for the free standing vertical plate. Henceforth, y_g will refer to the vertical distance along the glass surface with $y_g = 0$ being the bottom of the glass surface. It can be seen that the plots are similar, with h_x differing as mush as 5% near $y_g = 0.3$m but differing very little in the region of greatest interest where y_g is small.

The agreement between the CFD results and the semi-empirical models was determined to be acceptable and hence the mesh size was deemed to also be acceptable for the purpose of design calculations.

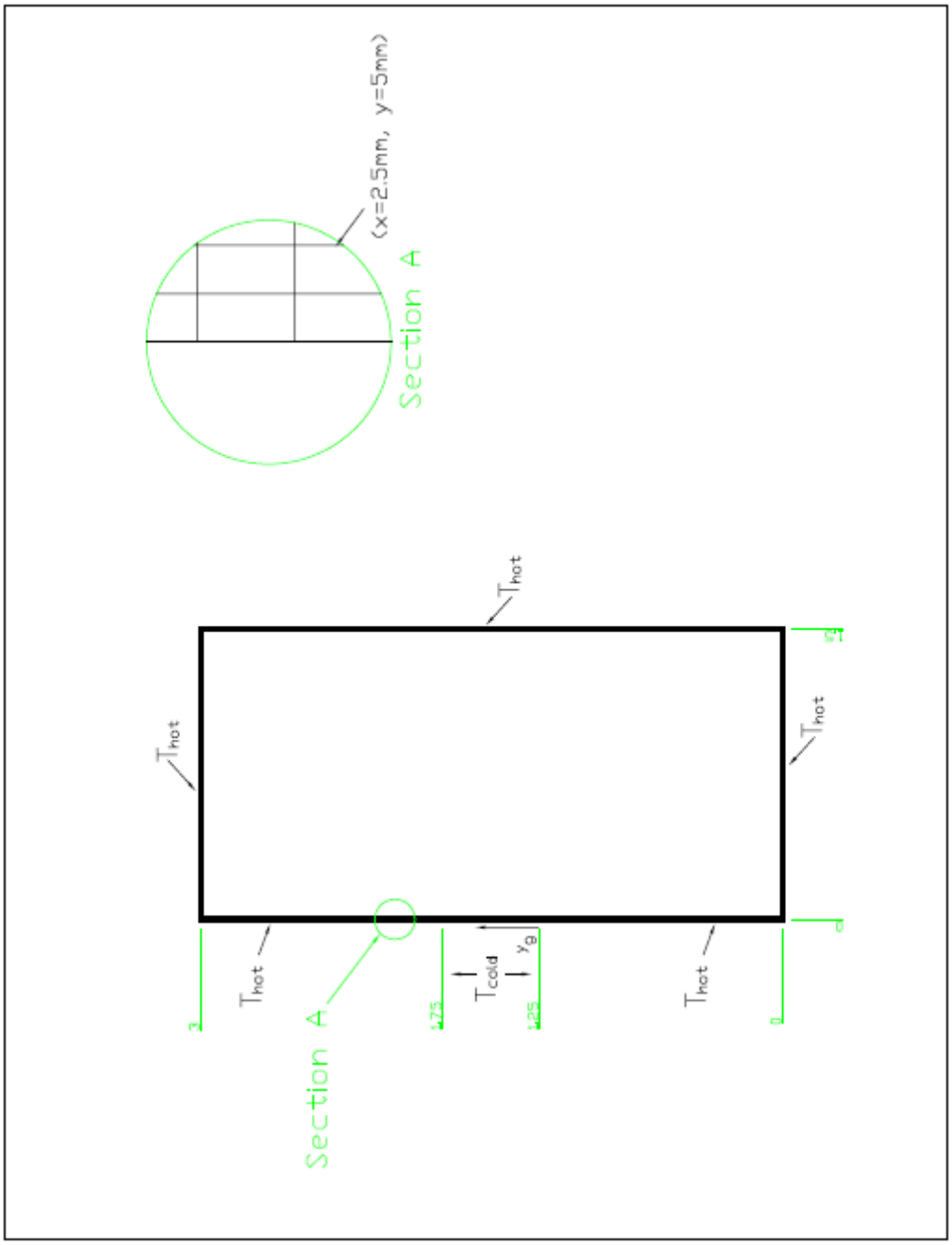

Figure 4.4: Detailed schematic of model used for validation

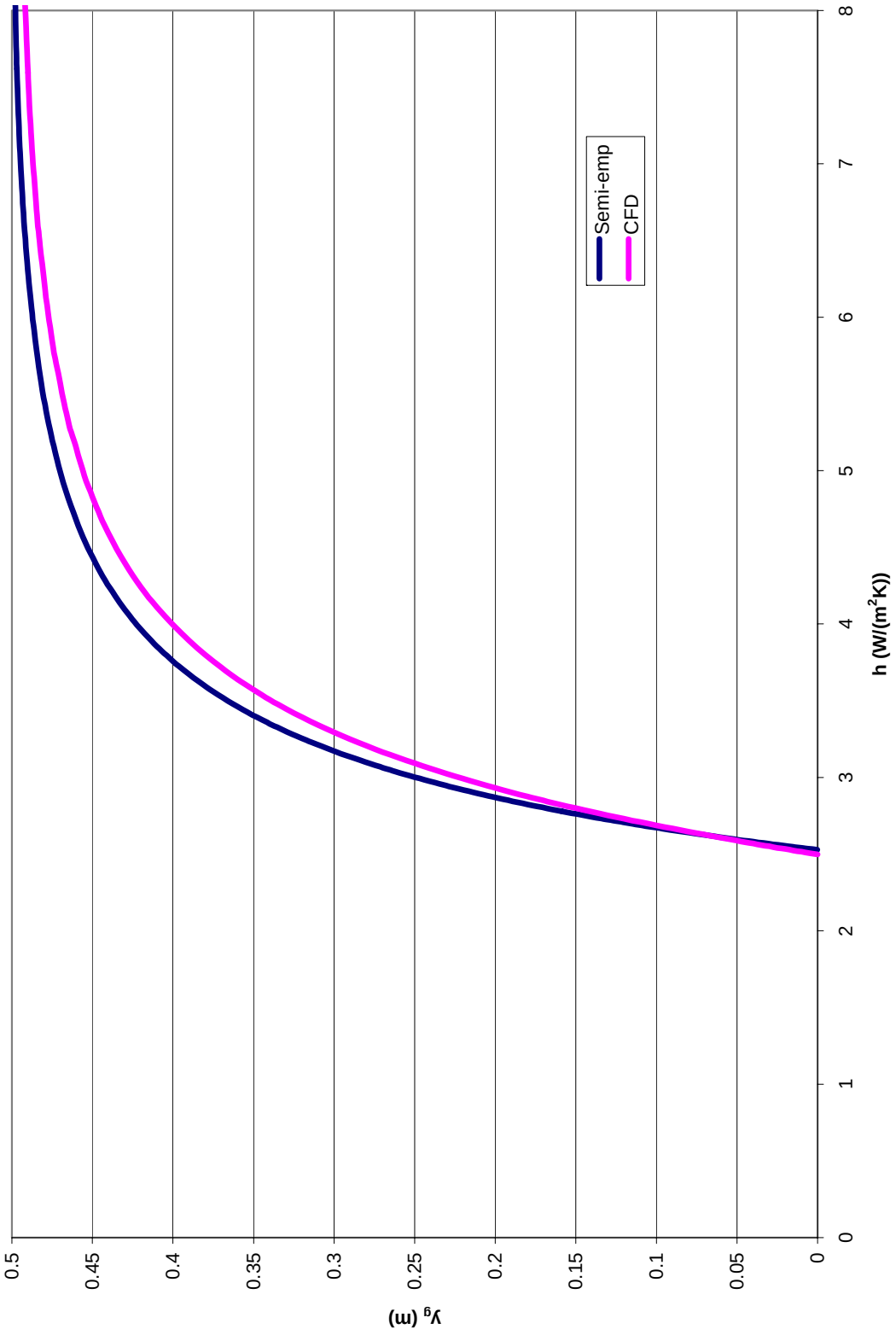

Figure 4.5: h_x versus y_g: free convection on a cooled (273.15K) vertical plate to air (293.15K)

4.4 CFD Models

Details regarding the CFD simulation can be seen in Figure 4.6. As shown in Figure 4.6, an aluminum plate is cooled at its bottom surface and attached to the glass sheet. This caused a temperature profile to develop along the height of the glass surface exposed to the enclosure. The resultant local heat transfer coefficient is shown in Figure 4.7. As can be seen in Figure 4.7, the local heat transfer coefficient profile varies at most by 15% over the bottom 0.012 m of the glass surface. The average convective heat transfer coefficient over the glass surface was 2.7 W/m^2K, similar to that of the glass surface under ASHRAE winter design conditions.

Most importantly, having the glass at a non constant surface temperature is similar to running multiple experiments at once. Each section of the glass can be segregated into sections with constant heat transfer coefficient. It was anticipated that condensation would proceed at a faster rate at lower surface temperatures. Accordingly, condensate run-off was expected to occur at the bottom portion of the glass before the top portion. This is important as it prevents run-off from any location interfering with sections of the surface where run-off has not yet occurred.

Figure 4.8 shows the free stream air temperature 0.1 m from the glass surface in the enclosure. It can be seen that the quiescent air is thermally stratified, 10°C at y_g = 0 m and 20°C at y_g = 0.5 m with an average air temperature of 14°C. This average air temperature was lower than required and hence more surface area at T_{hot} = 20°C was required to bring up the average air temperature to about 20°C.

The simulation also showed the temperature drops across the glass thickness were of order 10^{-2} °C. These values are well below the thermocouple accuracy and hence, for all experiments, thermocouple values were taken as exposed glass surface temperatures.

4.5 Reading RH and T_{db}

Determining the relative humidity in the enclosure is of great importance. To maintain an accurate experiment the relative humidity must be kept as close to constant as possible. Hence, an accurate RH sensor with a fast response time was sought. An off-the-shelf product with no additional modifications would be beneficial as well as ease of connection to a control system. The control system would be used to monitor the RH and then initiate moisture addition when necessary.

Two types of RH sensors available but not used are plastic optical fibre [Muto et al., 2003] and thermal sensors [Bhuyan & Bhuyan, 1995]. Fibre optics were not used as the technology is emerging and not readily available while thermal sensors did not provide sufficient accuracy and required a constant water input. A third method, thermoset polymer capacitive, was chosen and is described in more detail.

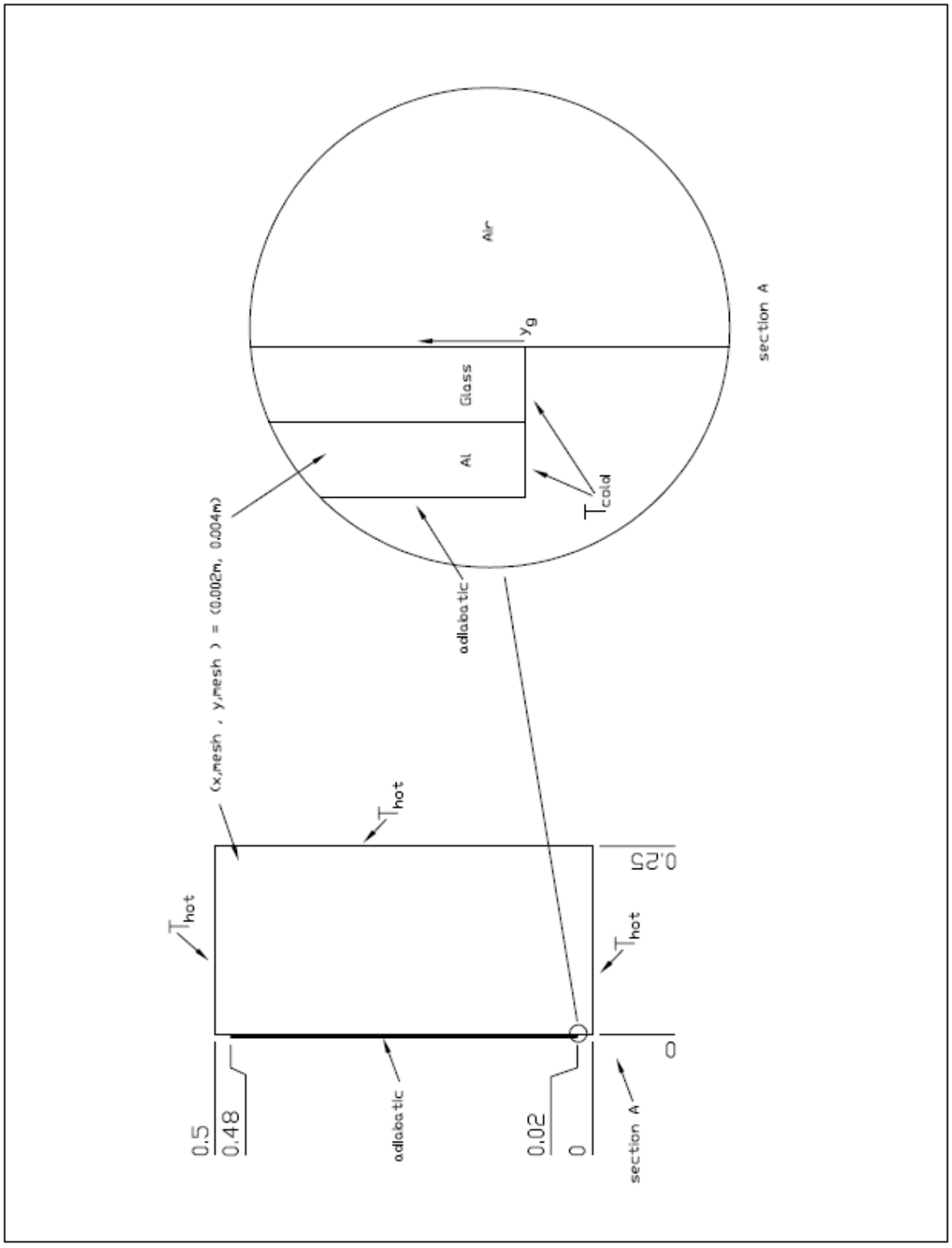

Figure 4.6: CFD schematic for simulation

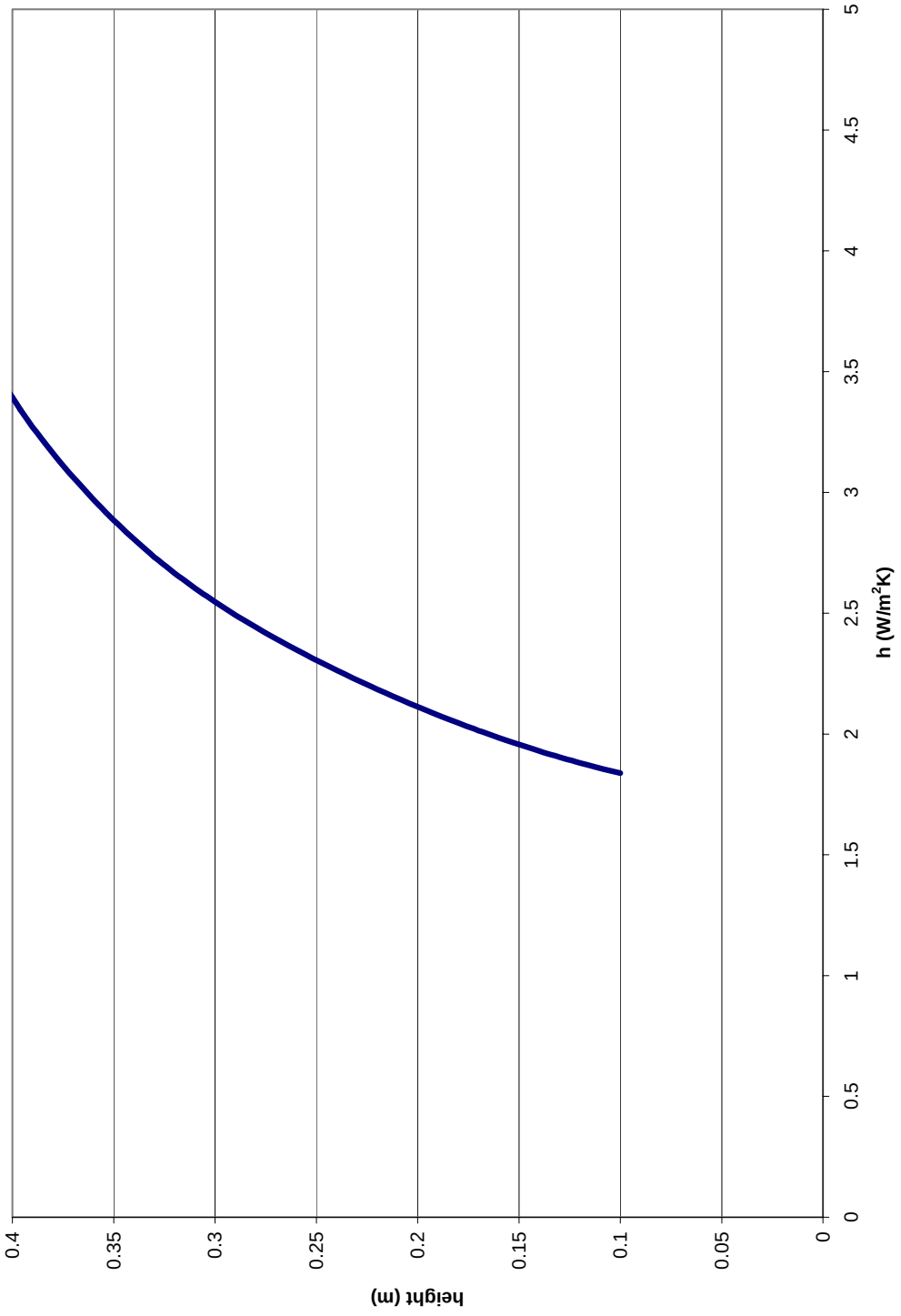

Figure 4.7: h_x at the glass surface versus height from the bottom of the enclosure for CFD simulation

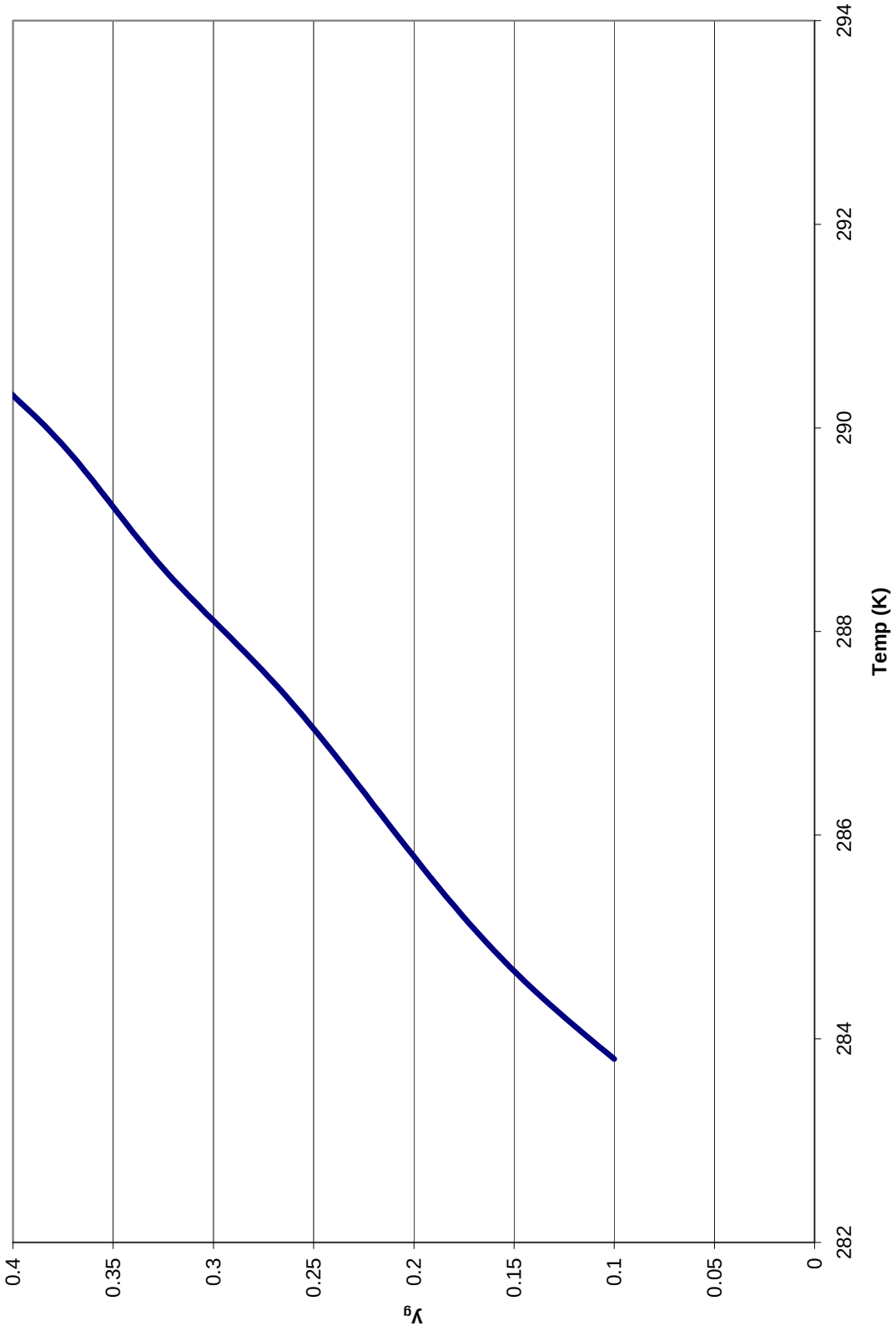

Figure 4.8: Temperature versus y_g for quiescent air in simulation, 0.1 m from the glass surface

4.5.1 Thermoset Polymer Capacitive

The thermoset polymer capacitive method is most common. Similar to a capacitor, the device has two plates of opposite charge. Each plate is coated with a special thermoset polymer. This polymer absorbs water when placed in a more humid environment. This absorption causes the polymer to expand thus altering the capacitance of the two plates. This change is then related to the increase in relative humidity. The opposite occurs when the environment drops in relative humidity. The polymer desorbs water and decreases in size. As before, the change is related to the drop in relative humidity. Two capacitive sensors currently on the market are the Honeywell HIH-3610 [Honeywell, 2006] and the Vaisala HMT333 [Vaisala, 2005].

The Honeywell sensor has a response time of 15 seconds in slow moving air (natural convection in the enclosure). The Honeywell sensor is accurate to ±2% RH and displays a hysteresis of ±1.2% RH maximum, calibrated to National Institute of Standards and Technology (NIST) specifications [Honeywell, 2006].

The Vaisala HMT sensor has a response time of eight seconds in still air. It is accurate to ±1.0% RH with a ±0.6% RH factory calibration uncertainty for RH levels between 0-40% and a factory uncertainty of ±1.0% for RH levels above 40%. This results in an overall uncertainty of ±1.17% RH for 0 to 40% RH and ±1.4% RH for 40 to 90% RH. It should be noted that this accuracy includes hysteresis. The module also contains a modest data acquisition system and two relay outputs. This allows the user to toggle the moisture

addition system when the RH drops below a specified level. In addition, the module reads T_{db} to an accuracy of 0.2°C [Vaisala, 2005].

It was decided the Vaisala HMT 333 sensor would be used for simplicity, ease of use, and accuracy. The relay/control module and data acquisition features eliminated the need for any other external devices or coding. Other humidity sensors following the capacitance technology did not claim accuracy better than that of the HMT333.

4.6 Maintaining Constant T_{db}

There were two main methods available for controlling T_{db} in the enclosure. The first was to heat all the (non-condensate) walls of the enclosure and the second was the heat an array of fins that would stand inside the enclosure.

The first option would require making the enclosure walls out of copper. Copper tubing would then be soldered to the back of the walls. The tubing would be connected to a heated water bath and transfer heat to the enclosure. This was the option assumed for the CFD simulation as mentioned above. The problem that arose with this solution was the low average air temperature and the thermal air stratification that occurred. This does not accurately simulate real world conditions as a normal house-hold window is exposed to a quiescent air temperature much closer to 20°C or normal indoor temperatures.

The second option was to run copper fins, with copper tubing soldered to each, within the air space. This option can be seen in the apparatus description as it was the one chosen.

This array of fins will help eliminate the stratification of air as they are of constant temperature and essentially fill up the entire space. They also provide more surface area to heat any cold air that pools at the bottom of the enclosure as was considered in CFD simulations. The larger surface area at a higher temperature would act to raise the quiescent air temperature. An average of 48 walls (24 fins, x 2 sides) at 293K and 1 wall at 273K, all undergoing heat transfer by natural convection, can be expected to yield an average quiescent air temperature of 292.6K. In addition, the reduction in thermal stratification is expected to produce a convective heat transfer coefficient at the glass surface that is more spatially uniform.

4.6.1 Copper Fins

Each fin was chosen to be 250 mm x 450 mm. This allowed the fins to span the entire enclosed space without interfering with the collar section which should be kept open for the possibility of interferometery. The fins rise from the bottom of the enclosure to heat the cooled pooling air and stop 0.05m from the top. This allows mixing at the top where the air leaves the fin array. This ensures a more uniform air temperature across the enclosure should any of the fins not operate at its intended capacity. A ¼" flexible copper tubing was chosen. This allowed for the tubes to be manually bent to the desired pattern. A semi-circular pattern was chosen and the tubes were soldered to each plate as shown in Figure 4.13.

The next step was to determine how many fins were required. This would be determined by the fin plate thickness and the space between the fins. Correlations for optimizing

spacing between natural convection cooled vertical parallel plates were developed by Bar-Cohen & Rohsenow (1984). They determined an optimal spacing (S_{opt}), maximizing heat transfer from the entire array of vertical channels and a maximum spacing (S_{max}), maximizing the heat transfer from each individual fin in the array. Both spacing correlations, for symmetric isothermal plates, are shown below.

$$S_{opt} = 2.71\left(\frac{Ra_s}{S_{opt}{}^3 L}\right)^{-1/4} \tag{4.7}$$

$$\frac{S_{max}}{S_{opt}} = 1.71 \tag{4.8}$$

It was decided that the maximum heat transfer from the entire array of fins would be the design condition, S_{opt}. Calculations showed that using, T_{hot} = 293K, T_{cold} = 273K, and $T_{mean(quiescent\ air)}$ = 292K; S_{opt} = 16 mm. The spacing was rounded down to 15 mm, resulting in 24 plates filling the 500 mm enclosure. The plates were kept 15 mm apart using threaded rods and copper spacers as shown in Figures 4.13 and 4.14. The copper spacers were made of 3/16" copper tubing cut into 15 mm lengths. The threaded rod was loosely fit through the spacers and holes punched into the copper sheets. The spacers were held in place by nuts at the end of the first and last plates.

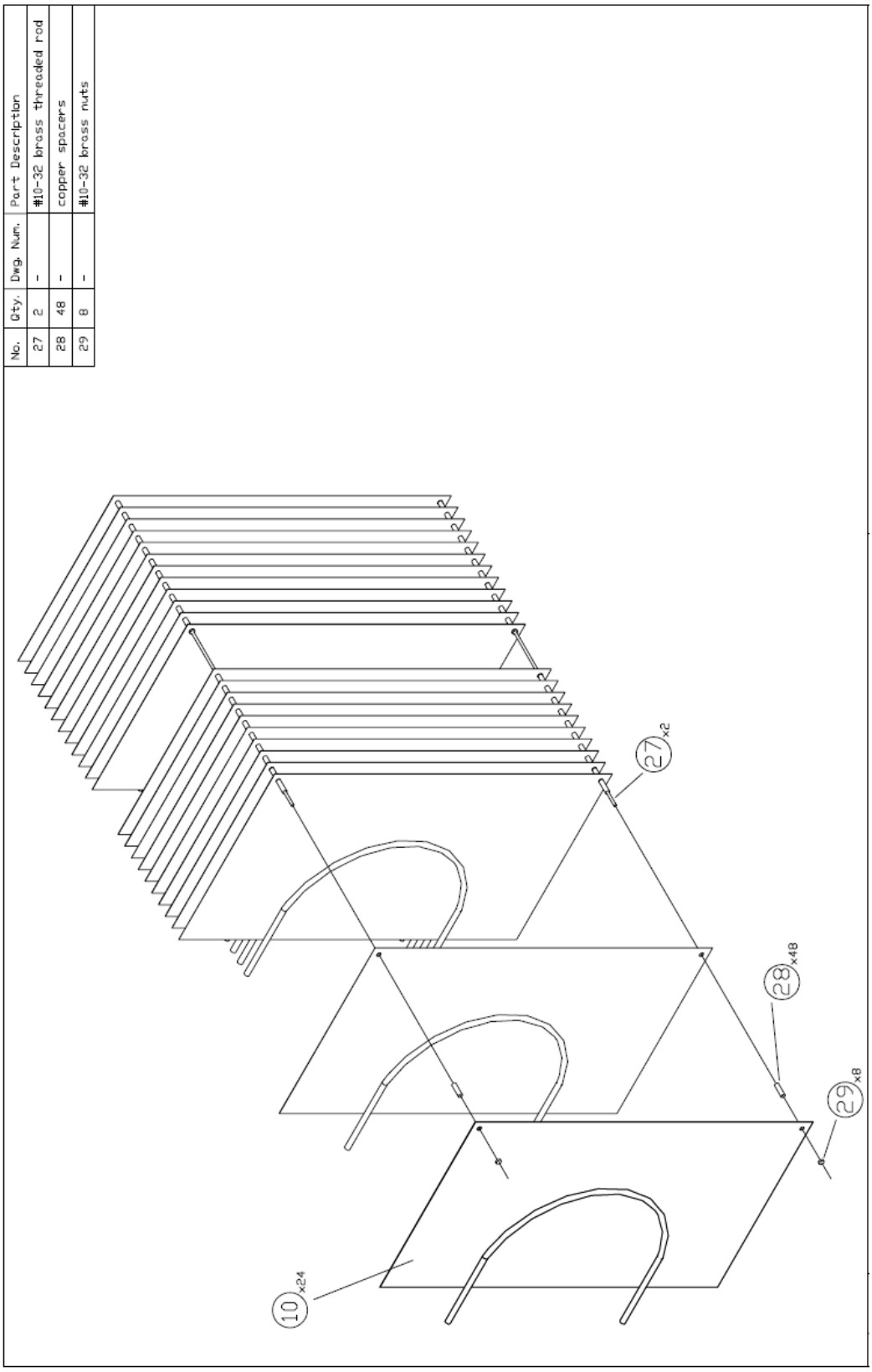

Figure 4.9: CAD drawing of copper fin assembly and spacers

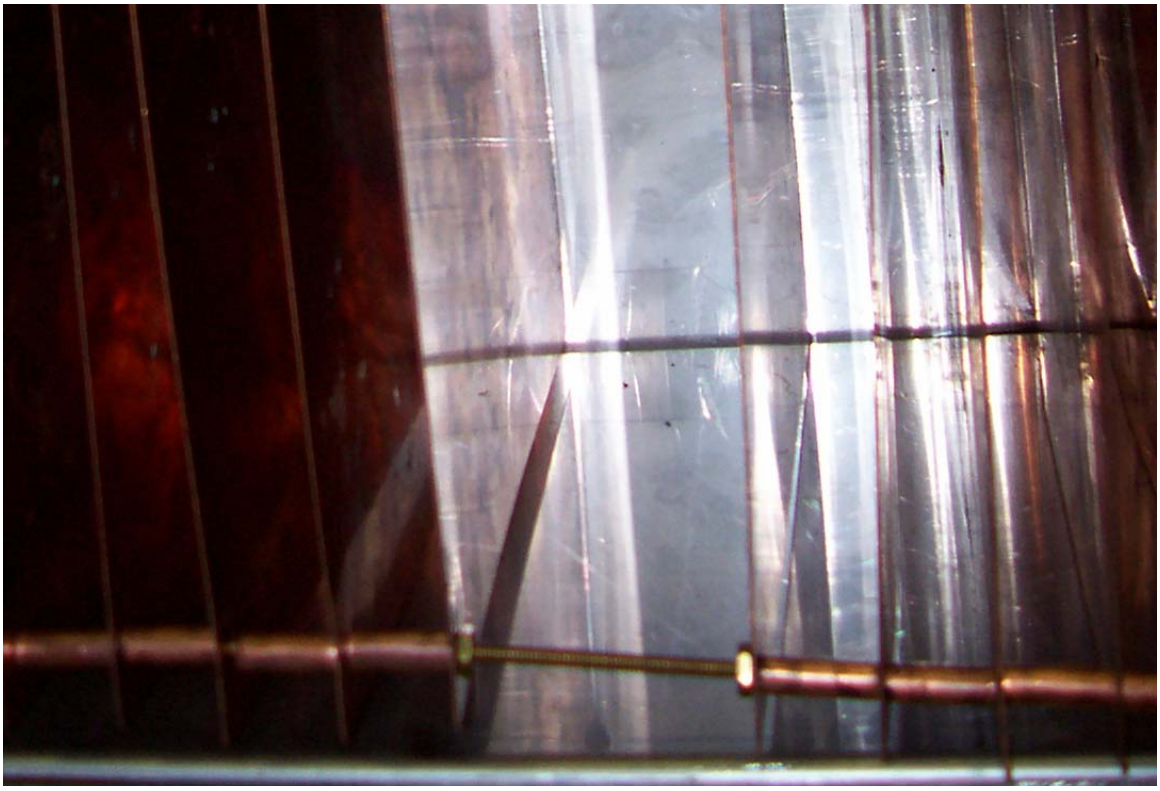

Figure 4.10: Copper fin and spacer assembly

4.7 Maintaining Constant RH

To bring an enclosed space to a set relative humidity it is best to look at the humidity ratio. This is because it shows the mass of water required rather then a vapour percentage. For example, approximately 5.95 g H_2O per kg of dry air is required to bring an enclosed space from a relative humidity of 0% to 40% at T_{db} = 293.15K. In the designed enclosure (0.5m x 0.5m x 0.3m), the addition of 0.53g of H_2O would b required. Under the same conditions an addition of 0.09g of H_2O would be required to bring the relative humidity from 35% to 40%. This shows that H_2O addition into the enclosed space must be done in small amounts at a slow rate.

The first method discussed is a low pressure, fine-misting nozzle. When required, a pressurised nozzle activates and a fine mist is released into the conditioned space. A low air pressure nozzle produced by Delevan Spray Technologies has the ability to emit water droplets averaging 100μm in diameter at a rate of 1.45 L/hr [Delevan, 2004]. Hence, to bring the conditioned space from 35% to 40% RH a spray burst lasting approximately two seconds would be required. It was also important to know how quickly the water will evaporate. Calculations for determining the evaporation rate of a liquid droplet are well documented by Turns (2000). Using species conservation equations and mass conservation equations Turns shows the derivation of the evaporation constant and the D^2 law for droplet evaporation, shown below.

$$K = \frac{8\rho D_{AB}}{\rho_l} \ln\left(1 + B_Y\right) \tag{4.9}$$

$$D^2(t) = D_O^2 - Kt \tag{4.10}$$

Both formulae used in conjunction with the conditions given in the enclosed space yield an evaporation time of approximately five seconds for a droplet 100μm in diameter. It should be noted that the formulae were derived under the following assumptions;

i. *The evaporation process is quasi-steady*
ii. *The droplet temperature is uniform*
iii. *The mass fraction (Y) of the vapour droplet surface is determined by liquid-vapour equilibrium at the droplet temperature*
iv. *All thermophyiscal properties are constant* [Turns, 2000]

A second option involves evaporating individual droplets of water on a heated plate. The water is fed via a pipette and controlled by a needle valve and a solenoid valve. The

water lands on a heated copper plate and then evaporates. A 20L container was used to provide the head to create the flow. A large container was necessary to provide an approximately constant head as water droplets fall. Tygon tubing connects the container to a needle valve. The needle valve restricts the flow and is used to control the flow of droplets through the pipette. The needle valve feeds a solenoid valve which in turn feeds the pipette. The solenoid valve was controlled by the humidity sensor. When the RH level drops, the relay in the sensor activates and opens the valve. The pipette provides a small opening making it possible to release water as droplets rather than a steady stream.

Various trials were run at different needle valve settings. This was done in order to find the valve setting that would provide an acceptable mass flow rate of water from the pipette. In choosing an acceptable mass flow rate it was necessary to consider the time required for each droplet to evaporate and then the time for the vapour to diffuse throughout the enclosure. To determine these values the mass of each droplet was obtained by massing 100 droplets with an ADAM AAA 250L scale (accurate to 10^{-4} grams). The total mass was then divided by 100 yielding an average droplet mass of 0.02475 grams. Assuming the water to be a saturated liquid at 293.15K it was determined that 60 J of energy was required to evaporate one droplet. The evaporation time of water droplets was used as the determining factor of mass flow rate.

A heating element was used to evaporate water droplets. The evaporation time was governed by the rate at which electrical energy is supplied to the heater. The additional energy gained from the heating element would act to disrupt the flow and properties

inside the enclosure. Hence it is necessary for the additional energy from the heating element to be minimal and stable. For simplicity it would be ideal for the heating element to run independent of a control system.

An acceptable solution resulting in an evaporation time of 60 seconds uses a small continuous 1 Watt heater. One Watt would cause very little disruption to the enclosed environment. Allowing the heated plate to run constantly eliminates the need to control the device and allows for maintaining a simple control system for the entire apparatus. Also of benefit, a one Watt heating element could be easily fabricated using generic components. A 5V power supply was used to supply current to the heating element. A 25 ohm resister was necessary to supply 1W of power with a 5V power supply. The final heating element consisted of a 25 ohm resistor fastened to the bottom of a small copper cup. Devcon aluminum epoxy was used as it provided excellent thermal conduction with poor electrically conduction. The cup was then insulated ensuring the inside of the cup, where the water would fall, would remain at an elevated temperature. The insulation also provided radiant shielding between the cup and glass surface.

The sensor relay was set to activate the valve, and hence start the water droplets, once the RH fell below the set point. Based on the average water droplet mass of 0.02475 grams, with droplets added at the rate of one every 60 seconds it was estimated that the RH level would increase 1% in approximately 60 seconds (e.g., from 39% to 40%, T_{db} = 293.15K). This was found to be suitable because the process of condensation on the glass was much slower.

4.8 Experiment Procedure

Ideally, each experiment would instantaneously start at the desired relative humidity. For instance, a 40% RH test would start at 40% at time zero. This is difficult as it would require bringing all surfaces to steady state temperatures without any moisture in the chamber, and then instantaneously adding the exact amount of moisture required. If moisture were present in the chamber it would start to condense on the glass surface as it was brought to a steady state and hence preclude a true test at a constant RH.

A more practical start-up would involve starting each experiment at an RH level below the desired experiment levels and at a level with a dew point temperature below the glass temperature. Once at start-up levels, water would be added quickly, bringing the RH level up to the experimental set-point. An appropriate start-up RH level would be at 25% or below. At 25% RH and 22.2°C T_{db}, T_{dp} is approximately 0°C. The glass temperature in the coldest region is above 0°C.

The start-up procedure must also entail moisture removal from the enclosure. This is necessary when conducting experiments in succession where all the moisture from the previous experiment must be removed before starting the next experiment. A simple method for removing moisture from the enclosure is the use of desiccant. To speed up the drying process between experiments it would be ideal to heat up the water already condensed on the glass surface, thus making it a vapour in the air and more easily absorbed. The glass surface was not cleaned between experiments as de-ionized water

was used and no mineral deposits were observed glass surface after all condensate was re-evaporated.

Using the criteria discussed above, the following start-up procedure was developed;

- The RH set-point was set to 1%, thus ensuring no water was added during the drying process
- The hot water bath was set to 27°C and the cold to 17°C, thus aiding in evaporation of the water on the glass surface from the previous run
- The desiccant was added
- After 4 hours, the desiccant was replaced with a fresh batch
- The previous step was repeated twice
- When the final batch of desiccant was inserted the temperatures of the baths were lowered every 15 minutes until the final temperatures were reached (bath settings: -3°C and 23°C)
- The apparatus was left for 60 minutes to allow the system to reach a steady state
- The desiccant was then removed
- For experiments run at 45% and 50% the RH point was set 2% below, while for tests at 30%, 35%, and 40% the RH point was set 5% below (i.e., 43% for a 45% run)
- The needle valve was opened to a rate of 1 drop every 3 seconds
- Once the set-point was reached, water addition stopped and the RH level still rose to the desired experiment level (e.g., water stopped at 43% but RH rose to 45%)

- The needle valve was then changed to a flow rate of; 1 drop every 3s for 50% RH, 1 drop every 10s for 45%RH, and 1 drop ever 30s for 30%-40% RH
- The RH point was then set to the desired level (e.g., 45%)
- A start-up was considered acceptable if the observed RH was within 1.5% of the desired value after 20 minutes

Once start-up was complete the experiment required little user input. Photographs were initially taken every 60 minutes for 30% and 35% RH experiments and every 30 minutes for 40%, 45%, and 50% RH experiments. Once condensation run-off began photographs were taken every 15 minutes. Approximate run-off times are listed in the results section. These values were determined from trial runs with the apparatus. Sixty minutes after initial run-off, pictures were taken every 60 minutes for 120 minutes and then every 180 minutes until a total run time of 950 minutes (approximately 16 hours) had elapsed.

When taking pictures it was important to minimise the time the halogen lamp was used so that it did not disturb the conditions in the enclosure.

Chapter 5

5 Results and Discussion

5.1 Introduction

This chapter presents RH versus time plots for each experiment, as well as photographs of the condensate taken at different time intervals. Observations showed that over time, a steady-state without run-off did not occur. In all cases run-off was observed and the run-off front progressed to the dew point line. Condensation was always in the form of droplets. At first, a fine mist consisting of small droplets, individual droplets were difficult to discern by eye, formed on the glass surface. As time progressed these small droplets coalesced and formed larger droplets. In turn, these larger droplets coalesced and formed still larger droplets. This progression continued until the droplets became large (heavy) enough to initiate run-off.

The progression that occurred was not uniform relative to height. In all cases, droplet progression occurred faster over the bottom portion of the glass relative to the top. A progression of droplet formation with respect to y_g could be seen in all cases, where larger droplets would exist at low y_g and would range all the way to a fine mist at high y_g.

A wave like pattern was noticed during droplet progression. This occurred after initial condensation when droplets were medium in size. These medium sized droplets aligned

to create a wave-like pattern. In general, a wave-like pattern indicates medium sized droplets.

5.2 Enclosure at 30% RH

The RH versus time plot for the enclosure held at 30% RH can be seen in Figure 6.1. The first main feature is the cyclic peak and valley nature of the plot. The RH for each cycle rises at a very fast rate and then, just as quickly, drops part of the way down. The initial jump ranges from 2% to 8% above the previous minimum and then RH falls to between 2% and 1% above the previous minimum. This is then followed by a slow decent until the next cycle commences. It can be seen that the local minima are initially at the RH = 30% (from 0 to 150 minutes) and then slowly drop to RH = 29.4% at t = 500 minutes. The local minima hold steady at RH = 29.4% until t = 650 minutes when they return to RH = 30%.

The local maxima do not vary appreciably except at two time intervals; 25 to 120 minutes, and 680 to 770 minutes. During these periods the local maxima are much larger compared to all other local maxima. Two manual changes of water mass flow rate were made during the experiment; at 20 minutes and 660 minutes. The higher peaks are due to two drops of water being dispensed. This occurs with all manual changes and sometimes at random times during an experiment as explained in the next chapter. Reasons for manual changes to the needle valve are also discussed in the next chapter.

Initial condensation run-off, observed through the view port, occurred between t = 630 and t = 660 minutes at y_g = 25mm. The average RH reading between 20 minutes and 630 minutes was 30.6 ± 0.8% RH (i.e., 29.8% RH and 31.4% RH) while the average RH reading between t = 660 minutes and t = 900 minutes was 30.9 ± 1.1%.

A second experiment at 30% RH was conducted until initial run-off to confirm repeatability. Initial run-off for the second experiment occurred between 660 and 690 minutes at an average RH of 30.9 ± 0.9 %.

Photographs shown in Figures 6.2, through 6.4, were taken at approximately t = 300 minutes, t = 800 minutes, and t = 900 minutes, respectively. It was difficult to observe the condensation detail because condensation at 30% RH occurred over a very small area. Much more detail was obtained in subsequent tests at higher RH levels. All photographs presented were taken 0.60 m from the glass surface at x 3 optical zoom. The images show the copper fins on either side of the condensate surface. A reflection of the glass surface can be seen on the copper fins (Figure 6.2).

It can be seen in all of the photographs, most evident at t = 300 minutes, that the condensation line is located at y_g = 33 mm (just below the second thermocouple) of the left side. It is also evident that the condensation line is not perfectly horizontal and drops about 8mm on the right hand side of the image.

At t = 300 minutes, a wave-like pattern is evident and occurs at y_g = 28 mm. At y_g = 10 mm (just below the first thermocouple) the surface appears smooth.

At t = 800 minutes the condensation front can be seen and is at y_g = 28 mm. It should also be noted that the run-off front, refer to Figure 6.4, has occurred very close the condensation line and does not progress up the glass at any significant pace progressing through to 900 minutes, as can be seen in the final image. At 900 minutes most of the condensation has run-off the glass surface.

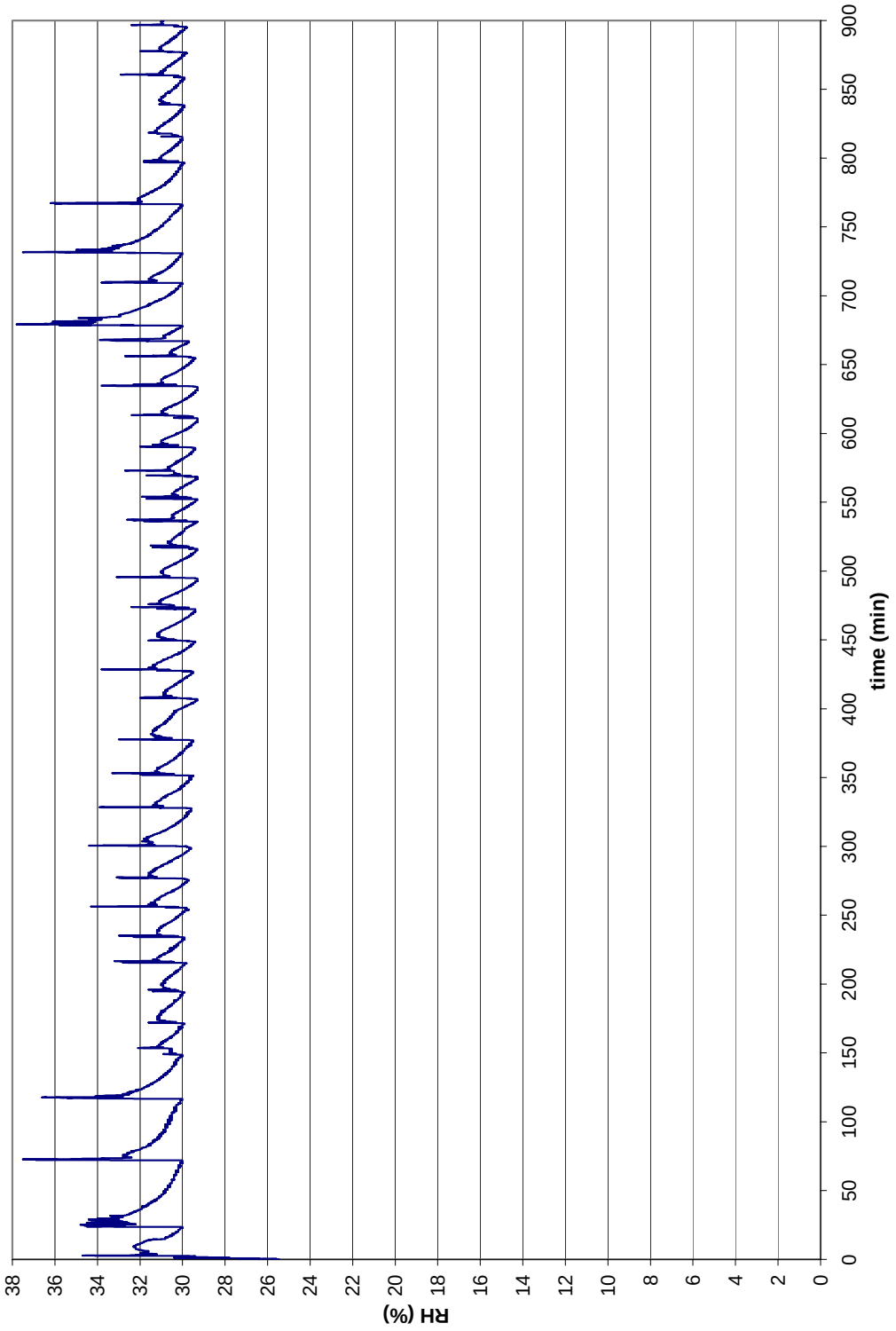

Figure 5.1: Time versus RH for enclosure held at 30% RH

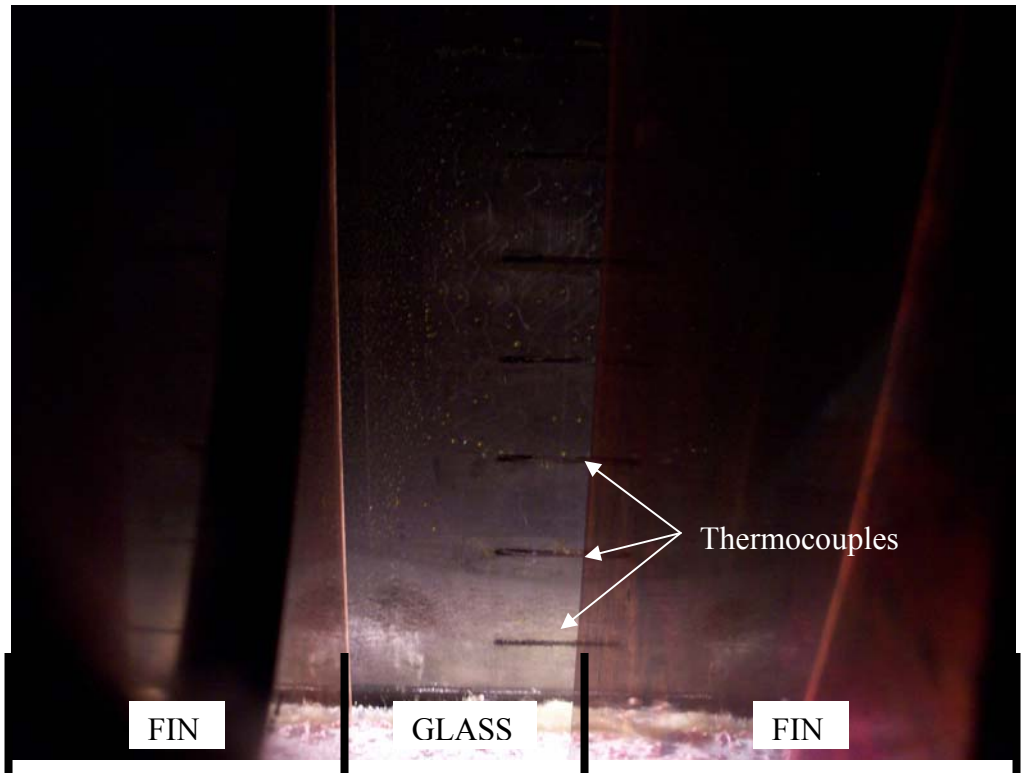

Figure 5.2: 300 minutes at 30% RH

Figure 5.3: 800 minutes at 30% RH

Figure 5.4: 900 minutes at 30% RH

5.3 Enclosure at 35% RH

The RH versus time plot for RH = 35% is shown in Figure 6.5. Again, a cyclic peak/valley profile was caused by the addition of water droplets. However, in this case, the main difference is there is no spike at the top of each peak. The larger peaks occur at minutes 210, 405, 505, and 640. Two of the peaks coincide with a manual increase of the needle valve (t = 210 minutes and t = 505 minutes). Of interest, the peaks that occur after each minima span a longer time period than those observed at 30% RH; this is apparent as the cycles take more of a concave-down "V" shape. There is also a significant drop in peak height between t = 275 minutes and t = 505 minutes, aside from one large peak at t = 400 minutes. Peaks then go back to a larger height before starting to tail off completely

below 35%. It is obvious that a manual increase in mass flow rate was required, but not made, at t = 800 minutes.

It became apparent that the experiment would require constant monitoring to ensure an increase in flow rate was given whenever required. This is virtually impossible over a 16 hour experiment that requires 3 hours of user-involved start-up. It was decided that an acceptable experiment would be one where the full progression of condensation could be observed over the condensate region. An entire progression of condensation consists of initial run-off and run-off front progression to the condensation line. Run-off front progression is discussed below.

Initial condensation run-off occurred between t = 310 and t = 325 minutes. The average RH between t = 20 and t = 310 minutes was 35.6 ± 0.6% and was 34.9 ± 1.3% from t = 325 to t = 900 minutes. A second experiment at 35% resulted in initial run-off between t = 310 and t = 325 minutes at an average RH of 35.4 ± 0.8%.

Figures 6.6 through 6.15 show photographs taken at t = 30, 120, 210, 300, 325, 400, 450, 560, 730, and 950 minutes. The first image, at t = 30 minutes, shows the condensation line located at y_g = 71 mm on the left side and at y_g = 63mm on the right side.

The second image (t = 120 minutes) is a good example of condensation droplet progression relative to y_g. It is described using three sections; y_g = 0 mm to y_g =13 mm, y_g =13 mm to y_g = 42 mm and y_g = 42 mm to y_g = 72 mm. These sections are labelled in

Figure 6.7. The first section appears smooth. The second section shows the wave like pattern and the third section is a smooth surface similar to the first section. A good comparison between the smooth initial condensation formation and the wave like pattern can be seen by comparing the first two thermo-couple wires to the third one. The first and second thermocouple wires appear distorted whereas the third wire appears only slightly distorted.

Looking to Figure 6.8 (t = 210 minutes), it can be seen that the wave like pattern is now present across the entire condensate surface. A further progression of droplet formation can be seen around y_g = 50 mm where larger droplets, relative to the photograph taken at t = 120 minutes, can be seen. This is further progressed after 300 minutes where droplets appear even larger.

Figure 6.10 (t = 325 minutes), shows initial run-off (condensation front) at y_g = 38 mm. In total three droplets appear to have run from 38mm (just below the second thermocouple), thus creating two "bands" of condensation. The first being condensate that has run, the second; condensate that has not run. Refer to Figure 6.10.

In the remaining photographs, a further progression of droplet formation and condensation front movement can be seen. From t = 400 minutes (Figure 6.11) to t = 450 (Figure 6.12) the run-off front has moved 10 mm to y_g = 48 mm.

The photograph at t = 560 minutes shows the run-off front did not moved appreciably. Looking closely below the run-off front, droplet formation has once again commenced. The droplets only appear in small pockets that stretch vertically along the surface creating a vertical striped pattern of clear condensate and droplets. The larger water droplets just above the run-off front are still apparent.

The photograph at t = 730 minutes shows the right side of the run-off front has progressed up towards the height on the left side. In total from t = 325 minutes to t = 730 minutes, the run-off front has moved from y_g = 38mm to y_g = 55mm, yielding a run-off front movement rate of 0.0425 mm/minute.

The photograph at t = 950 minutes shows the run-off front on the right side has caught up to the left and the larger droplets are few in number. The glass below the run-off front has once again formed the striped pattern.

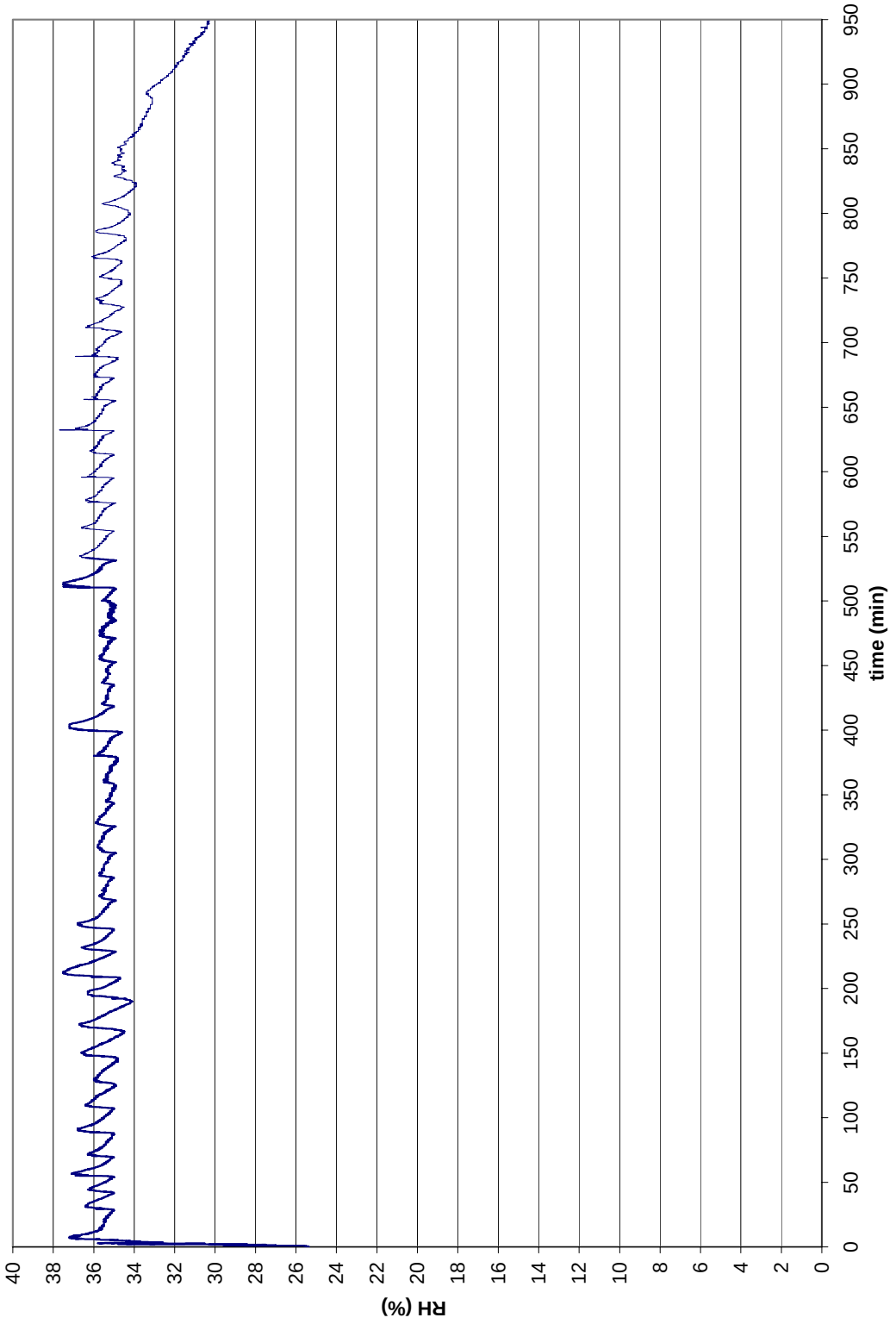

Figure 5.5: Time versus RH for enclosure held at 35% RH

Figure 5.6: 30 minutes at 35%RH

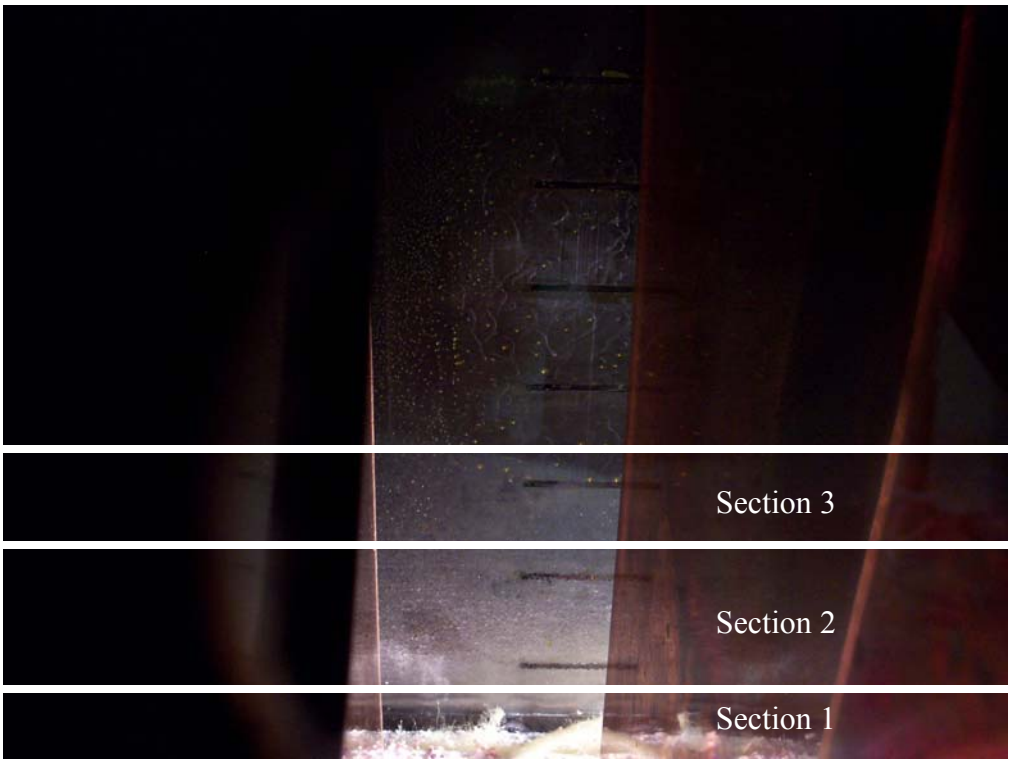

Figure 5.7: 120 minutes at 35% RH

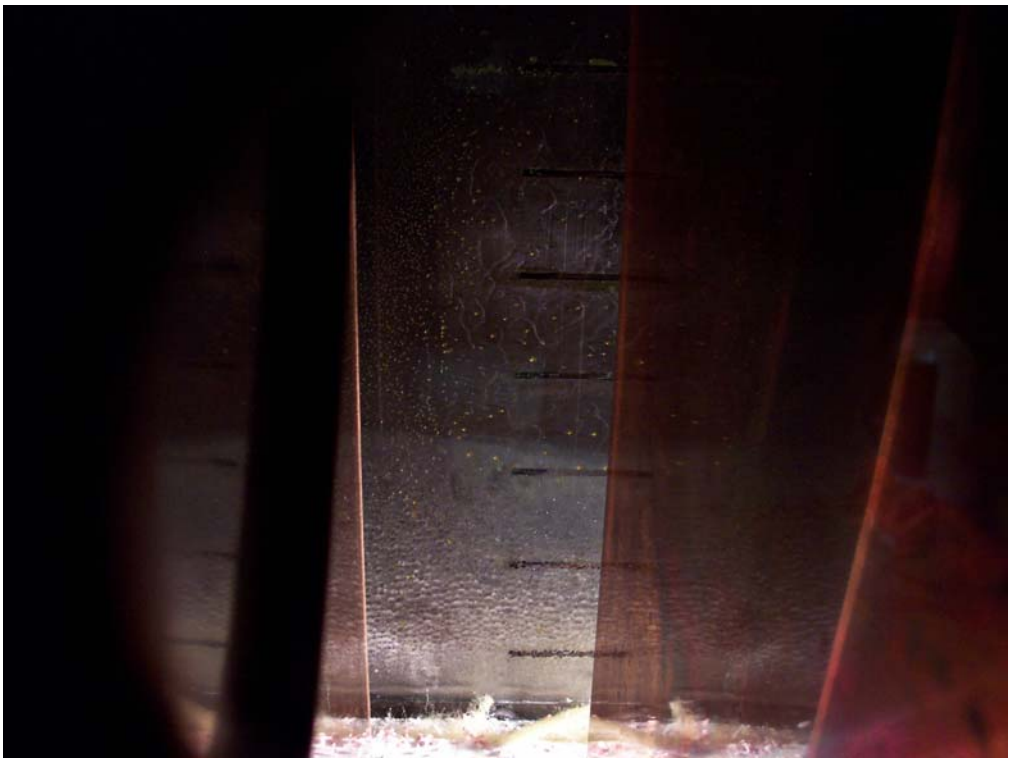

Figure 5.8: 210 minutes at 35% RH

Figure 5.9: 300 minutes at 35% RH

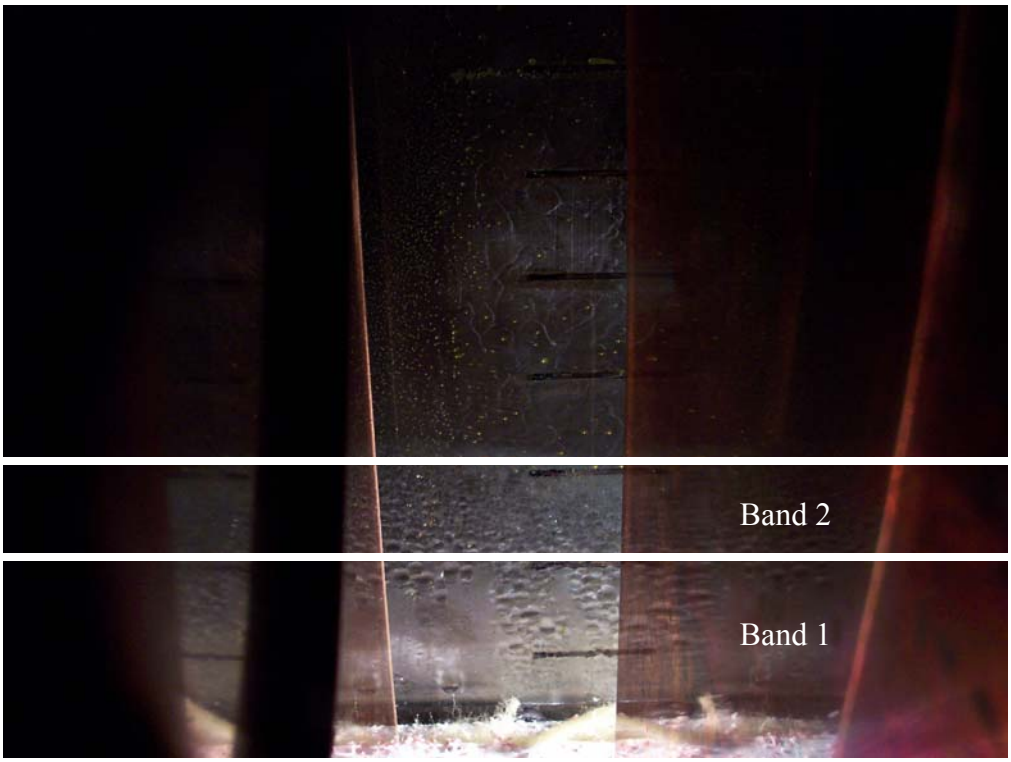

Figure 5.10: 325 minutes at 35% RH

Figure 5.11: 400 minutes at 35% RH

Figure 5.12: 450 minutes at 35% RH

Figure 5.13: 560 minutes at 35% RH

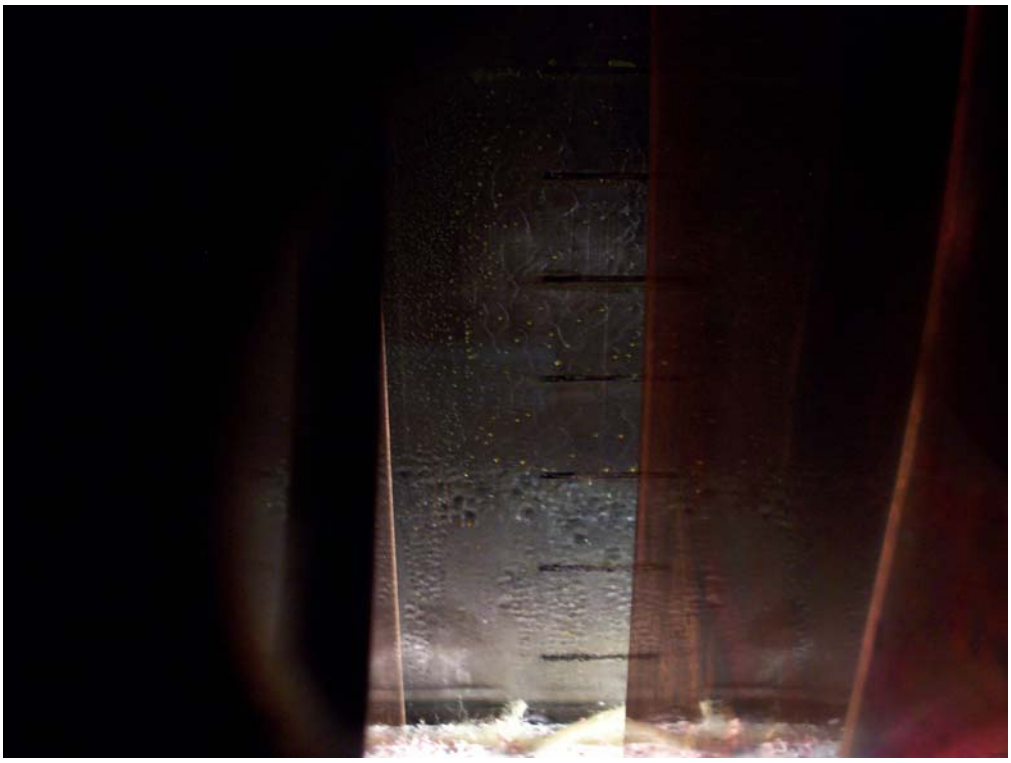

Figure 5.14: 730 minutes at 35% RH

Figure 5.15: 950 minutes at 35% RH

5.4 Enclosure at 40% RH

The RH versus time plot for RH = 40% is similar to that of RH = 35% with larger "V" shaped peaks followed by a group of smaller peaks, seen in Figure 6.16. At RH = 35% the pattern occurred once where at RH = 40% this pattern repeats three times; t = 200 minutes to t = 350 minutes, t = 530 minutes to t = 600 minutes, and t = 880 minutes to t = 950 minutes. In the first two cases the smaller cycle ended with a manual increase of mass flow rate; t = 350 minutes and t = 600 minutes. A manual increase was also made at t = 250 minutes.

Initial run-off occurred between t = 215 minutes and t = 230 minutes at y_g = 38mm. The average RH values observed pre and post run-off were 40.8 ± 1.3% and 40.7 ± 0.8%. Two additional runs were conducted at RH = 40%. Both runs showed initial run-off between t = 215 and t = 230 minutes at an average RH of 41.3 ± 0.8% and 41.7 ± 1.0%, respectively.

Figures 6.17 through 6.26 are photographs taken from the first RH = 40% experiment at minutes 40, 90, 215, 230, 400, 430, 510, 630, 840, and 950. The condensation line appears to have come closer to horizontal than at RH = 30% and RH = 35% with the right side at y_g = 88 mm and the left side at y_g = 95 mm. Figure 6.19 (t = 215 minutes) shows a good progression of water droplet formation with respect to y_g.

Initial run-off can be seen in Figure 6.20 (t = 230 minutes) at y_g = 38 mm. Movement of the run-off front can be seen in photographs after t = 430 minutes, t = 510 minutes, and t

= 630 minutes. The front has moved up 15 mm from t = 330 minutes to t = 510 minutes resulting in a run-off front speed of 0.083 mm/ minute. During this time, the run-off front is much more even across the visible area in comparison to the RH = 35% test.

Similar to the RH = 35% test, a striped pattern between smooth and wave-like condensate occurs, referring to images at t = 510 minutes and t = 630 minutes. Moving further, to 840 minutes, a pocket of larger droplets can be seen along the left side of the image in conjunction with the striped pattern. At t = 950 minutes all of the droplets have been wiped off except for a few that remain near the condensate line.

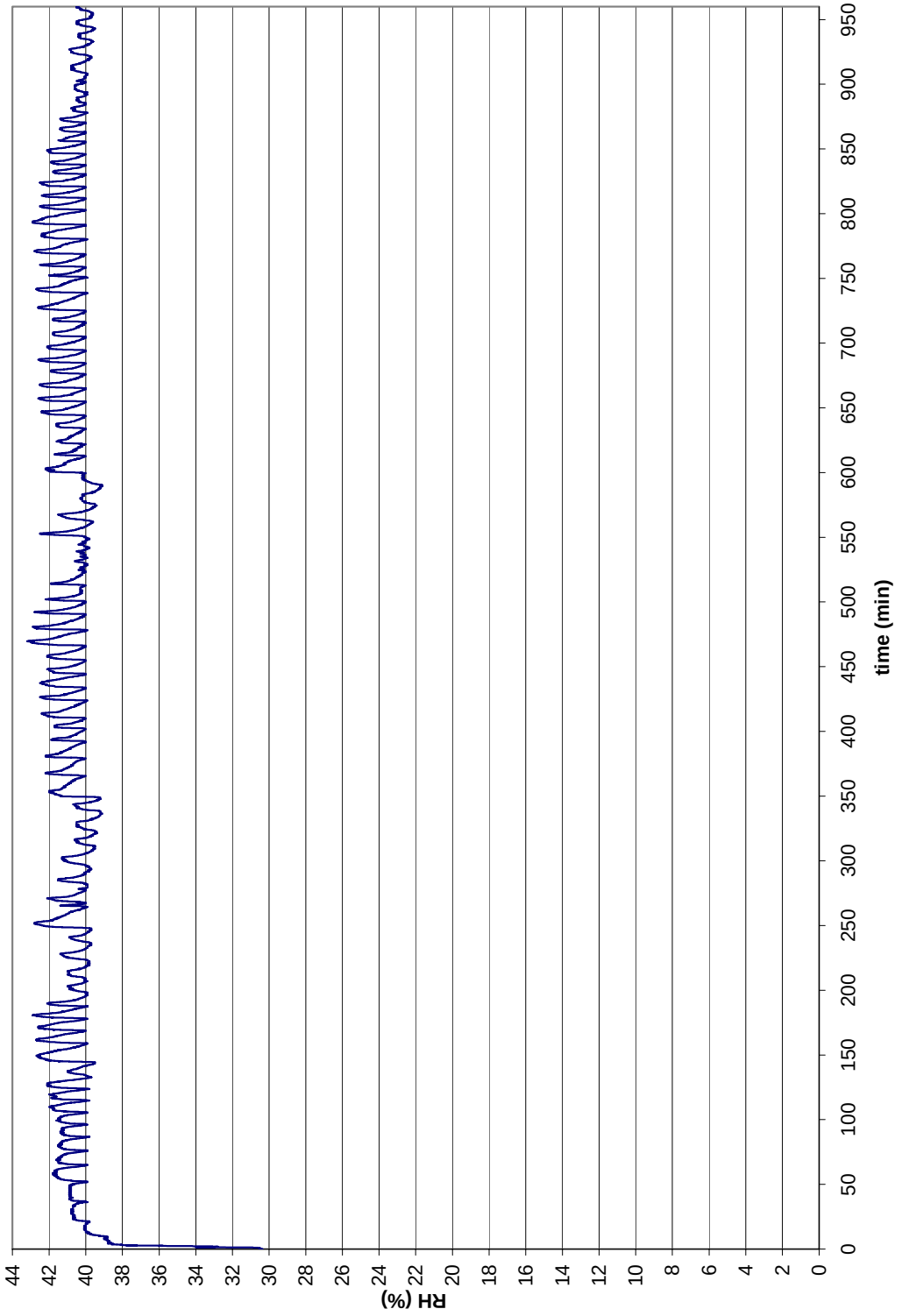

Figure 5.16: Time versus RH for enclosure held at 40% RH

Figure 5.17: 40 minutes at 40% RH

Figure 5.18: 90 minutes at 40% RH

Figure 5.19: 215 minutes at 40% RH

Figure 5.20: 230 minutes at 40% RH

Figure 5.21: 400 minutes at 40% RH

Figure 5.22: 430 minutes at 40% RH

Figure 5.23: 510 minutes at 40% RH

Figure 5.24: 630 minutes at 40% RH

Figure 5.25: 840 minutes at 40% RH

Figure 5.26: 950 minutes at 40% RH

5.5 Enclosure at 45% RH

The cycles at RH = 45%, shown in Figure 6.27, are much more compressed and are very difficult to see over the entire plot in comparison to tests at lower RH due to more frequent droplet addition. A section of Figure 6.27 is enlarged in Figure 6.28 (t = 50 minutes to t = 400 minutes, 20% to 48% RH), making the shape of the cycles visible. The peaks of each cycle progressively decrease in size until they eventually flatten around t = 725 minutes through to t = 800 minutes. At this point there is a sharp increase and then a more common "V" shape is seen. This sharp increase coincides with a manual increase in water flow rate.

Initial run-off occurred between t = 185 minutes and t = 200 minutes at y_g = 38 mm. The average RH pre and post run-off were 45.8 ± 0.6% and 45.5 ± 0.4%.

Three additional runs were conducted at RH = 45%. Run-off times ranged between 160 minutes and 185 minutes for RH levels of 45.6 ± 0.6%, 45.7 ± 0.7%, and 45.3 ± 0.2%.

Figures 6.29 through 6.48 are photographs taken from the second experiment at minutes 30, 60, 120, 185, 200, 240, 270, 280, 300, 330, 360, 390, 420, 480, 540, 600, 660, 810, 840, and 950. The first photograph, taken at t = 30 minutes, shows the condensate line peaks between the fifth and sixth thermocouple in the middle and drops on either side to the fifth thermocouple. In Figure 6.30 (t = 60 minutes) the condensate line is much clearer.

At t = 120 minutes the wavy-like pattern ranges from y_g = 13 mm to y_g = 38 mm. Also of interest, the condensation line is now level across the left side and drops 17 mm on the right side. At t = 185 minutes droplets have started to increase in size and the wave-like pattern extends further up the glass, now reaching y_g = 88 mm.

Initial run-off is apparent at t = 200 minutes at y_g = 38mm. Figure 6.35 (t = 270 minutes) shows the entire surface below y_g = 38 mm has been wiped from run-off. Photographs taken at 280, 300, 330, 360, 390, and 420 minutes show the run-off front moving up a total of 25mm, yielding a run-off front speed of 0.179 mm/minute.

Photographs taken after 480, 540, 600, and 660 minutes show a rise in the run-off front of 25mm on the left side and 12mm on the right side; yielding run-off front movement speeds of 0.104 mm/minute and 0.05 mm/minute, respectively.

Figure 6.46 (t = 810 minutes) shows condensation progression has started to repeat in the bottom sections with droplet formation, while larger droplets remain at the very top. The pin striped pattern is visible at t = 850 minutes and t = 950 minutes. The larger droplets at the very top, near the condensation line, still remain.

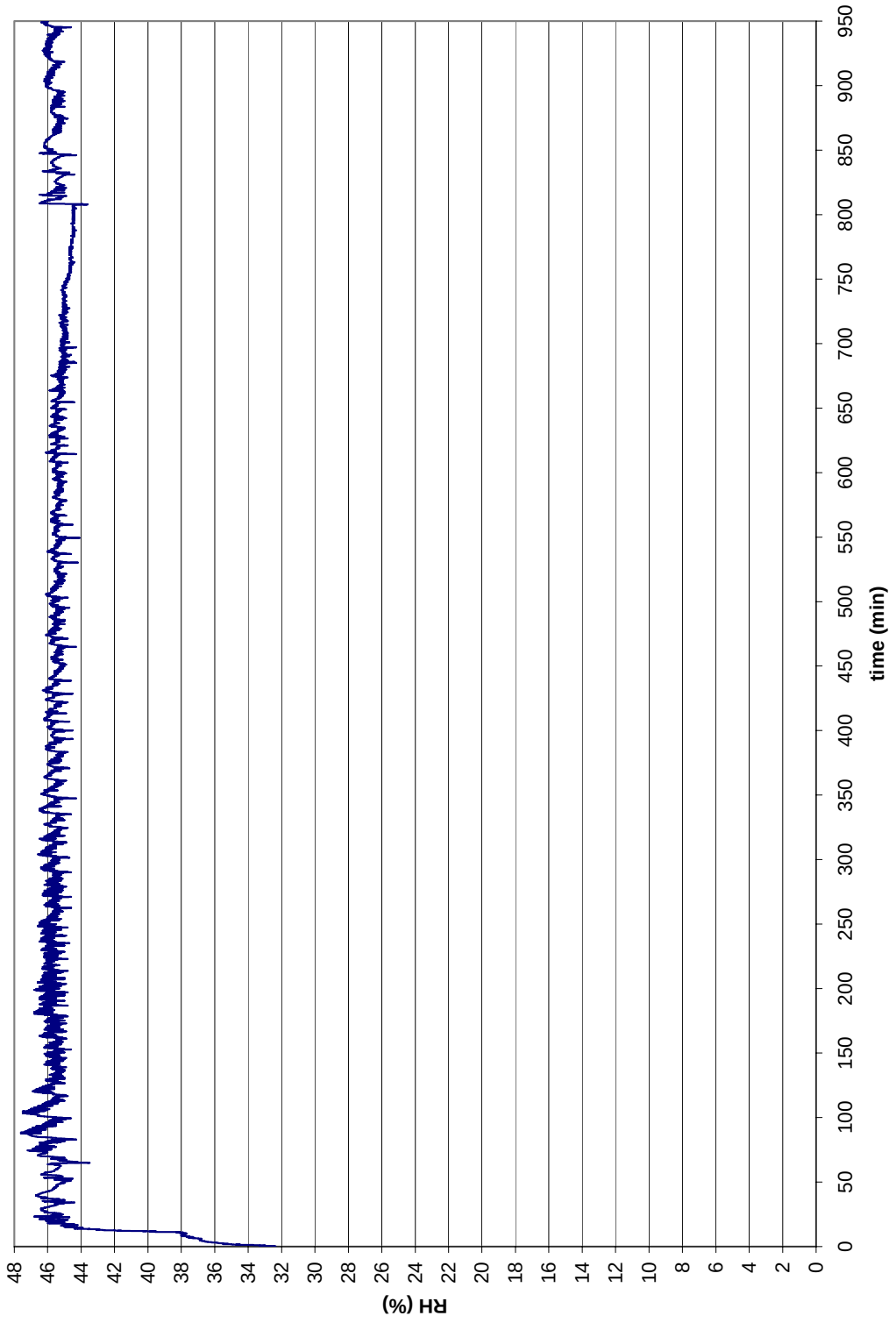

Figure 5.27: Time versus RH for enclosure held at 45% RH

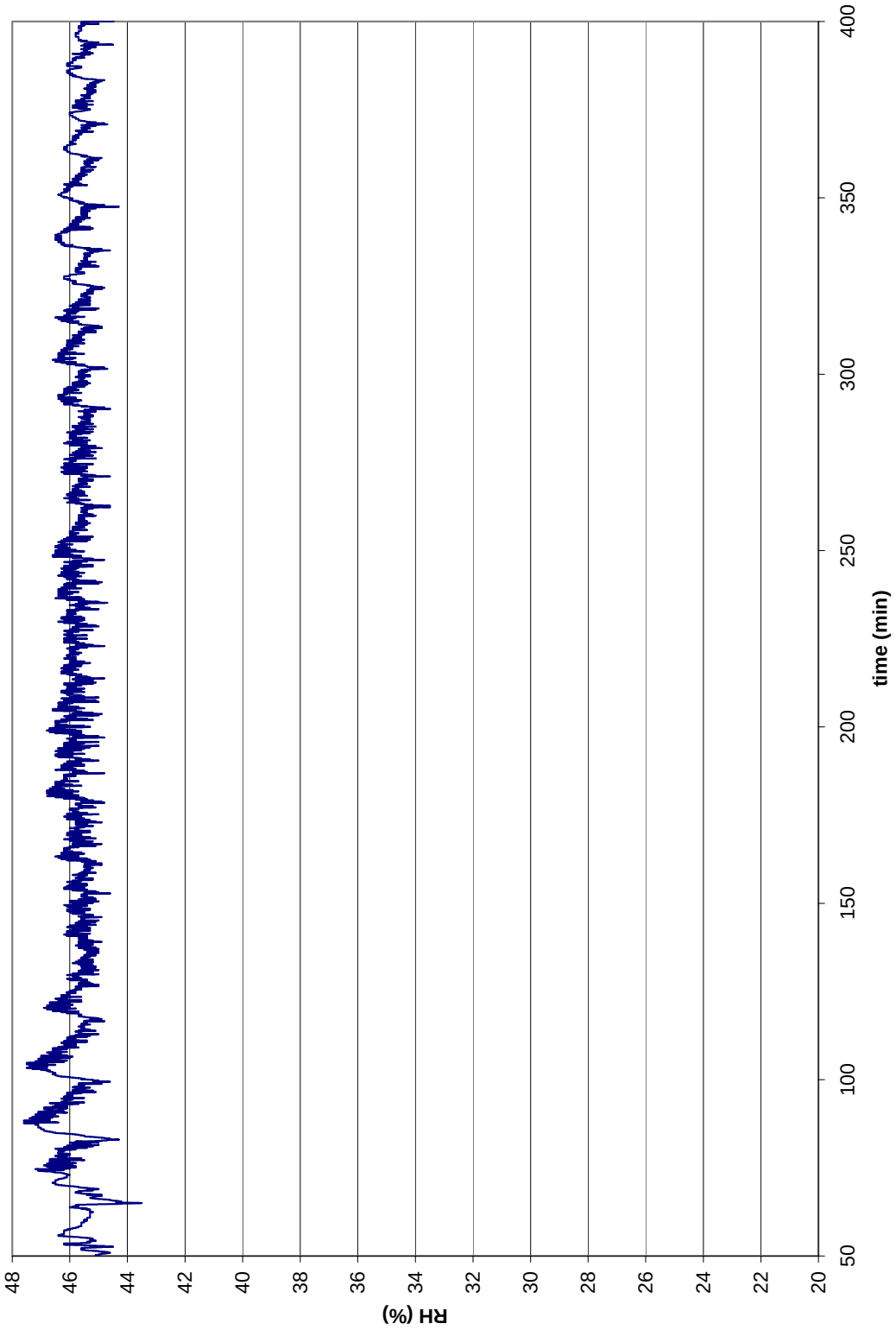

Figure 5.28: Expanded image of enclosure held at 45% RH

Figure 5.29: 40 minutes at 45% RH

Figure 5.30: 60 minutes at 45% RH

Figure 5.31: 120 minutes at 45% RH

Figure 5.32: 185 minutes at 45% RH

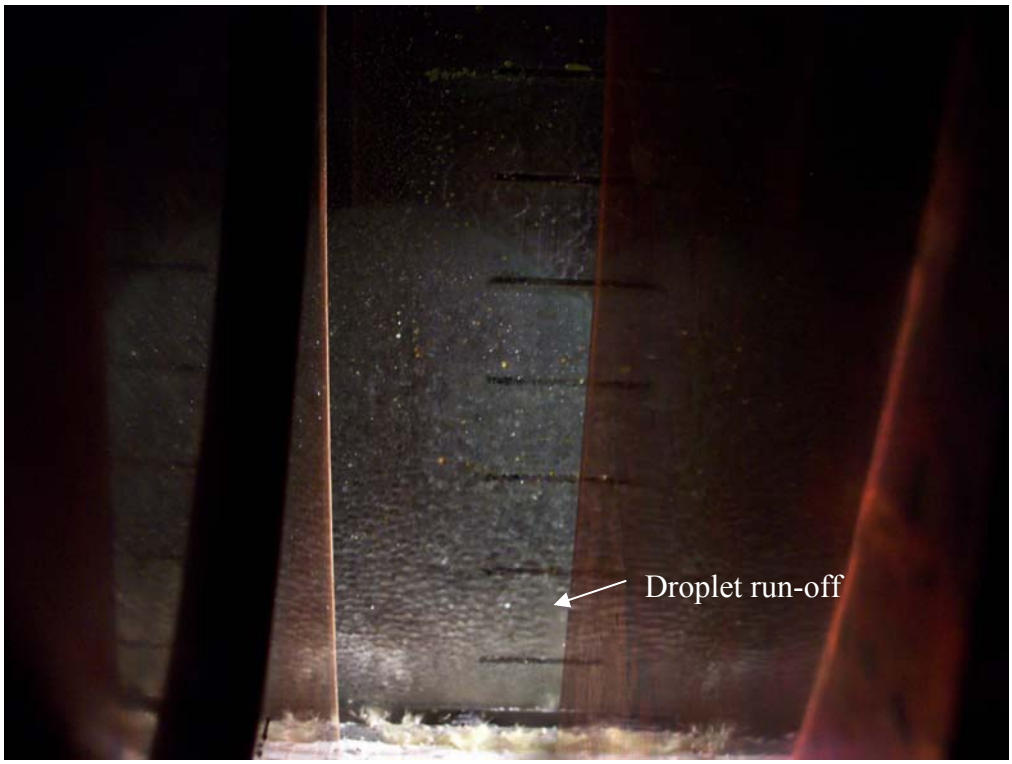

Figure 5.33: 200 minutes at 45% RH

Figure 5.34: 240 minutes at 45% RH

Figure 5.35: 270 minutes at 45% RH

Figure 5.36: 280 minutes at 45% RH

Figure 5.37: 300 minutes at 45% RH

Figure 5.38: 330 minutes at 45% RH

Figure 5.39: 360 minutes at 45% RH

Figure 5.40: 390 minutes at 45% RH

Figure 5.41: 420 minutes at 45% RH

Figure 5.42: 480 minutes at 45% RH

Figure 5.43: 540 minutes at 45% RH

Figure 5.44: 600 minutes at 45% RH

Figure 5.45: 660 minutes at 45% RH

Figure 5.46: 810 minutes at 45% RH

Figure 5.47: 840 minutes at 45% RH

Figure 5.48: 950 minutes at 45% RH

5.6 Enclosure at 50% RH

At 50%, the RH versus t plot does not show the full detail of the cyclic "V" shape at all over the entire test period, Figure 6.49. As with RH = 45% an enlarged section is required; shown in Figure 6.50 for t = 100 minutes to t = 200 minutes. Local maxima reach approximately 51% and no noticeable changes in cycle are visible. As well, no manual increase in mass flow rate was required. The only noticeable change occurred after 215 minutes where the local minima drop further below the set-point; similar to tests completed at RH = 45%.

Initial run-off occurred between t = 160 and t =175 minutes with average pre and post RH values of 50.3 ± 0.4% and 50.3 ± 0.4%. At RH = 50%, periods of only 100 minutes, before and after run-off, were used for calculations; t = 50 to t = 150 minutes and t = 300 to t = 400 minutes. Two additional tests were conducted at RH = 50% yielding initial run-off between 150 minutes and 165 minutes. The average RH readings were 50.7 ± 0.7% and 50.3 ± 0.7% respectively.

Figures 6.51 through 6.57 show photographs at minutes 60, 90, 170, 440, 740, 860, and 950 for the third experiment. The condensation line is fairly clear after 60 minutes reaching y_g = 153 mm on the left side and y_g = 125 mm on the right side.

The progression of droplet formation is evident through the photographs and initial run-off can be seen in Figure 6.53 (t = 170 minutes) at y_g = 38 mm. The run-off front can be seen rising from y_g = 38 mm to y_g = 87 mm between t = 170 and t = 440 minutes

(0.185mm/minute). The front further progresses to y_g = 122 mm between t = 440 minutes and t = 740 minutes (0.117mm/minute). The run-off front lags on the right side in comparison to the left and the striped pattern is evident throughout. Larger droplets can be seen below the run-of front, as with previous runs, at t = 860 and t = 950 minutes.

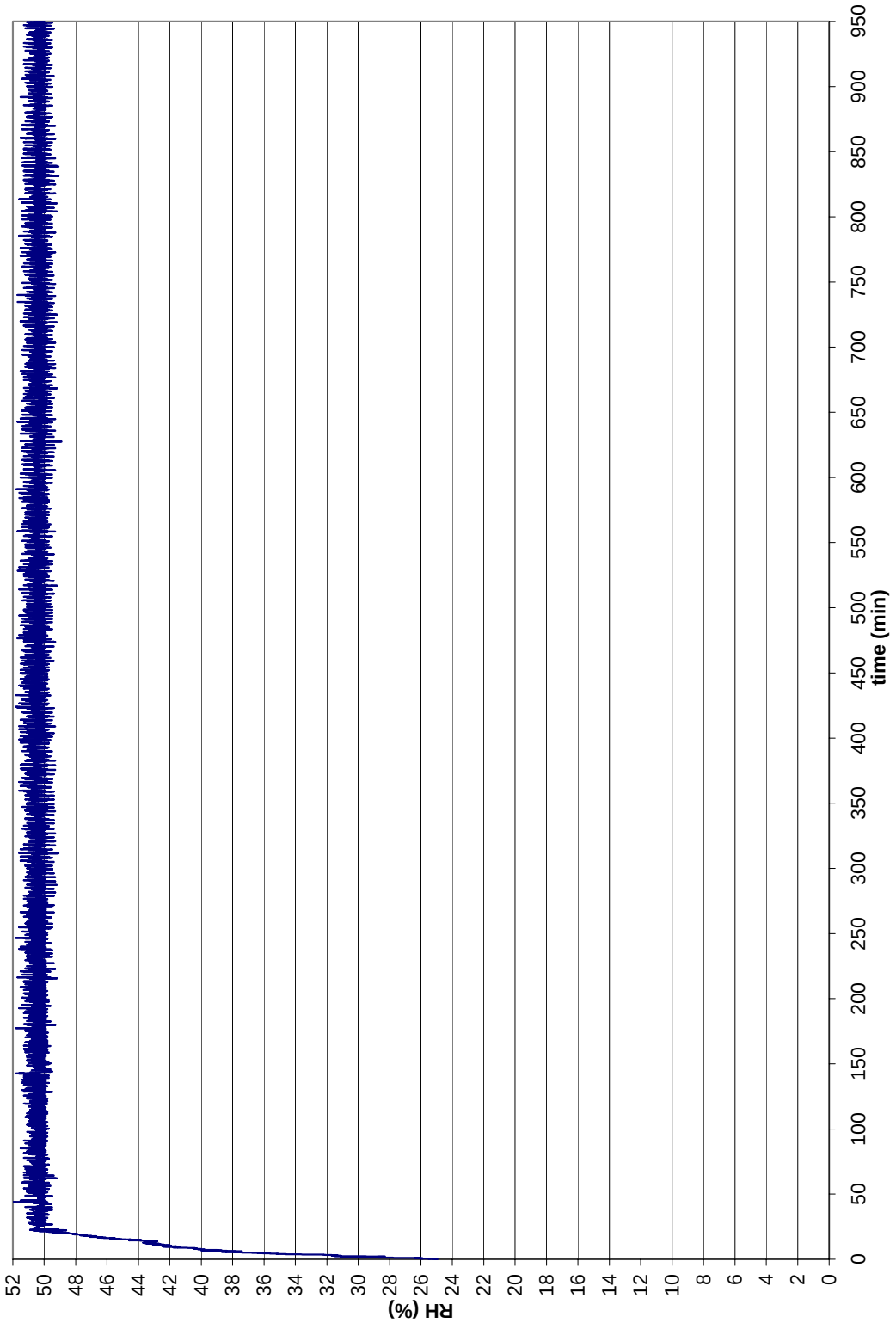

Figure 5.49: Time versus RH for enclosure held at 50% RH

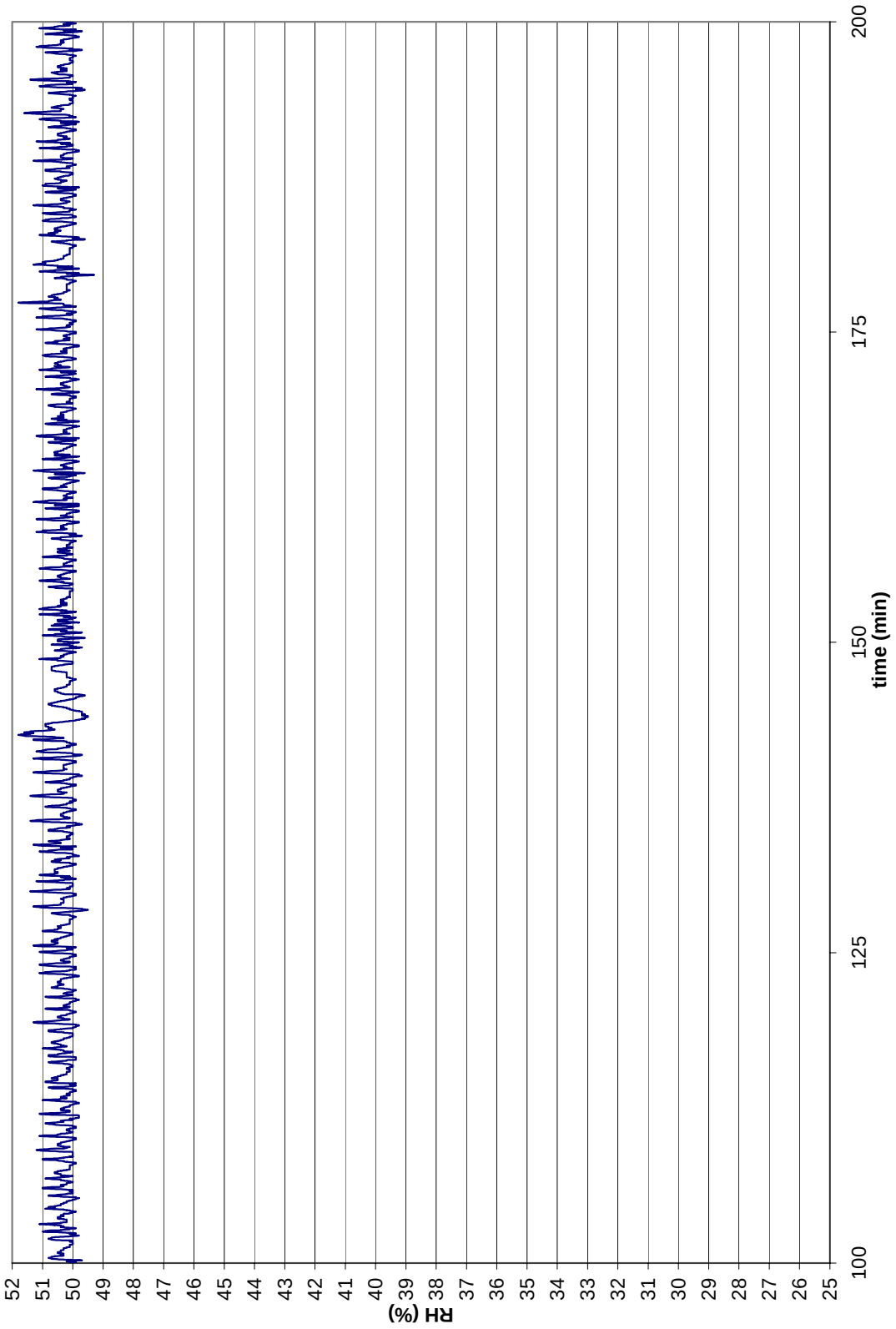

Figure 5.50: Expanded plot of enclosure held at 50% RH

Figure 5.51: 60 minutes at 50% RH

Figure 5.52: 90 minutes at 50% RH

Figure 5.53: 170 minutes at 50% RH

Figure 5.54: 440 minutes at 50% RH

Figure 5.55: 740 minutes at 50% RH

Figure 5.56: 860 minutes at 50% RH

Figure 5.57: 950 minutes at 50% RH

Chapter 6

6 Discussion

6.1 Introduction

This chapter provides a discussion of the different phenomena observed during the experiments. Sections will be broken down by phenomenon and will include a comparison for each experiment. The aspects to be discussed are; time of initial run-off (t_{ir}), run-off front speed, temperature along the glass surface, condensation line location, rate of droplet addition, and a summary plot.

6.2 Time of Initial Run-off

Figure 7.1 is a plot of t_{ir} versus nominal (RH - RH_{dp}). RH_{dp} is the RH level at which t_{dp} is 0°C. Any condensate that forms on the glass below 0°C will freeze before run-off occurs and hence, RH_{dp} acts as a vertical asymptote on the plot in Figure 7.1. RH_{dp} = 24% for the given enclosure (T_{db} = 22.1°C) and the asymptote is at (RH - RH_{dp}) = 0 or the y-axis.

The vertical axis of this plot shows the minimum time and maximum time for initial run-off for the multiple experiments conducted at each RH. For example, three experiments were conducted at 50%; initial run-off occurred between t =150 minutes and t = 165 minutes for two experiments and between t = 160 minutes and t = 175 minutes for the

third experiment. The low mark is plotted at t = 150, the high is at t = 175 minutes, and the diamond symbol (167.5 minutes) marks the average of 157.5 minutes, 157.5 minutes, and 167.5 minutes. It can be seen that RH has little influence on initial run-off time for cases with RH greater than 45%. Initial run-off time is strongly influenced by RH at low RH levels. In all cases run-off does occur within a 16 hour period.

It can be seen in Figure 7.1 that the data at higher RH (RH = 45% and 50%) appear to approach a horizontal asymptote near t_{ir} = 150 minutes. Using the R^2 function in Microsoft Excel it was found the data matched an exponential curve with an R^2 value of 0.997 assuming a horizontal asymptote of 153 minutes (t*). Figure 7.2 is a plot of nominal (t_{ir} - t*) versus nominal (RH - RH_{dp}). Also in Figure 7.2 is an exponential curve extended beyond the data points. It is believed that the initial run-off time at all RH levels for the given apparatus can be estimated using the exponential curve.

It was expected that condensation would commence run-off over a shorter period of time at a higher RH. A higher RH simply imposes a higher driving potential for mass transfer. Thus, a higher mass transfer rate and a faster progression through drop wise condensation, droplet growth, and condensation run-off.

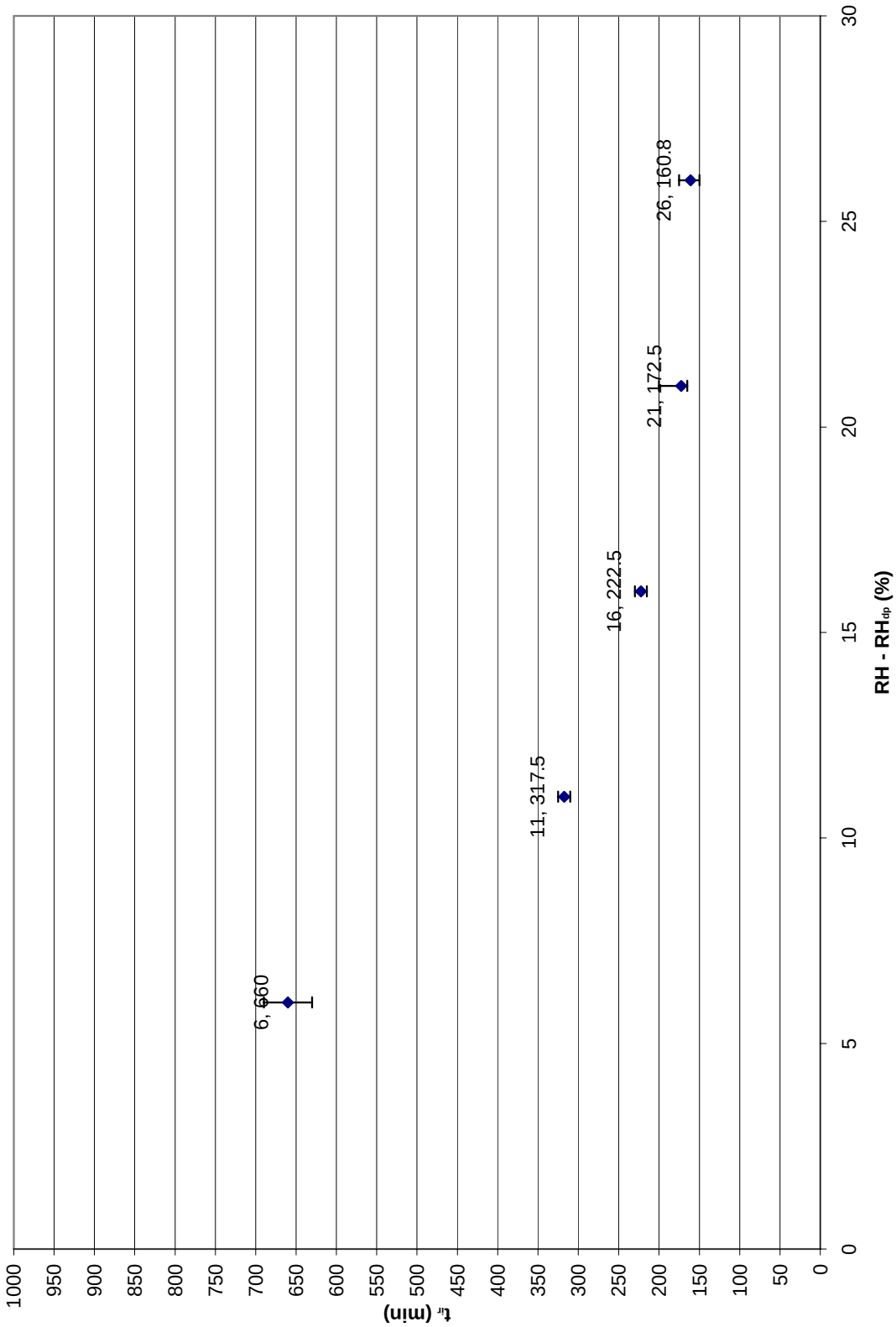

Figure 6.1: (RH - RH_{dp}) versus t_{ir} for initial run-off to occur

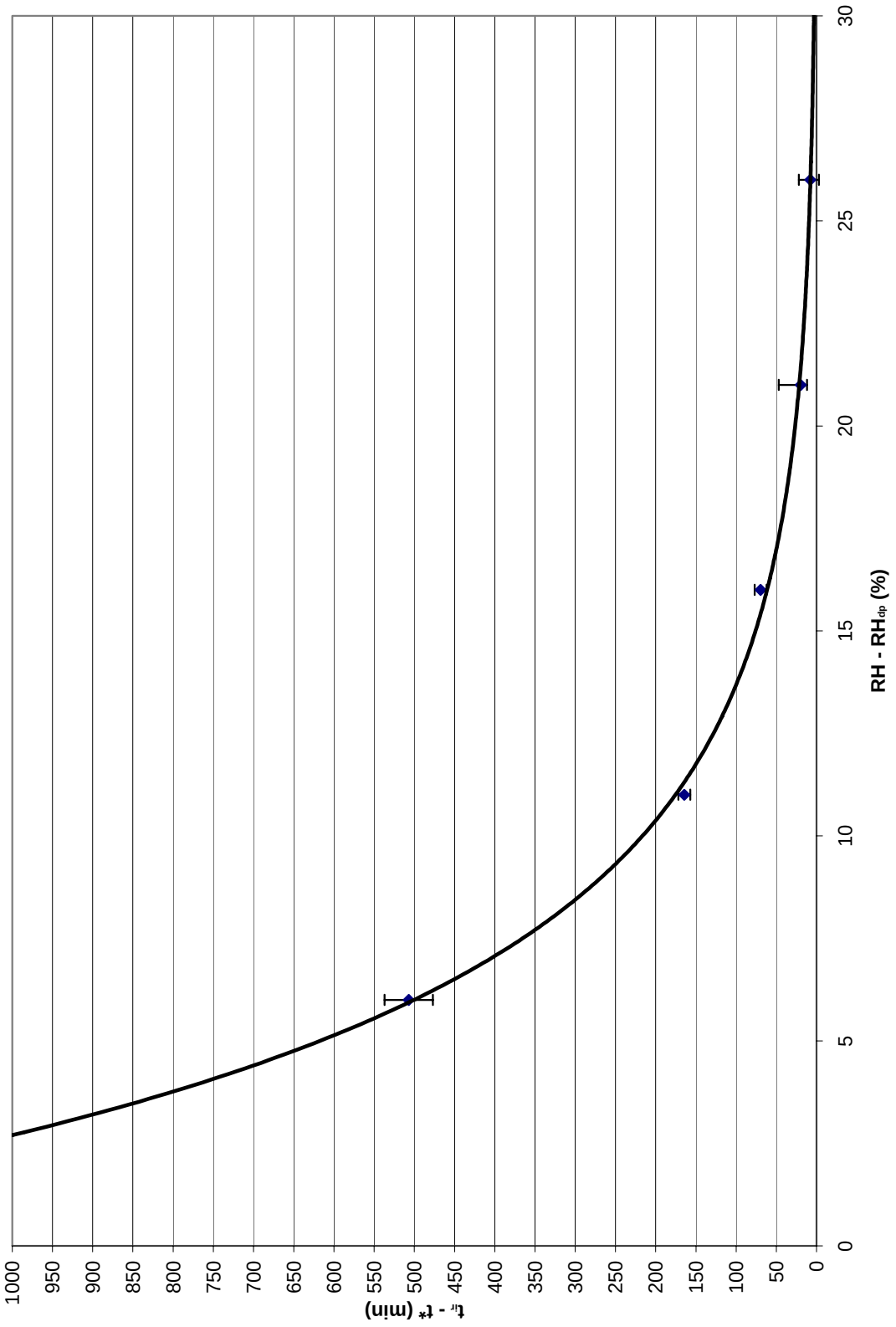

Figure 6.2: (RH - RH_{dp}) versus (t_{ir} – t*) for initial run-off to occur

6.3 Run-off Front Speed

A plot comparing run-off front movement versus (RH – RH_{dp}) is shown in Figure 7.3. The value plotted was the rate observed when the front began to move. The plot shows an increase in runoff front speed as RH is increased. This is expected as the higher RH imposes a higher driving potential for mass transfer. This in turn, results in a faster progression through droplet formation and hence, run-off and run-off front progression will occur over less time.

Estimated run-off speeds were obtained by observation and images captured were often 30 to 60 minutes apart. Hence, the margin of error for these values is significant.

It should be noted that the run-off front did not move appreciably over 950 minutes at RH = 30%. It is very much a possibility that the front did move, but did so at a rate that was too slow to be noticed. Clearly, run-off front movement speed must be zero at RH_{dp} as condensation run-off would not occur at RH_{dp}. The trend line plotted shows how the curve may start at (0,0) and then progress up similar to an exponential curve.

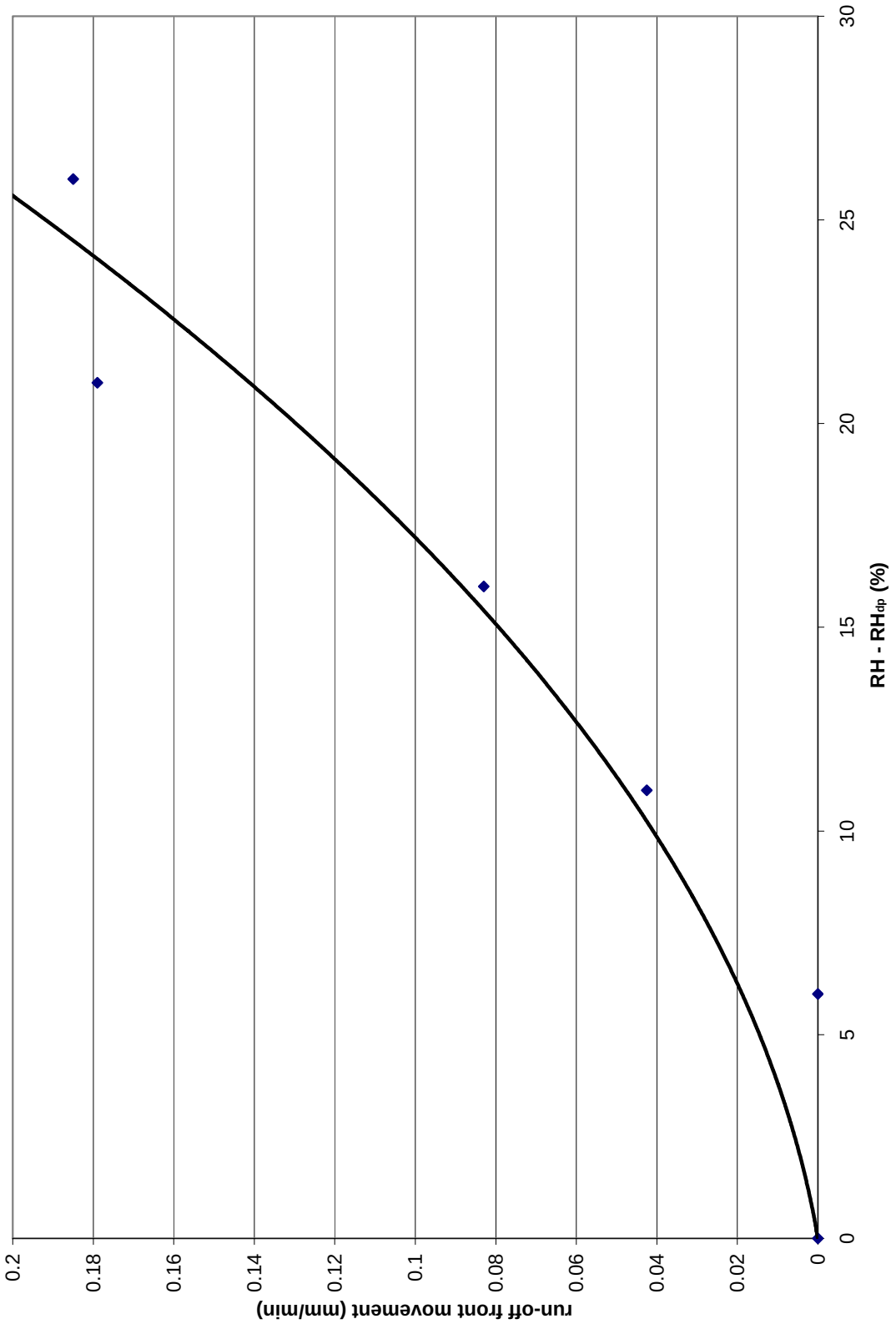

Figure 6.3: (RH - RH_{dp}) versus rate for condensation front movement

6.4 Surface Temperature

Thermocouple readings were recorded at the beginning and end of each experiment. As expected, the values did not vary appreciably between runs or between the beginning and the end of a run. At most there was a 0.7°C difference at any given thermocouple location between experiments. The thermocouples are accurate to 0.2°C and for the purpose of this experiment it can be assumed the aluminum surface temperature was the same for each experiment and constant throughout each experiment. The average temperatures for all readings are shown in Figure 7.4. Each point on the plot corresponds to a thermocouple location along the glass surface. Also in the plot is best fit curve that will be assumed to show the temperature at locations between the thermocouples.

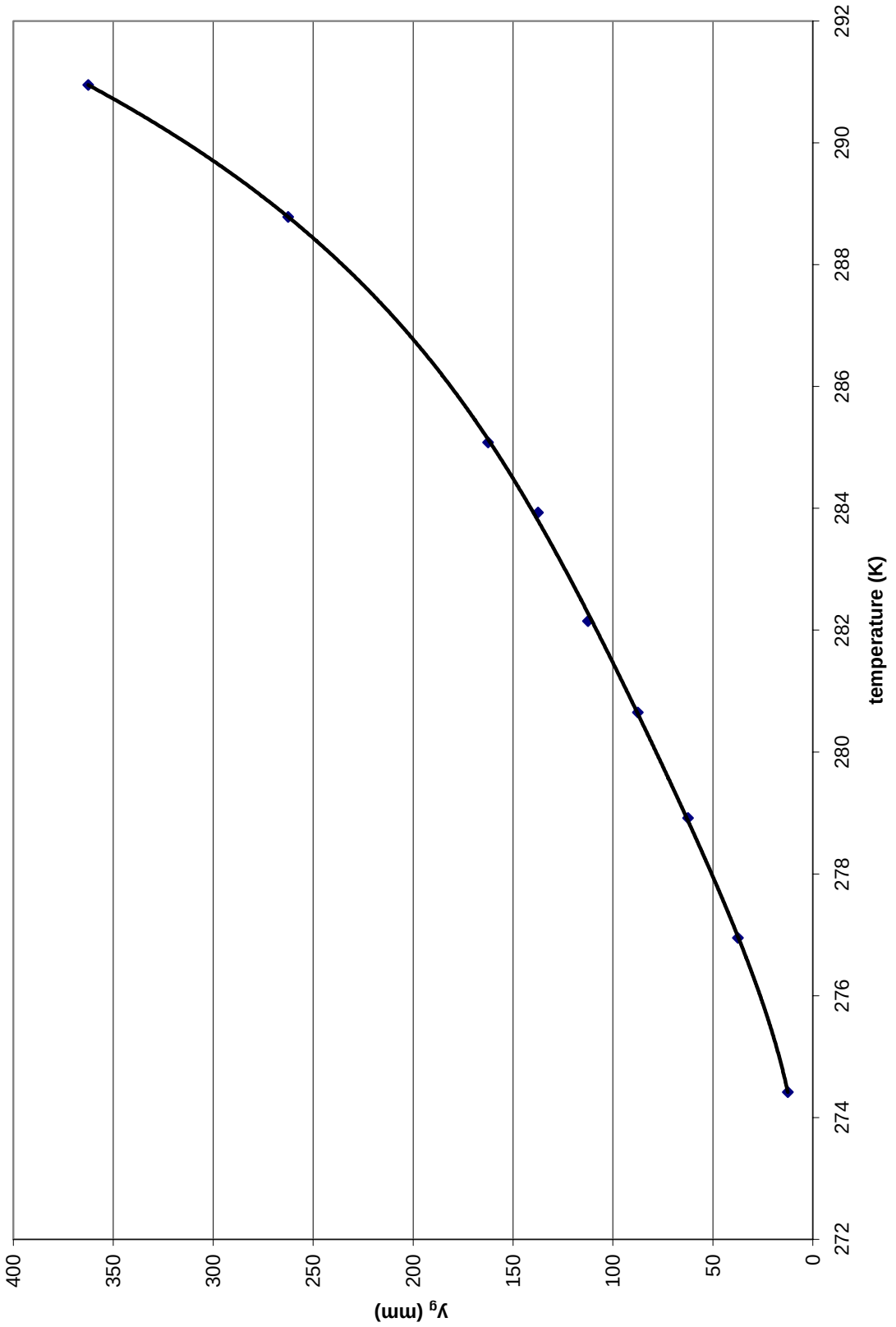

Figure 6.4: Temperature versus y_g; experimental values

6.5 Condensation Line

The condensation line was never horizontal. It stayed level starting from the left of the visible section until about the mid-point of the visible section, then dropped slightly moving further to the right, and levelled off again before leaving the visible section on the right side. This means the right side of the visible section was at a slightly higher temperature than the left side. It should be noted that the line that can be drawn across the condensation front does not continue past the visible section. The area visible is where the drop occurs and then balances off to form a horizontal line across the non-visible sections of glass. This was evident when a test was run with the glass portion exposed to the laboratory environment without the remaining enclosure. There are a number of possible explanations for this trend, although the exact cause is unknown. The first possibility may be an uneven glue layer between the glass and the aluminium. If the glue is thicker on the right side, the temperature of the exposed glass surface would be higher. A second possible reason; the thermocouple beads may have been slightly larger than the channel they sat in and hence prevented the glass surface from sitting directly on the aluminium surface during adhesion. The thermocouple channels were cut into the right hand section of the aluminum backing plate and the mass removed for the channels may have resulted in less thermal mass to store energy. Another possibility may be the edges of the channels were not filed down perfectly and any burrs on the channel edges may be preventing a flush mounting surface.

6.6 Droplet Addition

It should be noted that each spike at the beginning of each RH versus t cycle is associated with a single water droplet. The control device began droplet addition once the RH level dropped below the set-point. This trend did not continue throughout the duration of each individual experiment as the local minima decreased. This was due to a deficiency in the pipette system. It was observed that once the solenoid valve closed the water at the end of the pipette was drawn back up toward the valve. The longer the valve remained closed the further up the water traveled. Once the valve opened the water had to travel down the pipette before it could enter the chamber. The progression was slow and hence, a droplet was not immediately released on request from the control system. The second cause may be that because the pipette was not sealed to the chamber, some water in the pipette could have evaporated into the chamber; again, resulting in a greater distance for water travel before exiting the pipette.

Increasing the mass flow rate by a small amount did not increase the number of droplets added to the enclosure. For example, at 30%, the increase changed the flow rate from, 1 drop every 30 seconds to 1 drop every 20 seconds. Hence, the rate at which water traveled down to the pipette opening was increased and acted to offset the deficiencies described above. It seemed that by changing the water mass flow rate by a slight amount also acted to reset the system and provide immediate droplet addition when required. At higher RH levels where droplet addition was frequent, no manual input was required as the frequency of water addition was sufficient to avoid the problems mentioned above.

In some cases a much larger spike was observed amongst smaller spikes. It is believed that this was also a deficiency in the water system. On occasion, for unknown reasons the pipette would add a second droplet of water immediately after the solenoid valve closed.

6.7 Summary

Figure 7.5 is a summary of all results. It shows initial run-off, run-off rate, temperature profile, and run-off location at all RH levels. It is believed that this plot can be used to determine run-off properties of any glass surface that falls within the temperature range plotted and is exposed to a conditioned space at a T_{db} of 22.1°C with a RH within the plotted range. The lines labelled RH = 30% to 50% are condensation run-off plots (C_{plot}) for y_g versus time showing the location of the run-off front versus time.

Given the temperature of a section of glass and the RH of the space to which it is exposed, one can determine the time at which condensation run-off will occur. For example, refer to Figure 7.6, on a section of glass at 5°C, exposed to air at 22.1°C with a RH of 40%, condensation run-off will be observed after 325 minutes. If the same glass were exposed to air at RH = 35%, condensation run-off would commence at 540 minutes.

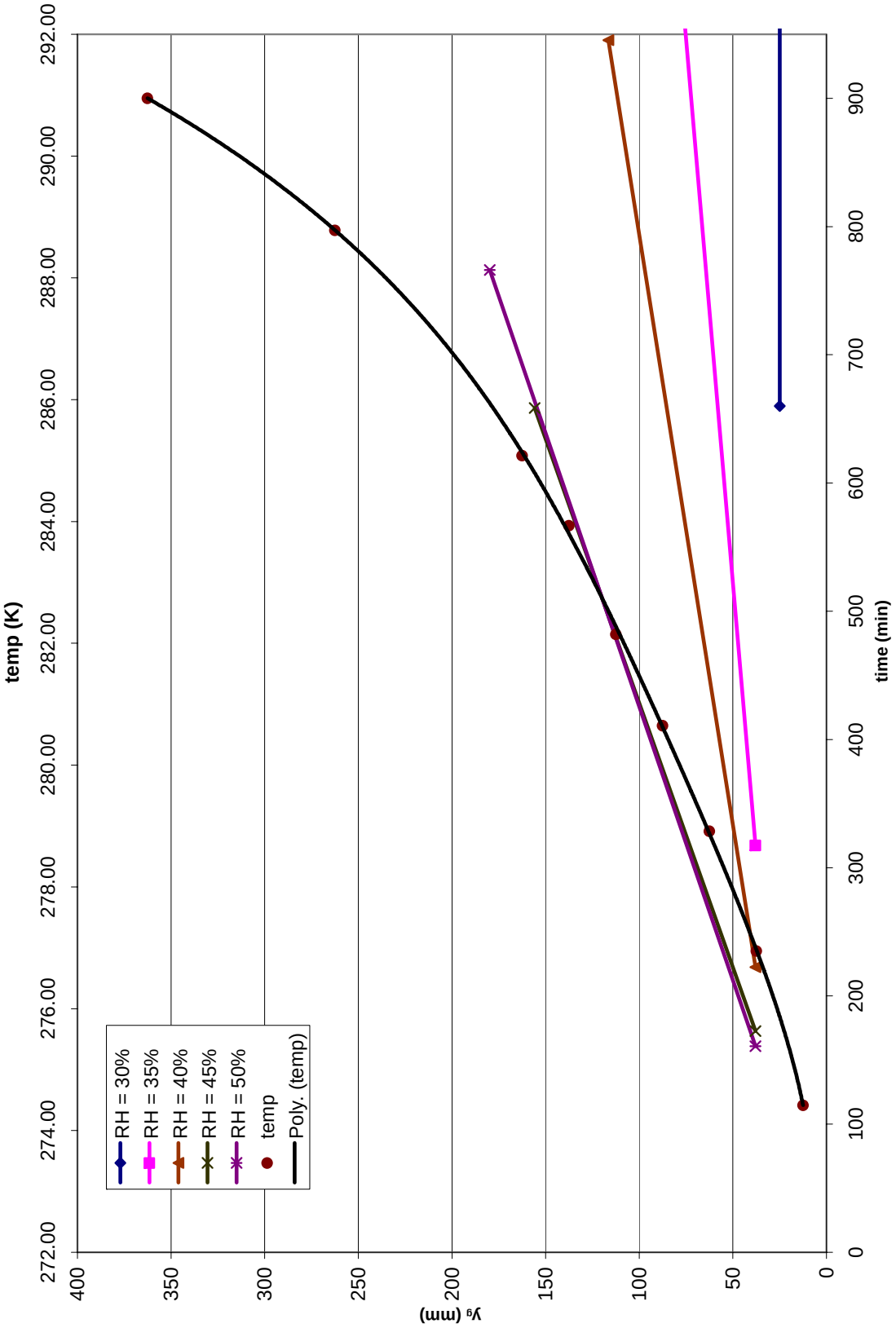

Figure 6.5: Location of condensate run-off front and surface temperature versus location

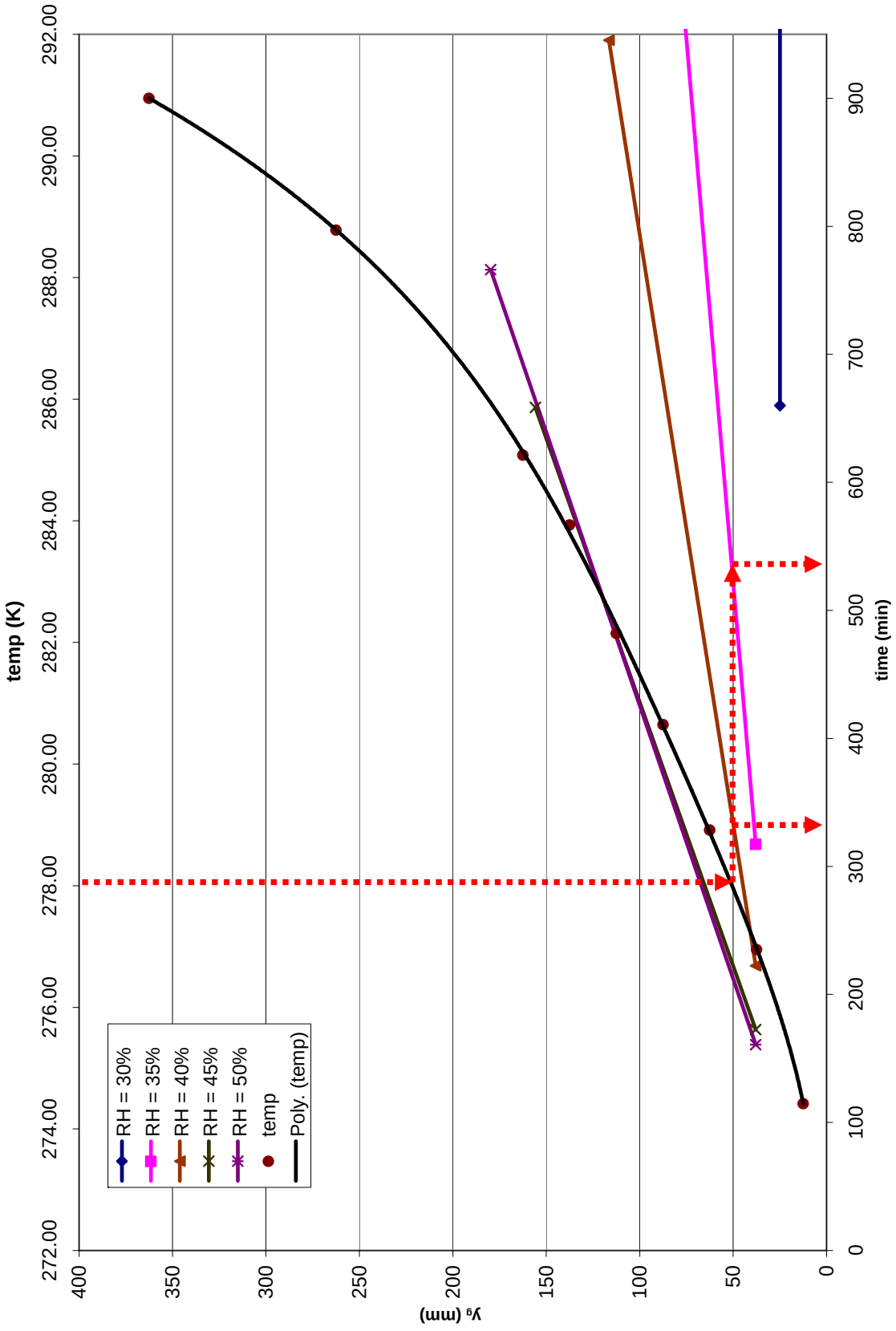

Figure 6.6: Location of condensate run-off front and surface temperature versus location example

Chapter 7

7 Conclusions and Recommendations

7.1 Conclusions

The main purpose of the apparatus was to determine if, and under what conditions, condensation would run-off a cooled vertical sheet of glass. It was shown that condensate on a cooled vertical glass surface with a temperature profile similar to that of a window did in fact run at relative humidity's of 30%, 35%, 40%, 45%, and 50% at a dry bulb temperature of 22.2°C. The initial run-off times at each RH set-point were approximately 630, 317.5, 222.5, 172.5, and 160.8 minutes. It was determined that initial run-off is sensitive at low RH (RH = 30%, 35%, 40%) and insensitive at high RH (RH = 45%, 50%).

It was determined that the RH versus time plots did not provide sufficient information to pin-point changes in condensation on the glass surface, and hence visual documentation was required.

It was seen, through qualitative analysis that the run-off front progressed up the glass at varying rates for each experiment; 0.043mm/min at 35%, 0.083mm/min at 40%, 0.18mm/min at 45%, and 0.19mm/min at 50%.

It was apparent that, because condensation at 30% was extremely slow and occurred over a small area, only the initial run-off time was obtainable from the experiment.

It was determined that the apparatus yielded logical and consistent results. These results, although approximate, provide useful information regarding the potential for condensation to cause damage as well as guidance regarding the design of subsequent experiments.

7.2 Recommendations

Numerous recommendations can be offered to improve the apparatus and experiments used within this study.

An improvement that became more obvious as the experiment progressed is the need for a more sophisticated automated water droplet system. With an automated system and a programmed controller the mass flow rate of water addition could be controlled and a more closely controlled RH could be achieved over an entire 16 hour time frame, without the need for manual adjustments.

Another benefit of importance, greatly reducing user interaction, is the need for an automated documentation system. A controller connected to a lamp and a fixed camera would eliminate the need for the user to collect images. The entire 16 hour experiment could be fully documented with pictures taken at shorter intervals.

A recommendation to determine mass flow rate of the condensate run-off is to install a device to measure the mass of water collecting in the collection system. If this device were connected to a data logger, the condensate mass could be monitored over the run as RH data is collected. The mass flow rate and times at which mass flow occurred would be available and could be possibly linked to changes in the RH plot.

It is also recommended that interferometery be performed on the condensate surface to obtain a heat transfer coefficient profile. These results would more accurately confirm the uniformity and magnitude of the heat transfer coefficient.

An alternative to the experimental apparatus that may simplify a few problems would be to greatly increase the size of the enclosure. Controlling the humidity would be much easier in a larger enclosure; in the current apparatus, one droplet of water increases the humidity ratio by 1 to 2 percentage points. In a larger enclosure with more air to dilute an individual droplet, such a large increase in RH will not occur. This would be most beneficial at lower relative humidity (30%) where it was difficult to bring the RH level to the set limit in a short time with out overshoot.

Of great importance, by using a larger enclosure or a small room, the air temperature may be controlled by a smaller, relative to the enclosure size, system. In the current apparatus the copper fin system is very large relative to the overall size of the enclosure and obstructs a great deal of the glass surface. It was first thought that only a small portion of the glass needed to be visible, but this made it difficult to know exactly when

condensation run-off began as run-off was determined visually and not by the RH sensor. The user was only able to detect condensate run-off by viewing the center portion of the glass. It was unknown if condensate began to run at an earlier time in an area not visible.

Chapter 8

8 References

Al-Doory, Y. & Domson, J.F., "Mould Allergy", *Philadelphia : Lee & Febiger* ©, 1984

Altman, L.C., Becker, J.W., & Williams, P.V., "Allergy in primary care", *Philadelphia: W.B. Saunders Company* ©, 2000.

AAMA, "AAMA 1503-98 voluntary test method for thermal transmittance and condensation resistance of windows, doors and glazed wall sections", *American Architectural Manufacturers Association*, 2004.

Arasteh, D.K., Beck, F.A., Griffith, B.T., Byars, N., & Acevedo, M., "Using infrared thermography for the study of heat transfer though building envelope components", *ASHRAE Transactions*, v.98(1), pp. 819-824, 1992

ASHRAE, "2004 ASHRAE handbook, HVAC systems and equipment", *American Society of Heating, Refrigeration and Air-Conditioning Engineers*., 2004.

ASHRAE, "2005 ASHRAE handbook, fundamentals", *American Society of Heating, Refrigeration and Air-Conditioning Engineers*., 2005.

ASTM 1363-87 "Standard test method for the thermal performance of building assemblies by means of a hot box apparatus".

Aydin, O., "Conjugate heat transfer analysis of double pane windows", *Building and Environment*, v.41(2), pp. 109-116, 2006.

Bailey, J. & Hall, G.H., "Fact sheet on controlling mold growth on window surfaces", *Mold Services Group – A Division of GHH Engineering Ltd*., http://moldservicesgroup.com/windowmold.asp, date accessed: May 14, 2006.

Baker, J., "Condensation resistance standards in North America", *Personal communication*., Friday, April 21, 2006.

Bar-Cohen, A. & Rohsenow, W.M., "Thermally optimum spacing of vertical, natural convection cooled parallel plates", *Journal of Heat Transfer*, v.106(1), pp. 116-123, 1984.

Barrett, J. R., "Mycotoxins: or molds and maladies", *Environmental Health Perspectives*., v.108(1), 2000.

Bartlett, K.H., Kennedy, S.M, Brauer, M., Ven Netten, C., & Bill, B., "Evaluation and a predictive model of airborne fungal concentrations in school classrooms", *Annals of Occupational Hygiene*, v.48(6), pp.547-554, 2004

Bhuyan, M. & Bhuyan, R., "An on-line method for monitoring of relative humidity using thermal sensors", *IEEE/IAS International Conference on Industrial Automation and Control*, No.95TH8005, pp. 7-11, 1995.

Bong, T.Y., Xue, H., & Liew, H.C., "Predicting window condensation potential for a large viewing gallery", *Building and Environment*, v.33(2,3), pp.143-150, 1998.

Brasel, T.L., Martin, J.M., Carriker, C.G., Wilson, S.C., & Sraus, D.C., "Detection of airborne stachybotrys chartarum macrocyclic trichothecene mycotoxins in the indoor environment", *Applied and Environmental Microbiology*, v.71(11), pp. 7376-7388, 2005.

CD adapco, "Tutorials", *CD adapco Group*, Star-CD, v.3.22, ©, 2004.

Carlson, N., "Fungal glossary", *University of Minnesota – Environmental Health and Safety*, http://www.dehs.umn.edu/IAq/fungus/glossary.html, date accessed: May 7, 2006.

Carpenter, S.C. & Hanam, M., "Rating the condensation potential of windows: results from testing and simulation", *ASHRAE Transactions*, v.107(2), pp. 550-555, 2001.

Carpenter, S.C. & McGowan, A.G., "frame and spacer effects in window u-value", *ASHRAE Transactions*, v.95(1), pp. 604 – 608, 1989.

Carson, S.E., "Toxic mold: latest construction defect", *Journal of Professional Issues in Engineering Education and Practice*, v.129(3), pp. 171-176, 2003.

Clark, M.D., "Builder sued after mold evicts woman", *The Cincinnati Enquirer*, June 3, 2002.

Cooley, J.D., Wong, W.C., Jumper, C.A., & Straus, D.C., "Correlation between the prevalence of certain fungi and sick building syndrome", *Journal of Occupational and Environmental Medicine*, v.55, pp. 579-584, 2006.

Crissey, J.T. et al. Lang, H., & Parish, L.C., "Manual of medical mycology" *Massachusetts: Blackwell Scientific* ©, 1995.

CSA, "Energy performance of windows and other fenestration systems/user guide to CSA A440.2-04, energy performance of windows and other fenestration systems", *Canadian Standards Association*, 2004.

Curcija, D. & Goss, W.P., "Two-dimensional natural convection over the isothermal indoor fenestration surface – finite element numerical solution" *ASHRAE Transactions*, v.99(1), pp. 274-287, 1993.

D'Andrea, C.M.S., "Guidelines on assessment and remediation of fungi in indoor environments", *New York City Department of Health & Mental Hygiene*, 2002.

Dalton, L.W., "Today's materials favor mold growth", *Chemical & Engineering News; Science & Technology*, v.82(7), pp.60-61, 2004.

Davis, P.J., "Molds, toxic molds, and indoor air quality", *California Research Bureau Note*, v.8(1), 2001.

De Abreu, P.F., "Modeling the thermal performance of windows using a two-dimensional finite volume model" *University of Waterloo, Department of Mechanical Engineering, Ph.D Thesi*s., 1997.

Dearborn, D.G., Yike, I., Sorenson, W.G., Miller, M.J., & Etzel, R.A., "Overview of investigations into pulmonary haemorrhage among infants in Cleveland, Ohio", *Environmental Health Perspectives Supplements*, v.107(S3), 1999.

Delevan Spay Technologies, "Total Control Industrial Nozzles and Accessories – Specifiers Guide (Model WBD)", *Develan Spray Technologies*, pp.C.1, 2004

Duffie J.A., & Beckman, W.A., "Solar Engineering of Thermal Processes – second edition" *NewYork: John Wiley & Sons, Inc.* © 1991

Eaton, R.A., "Bacterial decay of ACQ-treated wood in a water cooling tower", *International Biodeterioration & Biodegradation*, v.33(3), pp.197-207, 1994.

Edwards, D.K., "Solar Absorption by each element in an absorber-coverglass array", *Solar Energy*, v.19(4), pp.401-402, 1977

EEL, "FRAME: a computer program to evaluate the thermal performance of window frame systems" *Version 4.0, Enermodal Engineering Ltd,* 1995

Elmahdy, A.H., "Heat transmission and R-value of fenestration systems using IRC hot box: procedure and uncertainty analysis", *ASHRAE Transactions*, v.98(2), pp. 630-637, 1992.

Elmahdy, A.H., "Quantification of air leakage effects on the condensation resistance of windows", ASHRAE Transactions, v.109(1), pp. 600-606, 2003.

Elmahdy, A.H., & Devine, F., "Laboratory infrared thermography technique for window surface temperature measurements", *ASHRAE Transactions*, v.111(1), pp. 561-571, 2005.

Elmahdy, A.H., & Frank, T., "Heat transfer at the edge of sealed insulating glass units: comparison of hot box measurements with finite difference modeling", *ASHRAE Transactions*, v.99(1), pp. 915-922, 1993.

ElSherbiny, S.M., Raithby, G.D., & Hollands, K.G.T., "Heat transfer by natural convection across vertical and inclined air layers", *Journal of Heat Transfer*, v.104, pp.96-102, 1982.

EPA, "A brief guide to mold, moisture, and your home" *U.S. Environmental Protection Agency, Office of Air and Radiation Indoor Environments Division*, 2002.

EPA, "Mold remediation in schools and commercial buildings" *U.S. Environmental Protection Agency, Office of Air and Radiation, Indoor Environments Division*, 2001.

Etzel, R.A., Montana, E., Sorenson, W., Kullman, G., Allan, T., & Dearborn, D., "Acute pulmonary hemorrhage in infants associated with exposure to stachybotrys atra and other fungi", *Archives of Paediatrics & Adolescent Medicine*, v.152, pp. 757-762, 1998.

Fisk, W.J., Gomez, Q.L., & Mendell, M.J., "Meta-analyses of the associations of respiratory health effects with dampness and mold in homes", *Environmental Energy Technologies Division, Indoor Environmental Department., Lawrence Berkeley National Laboratory*, 2006.

Fraser, R.A., de Abreu, P.F., Wright, J.L., Sullivan, H.F., & Yao, H., "Critical issues in comparing edge-seal performance: modeling vs. experiment", *ASHRAE Transactions*, v.99(1), pp. 923-940, 1993.

Fredericton Student Housing, "UNB student union off-campus housing inspection form", *Student Union, University of New Brunswick*, 2006.

Gent, J.F., Ren, P., Belanger, K., Triche, E., Bracken, M.B., Holford, T.R., & Leaderer, B.P., "Levels of household mold associated with respiratory symptoms in the first year of life in a cohort at risk for asthma", *Environmental Health Perspectives*, v.110(12), 2002.

Godish, T., "Sick buildings: definition, diagnosis and mitigation", *Boca Raton: Lewis Publishers* ©, 1995

Godish, T., "Indoor environment notebook, everything you wanted to know about indoor air pollution and more", *Ball State University, department of Natural Resources and Environmental Management*, web.bsu.edu/ien/archives/2002/072002.htm, date accessed: May 14, 2006.

Grant, C., Hunter, C.A., Flannigan, B., & Bravery, A.F., "Moisture requirements of moulds isolated from domestic dwellings", *International Biodeterioration*, v.25(4), pp.259-284, 1989.

Greaves, H., "The bacterial factor in wood decay", *Wood Sciences and Technology*, v.5, pp.6-16, 1971.

Griffith, B.T., Turler, D., & Arasteh, D.K., "Surface temperature of insulated glazing units: infrared thermography laboratory measurements", *ASHRAE Transactions*, v.102(2), pp.479-488, 1996.

Griffith, B.T., Goudey, H., & Arasteh, D., "Surface temperatures of window specimens: infrared thermography laboratory measurements", *ASHRAE Transactions*, v.108(1), pp.525-536, 2002.

Hammond, G.P., "Thermal performance of advanced glazing systems", *Journal of the Institute of Energy*, v.74(498), pp.2-10, 2001.

Herdon, E.L & Yang, C.S., "Mold and mildew: a creeping catastrophe", *Claims Magazine*., pp. 38, August, 2000.

Hollands, K.G.T., Wright, J.L. & Granqvist, C., "Solar energy: a century of progress", *James and James, London, U.K.*, ©, 2001

Honeywell, "Humidity sensors HIH-3610 series", *Honeywell Sensing and Control*, 2006.

Incropera, F.P. & DeWitt, D.P., "Fundamentals of heat and mass transfer – fifth edition", *John Wileys & Sons: New York*, ©, 2002.

IOM, "Damp indoor spaces and health", *The National Academies, Washington: The National Academies of Sciences* ©, 2004.

Jarvis B. B., & Miller J. D., "Mycotoxins as harmful indoor air contaminants', *Applied Microbiology and Biotechnology*, v.66, pp. 367-372, 2005.

Jo, W.K. & Seo, Y.J, "Indoor and outdoor bioaerosol levels at recreation facilities, elementary schools, and homes", *Chemosphere*, v.61, pp. 1570-1579, 2005.

Kozak, P.P., Gallup, J., Cummins, L.H., & Gillman, S.A., "Factors of importance in determining the prevalence of indoor molds", *Annals of Allergy*, v.43(2), pp. 88-94, 1979.

Kuhn, R.C., "Prevalence and airborne spore levels of Stachybotrys spp. in 200 houses with water incursions in Houston, Texas", *Canadian Journal of Microbiology*, v.55, pp.25-28, 2005.

LBL, “WINDOW 4.1: a PC program for analyzing thermal performance-program description tutorial”, *Lawrence Berkeley Laboratory: Windows and Daylight Group*, 1993.

Mitchell, R., Kohler, C., & Arasteh, D., “THERM5/ WINDOW5 NFRC simulation manual”, *Lawrence Berkeley National Laboratory*, 2003.

Matsuyama, Y., Kotera, S., Shibuya, T., & Nagai, M., “Lifetime prediction of a resin spacer in insulating glass”, *Journal of Chemical Engineering of Japan*, v.38(3), pp.214-219, 2005.

McGowan, A.G., “Numerical prediction of window condensation potential”, *ASHRAE Transactions,* v.101(1), pp. 832-837, 1995.

McNeel S. V., & Kreutzer, R.A, “Fungi & indoor air quality”, *Health & Environment Digest*, v.10(2), pp. 9-12, 1996.

McQuiston, F.C., Parker, J.D., & Spitler, J.D., “Heating, ventilating, and air conditioning analysis and design”, *John Wiley & Sons, Incorporated* ©, 2000.

Miller, J.D., Laflamme, A.M., Sobol, Y., Lafontaine, P., & Greenhalg, R., “Fungi and fungal products in some Canadian houses”, *International Biodeterioration*, v.24(2), pp.103-120, 1988

Morrell, J.J, “Wood-based building components: what have we learned?”, *International Biodeterioration & Biodegradation*, v49(4), pp. 253-258, 2002.

Mortensen, G.K., Strobel, B.W., & Hansen, H.C.B., “Degradation of zearalenone and ochratoxin A in three Danish agricultural soils”, *Chemosphere*, v.62(10), pp. 1673-1680, 2006.

Muneer, T., & Abodahab, N., “Frequency of condensation occurrence on double-glazing in the United Kingdom”, *Energy Conversion and Management: An International Journal*, v.39(8), pp. 717-726, 1998.

Muto, S., Suzuki, O., Amano, T., & Morisawa, M., “A plastic optical fibre sensor for real-time humidity monitoring”, *Measurement Science & Technology*, v.14(6), pp. 746-750, 2003.

Natural Resources Canada, “2003 – survey of household energy use(SJEU) summary report, december 2003”, *Energy Publications, Office of Energy Efficiency, Her Majesty the Queen in Right of Canada* ©, 2006.

Nilsson, T., “Cavitation bacteria”, *The International Research Group on Wood Preservation*, Document No. IRG/WP/1235, 1984.

Nilsson, T. & Daniel, G., "Tunnelling bacteria", *The International Research Group on Wood Preservation*, Document No. IRG/WP/1186, 1983.

Nilsson, T. & Rowell, R.M., "Decay patterns in butylene oxide modified ponderosa pine attacked by fomitopsis pinicola", *The International Research Group on Wood Preservation*, Document No. IRG/WP/1183, 1983.

NFRC, "NFRC 102-2004 Procedure for measuring the steady-state thermal transmittance of fenestration systems", *National Fenestration Rating Council Incorporated*, 2004a.

NFRC, "NFRC 500-2004 Procedure for determining fenestration product condensation resistance values", *National Fenestration Rating Council Incorporated*, 2004a.

O'Neill, A., "Ed McMahon sues over mold in house", *Los Angeles Times*, April 10, 2002.

Pasanen, A.L., Heinonen-Tanski, H., Kalliokoski, P., & Jantunen, M.J., "Fungal microcolonies on indoor surfaces- an explanation for the base-level fungal spore counts in indoor air", *Atmospheric Environment*, v.26B(1), pp.117-120, 1992.

Porter, P., "Mold is growing as insurance problem", *The Columbus Dispatch*, February 22, 2003.

Post, N.M., "Containing Noxious Mold", *Engineering News Record*, v.242(17), pp.32, 1999.

Reilly, S., "Spacer effects on edge-of-glass and frame heat transfer", *ASHRAE Transactions*, v.100(1), pp. 1718-1723, 1994.

Reilly, S., Arasteh, D., & Rubin, M., "Effects of infrared absorbing gasses on window heat transfer. A comparison of theory and experiment", Solar Energy Materials, v.20(4), pp. 277-288, 1990.

Ridder, J.A., "Toxic mold; a growing headache-Moisture usually to blame in energy-efficient homes; pulmonary haemorrhage, memory loss among woes", *The Akron Beacon Journal*, February 25, 2002.

Robbins, C.A., Swenson, L.J., Ger, W.T., & Kelman, B.J., "Mold in indoor environments: a critical review of research studies", *Injury Insights, National Safety Council Research & Statistical Services*, April/May 2003.

Rubin, M., "Calculating heat transfer through windows", *International Journal of Energy Research*, v.6(4), pp. 341-349, 1982.

Schrey, A.C., Fraser, R.A., & de Abreu, P.F., "Local heat transfer coefficients for a flush-mounted glazing unit", *ASHRAE Transactions*, v.104(1B), pp. 1207-1221, 1998.

Shelton, B.G., Kirkland, K.H., Flanders, W.D., & Morris, G.K., "Profiles or airborne fungi in buildings and outdoor environments in the united states", *Applied and Environmental Microbiology*, v.68(4), pp. 1743-1753, 2002.

Sullivan, H.F., Wright, J.L., Fraser, R.A., "Overview of a project to determine the surface temperature of insulated glazing units: thermographic measurement and two dimensional simulation", *ASHRAE Transactions*, v.102(2), pp. 516-522, 1996.

Sullivan, R., Arasteh, D.K., Beck, F.A., & Selkowitz, S.E., "Energy performance of evacuated glazings in residential buildings", *ASHRAE Transactions,* v.102(2), pp. 220-227, 1996.

Turns, R., S., "An introduction to combustion – concepts and applications – 2nd edition", *The McGraw-Hill Companies Inc* ©, 2000

Underwood, A., "A hidden health hazard", *Newsweek Magazine: New York*, v.136(23), pp. 74, 2000.

Upsher, F.J., "Fungal colonization of some materials in a hot-wet environment", *International Biodeterioration*, v.20(2), pp.73-78, 1984

US Environmental Protection Agency (EPA), "Mold Web Course", Last updated March 13, 2006.

UW, "VISION4 computer program" *University of Waterloo, Advanced Glazing Laboratory*, 1995.

Vaisala Oyj, "Vaisala HUMICAP humidity and temperature transmitter series HMT330 user's guide", *Vaisala* ©, 2005.

Wang G-S., Yang, K.Y., & Perng, R.P., "Life-threatening hypersensitivity pneumonitis induced by docetaxel (taxotere)", *British Journal of Cancer*, v.85(9), pp. 1247-1250, 2001.

Weir, G., & Muneer, T., "Energy and environmental impact analysis of double-glazed windows", Energy Conversion and Management, v.39(3-4), pp. 248-256, 1998.

White C. W., & Kuehl. M. H, "The Role of Construction Textiles in Indoor Environmental Pollution", *Journal of Industrial Textiles*, v.32(1), 2002.

Wright, J.L., "Calculating center-glass performance indices of windows", *ASHRAE Transactions*, v.104(1B), pp. 1230-1241, 1998a.

Wright, J.L., "A simplified numerical method for assessing the condensation resistance of windows", *ASHRAE Transactions*, v.104(1B), pp. 1222-1229, 1998b.

Wright, J.L., “Correlation to quantify convective heat transfer between vertical window glazings”, *ASHRAE Transactions*, v.102(1), pp. 940-946, 1996.

Wright, J.L., “Summary and comparison of methods to calculate solar heat gain”, *ASHRAE Transactions*, v.101(1), pp. 802-818, 1995.

Wright, J.L., Jin, H., Hollands, K.G.T., Naylor, D., “Flow visualization of natural convection in a tall, air-filled vertical cavity”, *International Journal of Heat and Mass Transfer*, v.49(5-6), pp. 889-904, 2006

Wright, J.L. & Kotey, N.A., “Solar absorption by each element in a glazing/shading layer array”, *ASHRAE Transactions*, v.112(2), 2006.

Wright, J.L. & McGowan, A.G., “A comparison of calculated and measured indoor-side window temperature profiles”, *ASHRAE Transactions*, v.109(2), pp. 857-870, 2003.

Wright, J.L. & Sullivan, H. F., “Natural convection in sealed glazing units: a review”, *ASHRAE Transactions*, v.95(1), pp. 592-603, 1995.

Wright, J.L. & Sullivan, H. F., “A two dimensional numerical model for glazing system thermal analysis”, *ASHRAE Transactions*, v.101(1), pp. 819-831, 1995.

Zhao, Y., Curcija, D., & Goss, W.P., “Condensation resistance validation project – detailed computer simulations using finite-element methods”, *ASHRAE Transactions*, v.102(2), pp. 508-515, 1996.